FABRICATION OF SERS AND FLUORESCENCE SENSORS USEFUL IN DETECTION OF R6G AND IONIC PHOSPHATE RESPECTIVELY

By

ANJULI BHANDARI

A DISSERTATION

Submitted to the faculty of Delaware State University in partial fulfillment
of the requirement for the degree of Doctor of Philosophy
of Applied Chemistry in the Department of Chemistry

DOVER, DELAWARE
August 2019

This dissertation is approved by the following members of the Final Oral Review Committee:

Dr. Gulnihal Ozbay, Committee Chairperson, Department of Agriculture and Natural Resources, Delaware State University
Dr. Cherese Winstead Casson, Committee Co-Chairperson, Department of Chemistry, Delaware State University
Dr. Bizuneh Workie, Committee Member, Department of Chemistry, Delaware State University
Dr. Gabriel Gwanmesia, Committee Member, Division of Physical and Computational Sciences, Delaware State University
Dr. Dominik Berg, External Committee Member, Department of Physics and Astronomy, Rowan University

DEDICATION

I would like to dedicate this dissertation to my husband and family. Nick, you have supported me in all of my endeavors, even when they take me far away, and I will forever be thankful for that. To my loving parents and sister; Kathleen, Billa and Kiran - thank you for being such a strong and supportive family to help me reach my goals whether it was grade school or grad school. Lastly, thank you to my in-laws and the friends who have turned into family who have been so kind, thoughtful and encouraging along the way. It has been a long journey but I am beyond grateful to you all for everything you have provided. I owe all of my success to this group of people, who have been my support system throughout my academic career.

ACKNOWLEDGEMENT

I would like to express my appreciation towards the individuals who have guided me academically and aided in my success throughout my journey to becoming a Doctor of Philosophy in Applied Chemistry at Delaware State University. To my mentors, Dr. Daniela Radu and Dr. Cheng-Yu Lai, thank you for all of your support, motivation, and continued trust over the course of this program. The experiences and knowledge I will take away from working with you will be something I will never forget and have helped shape me into the Chemist I am today. Thank you for being wonderful mentors and never losing faith in me!

In addition, I would like to take the time to say thank you to my colleagues and friends I have met along the way; Dr. Po-Yu Hwang, Dr. Dominik M. Berg, Dr. Mimi Liu, Nicholas Pizzi, Martin Chi, Aaron R. Legar, Dylan R. McConnell, and Miranda L. Penny. Thank you for the shared experiences, whether in or out of the laboratory. Your company is cherished.

Lastly, I would like to thank both Co-Chairpersons from my committee; Dr. Cherese Winstead and Dr. Gulnihal Ozbay. Dr. Ozbay, thank you for continuing to mentor and provide full support in my academic pursuits. Your help and motivation has continued to guide both my work and passions and I am forever thankful for the experience to work alongside you. Dr. Winstead, thank you for the opportunities you have provided me and for the constant support. I would also like to acknowledge my committee members; Dr. Gabriel Gwanmesia, Dr. Dominik Berg and Dr. Bizuneh Workie, thank you for taking the time to provide guidance throughout my career. I could not be more thankful for all of the individuals who provided this wonderful experience.

Lastly, I would like to acknowledge and thank Deborah Powell DBI for the SEM/TEM images provided as well as Michael Moore from DSU Optics Center for the training and access to SEM and AFM. I'm grateful for the opportunity the RISE-ANERA Fellowship provided me.

ABSTRACT

This dissertation focuses on organically synthesized sensors. A variety of projects were worked on to find the best method of a selective and sensitive sensor. Findings presented in this dissertation will cover a fluorescence based sensor used to detect ions as well as a Surface Enhanced Raman Spectroscopy (SERS) active sensor that can achieve low Rhodamine 6G (R6G) quantification.

Fluorescent probes are of vast research interest due to the ease of fabrication, high sensitivity, selectivity, and application in both in vivo/in vitro studies. Coumarin compounds are innately fluorescent and are ultimately suitable as fluorescent probes. By altering the mechanism used as well as the probe compound, the target analyte can vary. Work performed in this dissertation synthesized a variation of Coumarin that was suitable in phosphate and sulfate detection methods. When in solution, the chemodosimeter proved to be selective in distinguishing between four ions out of the eleven tested. Beyond detection, the sensor was capable of quantification of these ions when in solution.

Raman SERS substrates are another type of sensor that can prove incredibly useful by increasing the intensity in a given spectrum. Using a metallic nanoparticle material, the localized surface plasmon resonance helps achieve an amplified signal. A novel SERS substrate was fabricated utilizing both silver nanostars and mesoporous silica nanoparticles that was suitable in R6G detection. Using this sensor, R6G was capable of being quantified down to 100 pM.

Findings presented in the work below were achieved using prior research and new concepts. Both sensors described proved to be reproducible and stable materials. This dissertation will go into detail of the fabrication and utilization of these sensor based materials and applications of testing methods.

TABLE OF CONTENTS

LIST OF TABLES

LIST OF FIGURES AND SCHEMATICS

LIST OF ABBREVIATIONS

AgNS	Silver Nanostars
PMMA	Poly(methyl methacrylate)
AgNP	Silver Nanoparticles
R6G	Rhodamine 6 G
Pi	Inorganic Phosphate
MSN	Mesoporous Silica Nanoparticles
PSP 281	Guo *et al* chemodosimeter material
HEPES	4-(2-hydroxyethyl)-1-piperazineethanesulfonic acid
PSP 286	4-chloromethyl-7-hydroxycoumarin
PSP 287	7-hydroxy-4-(hydroxymethyl)-2H-chromen-2-one
SERS	Surface Enhanced Raman Spectroscopy

CHAPTER I: INTRODUCTION

Throughout this dissertation, the synthesis of varied sensors and their capabilities will be discussed in depth. Each sensor is conceptually different and provides contrasting abilities along with instrumental technique, characterization and application. Using prior research applications, these novel sensors were built using both new and prior knowledge to acquire the most efficient model possible. This dissertation will cover two synthetic sensor methods, their applications, sensitivity and selectivity at a detailed level.

1.1. The History Behind Sensors

The first industry sensor to be synthesized and utilized occurred in 1860.[1] Materials were noted to sometimes be affected by either temperature or electrical resistance earlier than this time, but Wilhelm von Siemens was the first to apply the theory. [1] Using a resistor made of copper material, Siemens effectively created a thermal sensor, thus creating the industrial exploration of sensors and applications in the years to follow. [1]

Sensing is a mechanism widely used in everyday objects where many are unaware of the impact it has in one's daily life. For example, iPhones use touch key pads which sense the pressure of the finger and uses biometric identification for unlocking mechanisms. This classifies as a tactile sensor, where the sensor detects physical disruption.[2] Technology seems keen on these types of sensors, where a plethora of computer systems as well as automobile systems rely on a variation of this style to be more independent in function.

Beyond tech savvy sensors, there are those that exist in nature. For instance, the human body is capable of detecting various parameters that include; temperature, moisture, sound, light, the list goes on. Although the body is capable of reacting to a variety of environmental changes,

there are also systems that can be applied to the body which can then respond to changes other than the environmental ones. To elaborate, it is well known that elderly individuals have a higher risk of taking a fall that could potentially cause either grave physical harm or could ultimately prove fatal. To combat this epidemic, a multitude of sensors were created to detect if a fall had occurred, which would automatically alert first responders to come render aid.[3] Phillips, which is a company that markets these products, uses sensors that either detect barometric deviations indicating a fall as well accelerometers which can detect acceleration force indicating a fall took place.[3] There are also similar styles available which allow the user to call for help, or the aforementioned automatic detector which evaluates on its own and calls for help.

1.2. Chemical Sensors

Sensors carry the ability to detect a targeted and specified presence. In the case of chemical sensors, that object is a chemical analyte or molecule. The sensor detects this chemical and transforms the positive signal into information that can be collected and prove useful in further work, **Fig 1.1**. Some sensors go beyond simple detection and are capable of quantification. There are a multitude of sensors that can be created for detection using different techniques, it is important to focus on finding the right application, method, and material when synthesizing such a sensor.

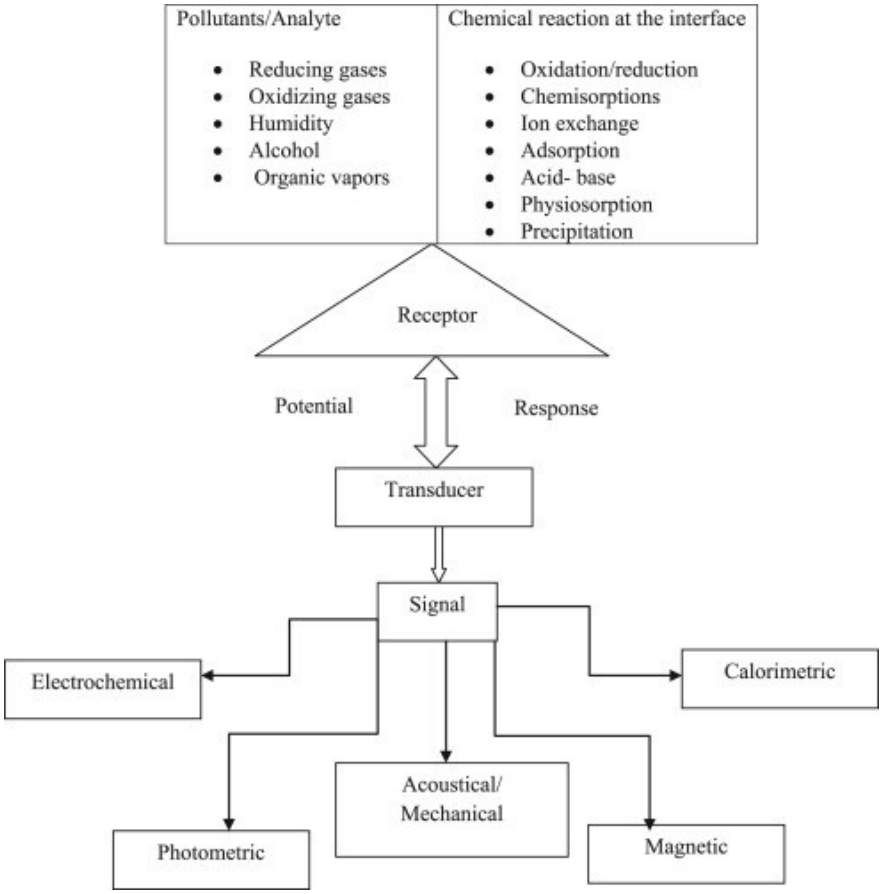

Figure 1.1. Chemical sensors and mechanism possibilities.[4]

The chemical sensor can be applied in a variety of settings and applications. This alone creates interest in investigation of chemical sensors since there is universal application and unlimited analytes that could be potentially quantified. Generally, there are two methods of how this sensor works. First, there is the chemical reaction that takes place between the analyte and receptor.[5] If this occurs, the system can be manipulated to search for the product of the reaction, such as a bound molecule.[5] The other option is that a physical change takes place when the receptor is adhered or bound with target molecule creating a change in physical properties, like fluorescence or a colorimetric response.[5]

1.3. Optical Chemical Sensors

In an optical chemical sensor, the same relationship is exhibited between receptor and transducer as in a chemical signal. However, an optical transduction is used to observe any analytical information regarding the molecule or target system of interest.[6] These types of analytical transducers include absorbance, luminescence, refractive index, and reflectivity.[6] The efficiency of the sensor is determined based on compatibility of the mechanism used for sensing or essentially which optical transducer is used.[6] Between the cost efficiency, relative ease of use and selectivity, optical chemical sensors are great alternatives to standard electric-based sensors, **Fig 1.2**.[7]

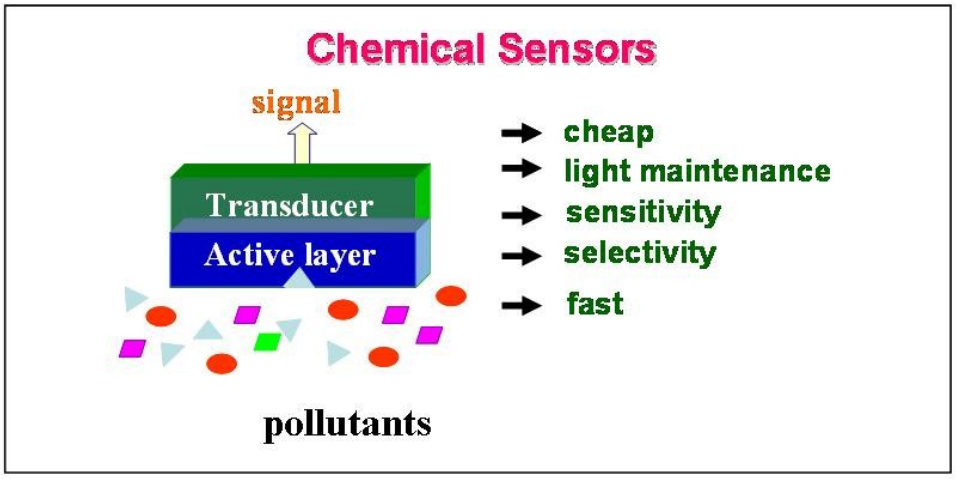

Figure 1.2. Chemical sensor mechanism and advantages.[7]

Optical chemical sensors tend to be favored in today's research climate for a multitude of reasons. When dealing with an electric-based sensor there are many factors that can cause influence or disruption including; lack of selectivity, electromagnetic interference, and absence of stability when dealing with hazardous compounds.[8] When dealing with an optical sensor,

many of these hazards are diminished making the sensor relatively safer resulting in more stability and general favorability.[8]

Direct spectroscopic sensing appears to hold the largest interest for optical chemical sensors. This may be due to the wide variety of applications and instrumentation that can be used to accommodate a plethora of analytes. For instance, In spectroscopy is typically used when distinguishing the presence of gases such as; carbon monoxide and dioxide, nitrogen dioxide, ammonia and methane.[6] In using Fourier Transform Infrared Spectroscopy (FTIR), the detection limit is even lower, detecting into the ppb range of these gases.[6] The application of this kind of sensor displays great importance when measuring pollution and environmental levels, proving suitable for sampling in any type of environment.[6, 9]

This application is highly sought after when fabricating new sensors; something that is highly sensitive and holds the ability to be used in a large variety of testing environments. However there are other analytical methods beyond FTIR that can be equally, if not more, sensitive. It is important to explore characteristic methods to determine the best combination of sensor, instrumentation, and analyte.

1.4. Raman and SERS Sensing Mechanism

Raman Spectroscopy is an analytical technique that can identify molecules based on distinct vibrations specific to each molecule.[6] A laser source is used to excite the sample which causes both elastic (also known as Rayleigh scattering) and inelastic scattering.[10] Elastic scattering occurs from photons at the same frequency as the excitation source and are therefore negated due to the lack of energy loss or gain.[10] Inelastic scattering occurs from photons of a different frequency than the excitation source which results in a Raman effect.[10]

Aside from Rayleigh scattering, there are also two other possibilities in regards to outcomes of scattering. Stokes Raman scattering occurs when energy is shifted from the incident beam (or laser) to the molecule, causing a lower energy by absorption.[11] Anti-stokes Raman scattering arises when the opposite takes place; energy is shifted from the molecule to the incident photon, causing the molecule to lose energy and resulting in higher energy, **Fig 1.3**.[11]

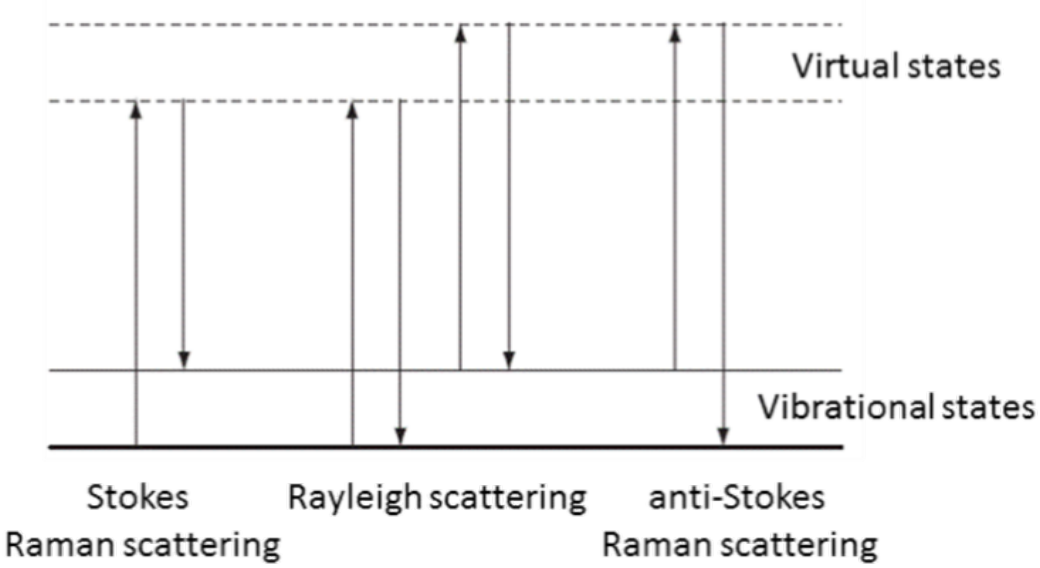

Figure 1.3. Raman scattering variation depiction.[11]

Besides the fact that Raman Spectroscopy is nondestructive, it is also advantageous over using other characterization methods including (FTIR). FTIR is an instrument that can also provide fingerprints of molecules, but not at the same caliber as Raman. For instance, if water is present in a sample when using FTIR, the spectrum will show the water present. When using Raman, water will not interfere with sample vibrations.[6] This alone makes Raman suitable for biological research.[6] Although this research is not biologically based, this is an ideal characterization method in the sensor application discussed further throughout this dissertation due to the instrument's sensitive capabilities and ability to uniquely characterize molecules.

Further into the realm of Raman Spectroscopy yields a newer technique; Surface Enhanced Raman Spectroscopy (SERS). SERS effect is due to the localized surface plasmon interaction between a metal and analyte that is specifically targeted. The exact nature of the mechanism that results in the enhancement effect for SERS is still debated. The two primary theories and their mechanisms differ substantially, and distinguishing them experimentally has not been straightforward. According to some literature, the increased electromagnetic field will activate a dipole-dipole moment causing a significant increase in the Raman measurement.[6, 12] Essentially, the electromagnetic theory claims the SERS is a result of localized surface plasmons where the chemical theory proposes formed charge-transfer complexes.

For a substrate to be SERS active, there are two necessities. First, there must be a metal nanoparticle present that can aid to enhance the signal, **Fig 1.4**.[6] When the metal is present, the electromagnetic field is enhanced solely due to this presence.[6] Secondly, the target molecule of interest needs to be incapacitated on the substrate and close to the surface.[6] Typical metals used for SERS include copper, silver and gold.[13] However, copper is more reactive and less stable than silver or gold leaving these two metals to be more typical in SERS substrates.[13] When incorporating these aspects of SERS, the signal can be enhanced by up to a factor of 10^8.[6] The ability to intensify and increase the signal of a positive detection caused SERS research interest to amplify.

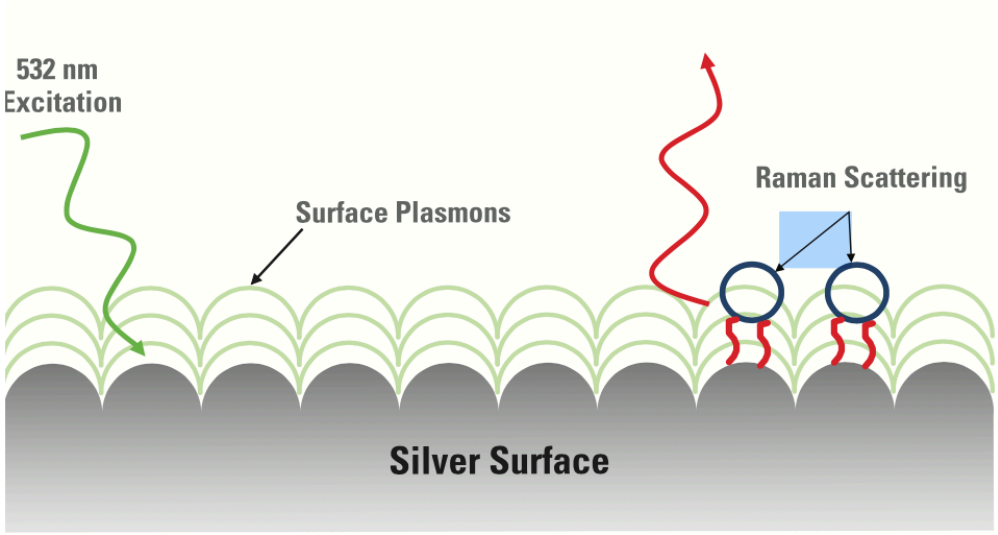

Figure 1.4. Depiction of SERS mechanism.[14]

Although silver, gold and copper are some of the more common SERS based metals, there exist a variety of options. Lithium, palladium, sodium, nickel and cadmium are all possibilities when examining a SERS active substrate.[15] The key aspect when manufacturing a substrate is maintaining a stable and suitable product. If using a substrate composed solely of lithium, oxidation will then occur quickly and leave the sensor compromised and unstable for detection methods.[15] These types of possibilities exist when using lithium, copper, or sodium due to their lack of stability as materials.[15] For copper specifically, if in an open environment, the air would cause the substrate to corrode which would render it useless as a substrate.[15] These limiting factors are not ideal for suitable sensor material.

In older models, roughened metallic surfaces were used for SERS methods. [15, 16, 17, 18] In 1973, Fleischmann *et al* conducted a SERS substrate using roughened silver nanoparticles as their surface.[19] The material was suitable for pyridine which, when adsorbed to the roughed particles, yielded a significant enhancement in spectrum.[19] Since the 1970s, many other discoveries have been made in terms of SERS, such as the type of material's direct effect

including how shape, morphology, uniformity, type of metal and innate stability affect the sensor.

Silver is ideal in other aspects besides stability. According to Faulds *et al*, the scattering to absorption ratio of silver is much larger than that of gold.[15] This is indicative of the larger excitation that occurs with silver. Specifically, at 514 nm excitation, silver is much more excitable than the gold particles are.[15] This is not to say that gold is inefficient in SERS research, rather simply that silver appears to be more ideal by resulting in larger intensity. However, there are surely molecules that gold would be more suitable for in detection apparatus', since the molecule detection depends on material and the material's properties.

1.5. Hot Spots

It has been discussed that SERS active substrates incorporate metal nanoparticles to yield enhanced Raman signals. Within this SERS substrate, there are locations commonly referred to as hot spots. A hot spot is referenced when the optical field of that specific loci is significantly more intense than the remainder of the surrounding substrate.[20] Hot spots occur randomly and are difficult to reproduce.[20] With this in mind, it is not uncommon when measuring analyte via SERS active substrate that there can be higher detection in some areas versus others. Ultimately, some areas may detect a lower concentration than others. However, the reproducibility is the key and although this can occur, if it only occurs seldom then it is due to presence of a hot spot and can be noted but negated in terms of reproducible detection.

Generally, these hot spots occur when a target molecule comes into close contact with the metallic nanoparticle. When in the right location and in close proximity to the metal's electromagnetic field, the signal is largely intensified, **Fig 1.5**. Radziuk *et al* examined the hot

spot formation when controlling interparticle space.[21] In **Fig 1.5 a)**, the particles were coated using polyethylene glycol and using a polymer chain length of 8000 Da.[21] Using this length, the particles were so evenly spaced that the target molecule fit perfectly between and created a hot spot.[21] In **Fig 1.5 b)** the polymer chain length was shortened to 1000 Da, leaving less interparticle space for the target analyte and resulting in normal SERS without hot spots.[21] Even when these hot spots are not present and the substrate is more uniform, SERS still occurs. A hot spot is a focal point where the intensity goes beyond SERS. However, it is typically not reproducible and often discounted when examining limit of detections due to the lack of repeatability for measurements.

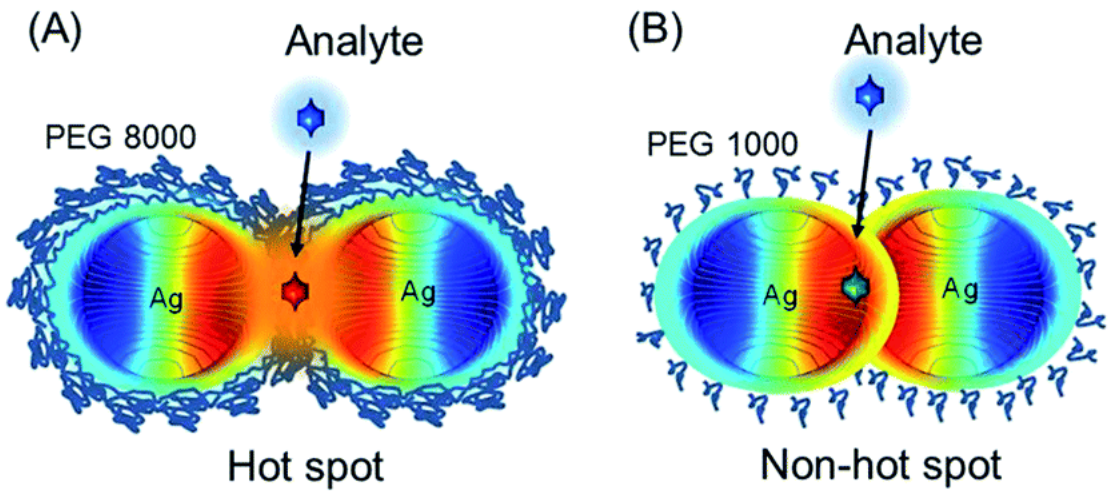

Figure 1.5. SERS hot spot versus non hot spot by controlling polyethylene glycol chain length of a) 8000 Da and b) 1000 Da.[21]

In the conducted polymer hot spot research, the hot spot formations were controlled by the polymer chain length.[21] This is one of many directions that SERS research is pursued in. By manipulating hot spot formation, substrates will be more accountable when it comes to

repeatability of sensing. Controlling hot spots can be useful in methods such as intracellular research, which was the focus of the Radziuk and colleagues project.[21]

1.6. Classifications of SERS Substrates

According to one review, there are three different categories when synthesizing a SERS substrate.[22] These three variations include; colloidal substrates, non-colloidal substrates, and hybrid substrates.[22] Generally nanoparticles of spherical morphology are used, however other morphologies can and have been used in SERS research.

Of the three categories, colloidal substrates, appear as the most popular for research studies. Colloidal solutions are typically easy to fabricate and are on the lower end of cost for production.[22] Some research groups had success when adding their colloidal solutions directly to sample, such as Loren *et al* (2001) and Yan *et al* (2008).[22, 23, 24] Loren and colleagues conducted investigations into detection of doxorubicin in bovine serum by aggregating colloidal solutions.[22, 23] Using the colloidal substrate, they could quantify doxorubicin between 100 and 750 nM concentrations.[22,23] Yan *et al* conducted research of paclitaxel in human serum albumin again via colloidal substrate method.[22, 24]

The direct method was used in several other research findings but in a modified process. Rather than incorporating all solutions at once, a flow system was used to increase reproducibility.[22] In work performed by McLaughin *et al* they used a pump to aggregate the silver nanoparticles first with enzyme (either sodium chloride or poly-L-lysine) which would then enter a pump with sample.[22, 25] Using this method, the SERS substrates were made in a much simpler process as well as creating reproducible results.

Aside from colloidal substrates, there are non-colloidal substrates which are less equally dispersed than colloids and are easier to separate. These non-colloidal solutions have proven efficient in current SERS research. Non-colloidal substrates are ideal due to their ability to be functionalized.[22] This allows for the substrates to work better for detection as well as overall replicating of results with little deviation.[22] Although this substrate sometimes requires more work in terms of fabrication, these advantages can be favorable if attempting detection of a molecule that requires a functionalized sensor for binding

In work performed by Litti *et al*, anti-cancer drug concentrations were detected using a SERS non-colloidal substrate. The substrates were commercially purchased Klarite from Renishaw Diagnostics. Using silicon, etchings were prepared to create a pyramidal formation which was then covered with "gold islands".[26] Then prepared substrates (Klarite) was covered with a "Viton mask" with a small opening to allow for analyte deposition.[26] Target analytes, which included; paclitaxel, sunitinib, SN-38 of irinotecan, and irinotecan, were deposited using a volume of 6 μL.[26] Once the substrate containing analyte had dried, the Viton mask was physically sealed, creating a one-time use SERS substrate for anti-cancer drug detection.[26] With exception to paclitaxel, the three other drugs and metabolite were detectable between ranges of 20-70 ng using the Klarite SERS active substrate.[26] This research proved that non-colloidal substrates have promise as SERS active substrates, and gave highly sought after results.

Aside from Litti *et al*, there are endless possibilities for the non-colloidal category. Research ranges broadly due to the feasibility and variability of functionalization this group possesses. In 2013, Li *et al* functionalized silver nanoparticles with graphene to create a SERS substrate that worked in conjunction with electrophoretic preconcentration (EP-SERS).[27] This sensor was capable of detecting antibiotic samples present in water.[27]

The applicability of non-colloidal SERS substrates are endless. Research has been expanding theorizing the near use of functionalized non-colloidal solutions as is, with sample, directly measuring from patient (ideally).[22] This particular group of substrates cannot be limited due to the vast variability that could be attained. This in particular makes these substrates well admired when researching into SERS active substrates.

However, there is another type of substrate; hybrids. Hybrid strategies involves the trapping of target analyte between two substrates.[22] Ideally, the analyte is sandwiched allowing for the SERS measurement to be observed. In 2014, Yang *et al* performed work using the hybrid technique to detect for folic acid and methotrexate.[28] The hybrid sensor was made of two layers; a bottom layer of silver nanoparticles templated to copper foil, and a top layer of more silver nanoparticles.[28] Behind this mechanism, the plasmonic coupling that takes place between the top and bottom layer of silver accounts for an increase in intensity from the SERS.[28] Realizing the enhancement factor here, the hybrid strategy is more ideal in this case for detection of the two analytes.

1.7. Factors Affecting the Enhancement

There are various ways that SERS substrates can be synthesized or manipulated. This makes material much more versatile and functional in finding target analyte for detection. As previously stated, materials can be functionalized for better recognition or even reproducibility. Beyond that, there are other factors that can be tweaked for favorable substrates.

When the materials are altered, even just by morphology, the plasmonic properties also alter, **Fig 1.6**. As plasmonic characteristics change, ultimately the SERS spectrum will as well. These values are what allow for better specificity of target analyte. According to Lu *et al* in

2012, silver has very strict characteristics in prior research.[29] Previous publications generally resulted with silver nanoparticles in the UV-blue area.[29] However, more research is being performed to alter the plasmonics in today's research and ultimately has changed the perception of SERS based sensors.

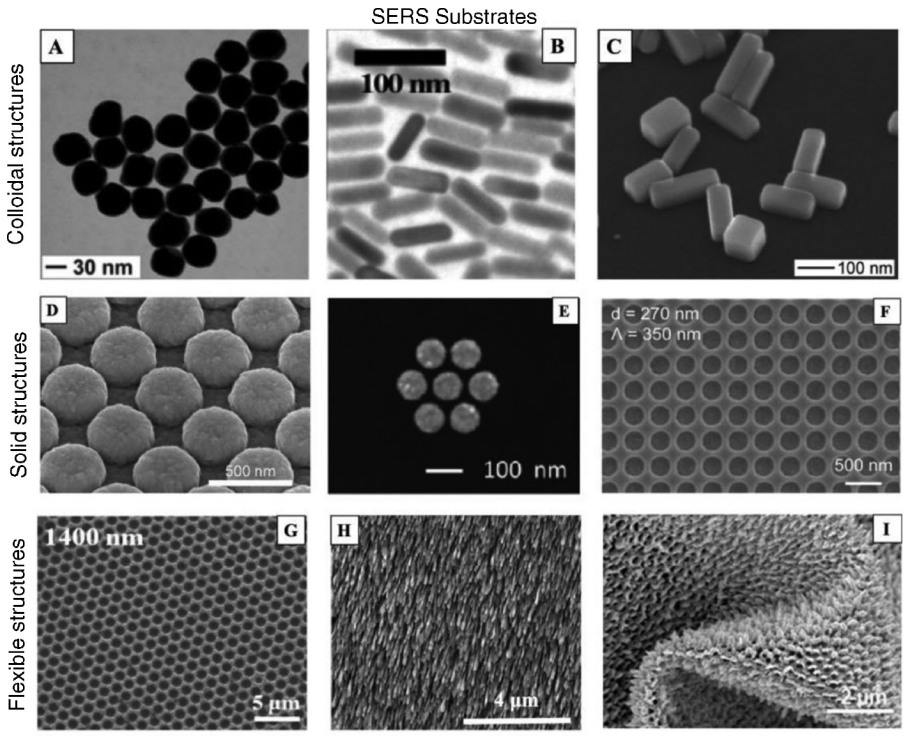

Figure 1.6. SERS substrates examining different metals (silver and gold) with various morphologies that include nanorod, nanospheres, etc obtained from Kahraman *et al* (2017).[30]

Simply by changing the dimension of the silver particles, the wavelength has shifted.[29] Lu and colleagues work was theorized to be successful off of prior work by Zhang in 2010.[31] In Zhang's research, silver nanocubes were synthesized that shifted the wavelengths from primarily blue area to the blue-green region between 420 and 500 nm.[29, 31] Determining how the shape could alter the wavelength, Lu then decided to synthesize nanodecahedrons, which were predicted to shift into the red area.[29]

Even just due to morphology, results from SERS substrates can be altered. Aside from the shape, size of the material can also be a factor. When fabricating a SERS active substrate, it is important to take these considerations into account. Although detection may not necessarily work under one type of morphology or diameter, it does not mean the same material will not work with slightly different characteristics.

To calculate how much more efficient the SERS method is comparative to the Raman method alone, an enhancement factor is typically calculated. This factor allows for the comparison between the two methods and determine quantitatively how much more efficient the SERS method can be over the Raman method. Enhancement factor calculation is given as the equation below;

$$EF = \frac{I_{SERS}}{I_{Raman}} \times \frac{N_{Raman}}{N_{SERS}}$$

where I is representative of the intensity of measured signals, either from Raman or SERS.[32] If identifying the Raman measurement, the experiment was performed without the metal nanostructures and the SERS experiment was performed in the presence of the metal.[32] N is denoted for the number of molecules within the solution, which can be calculated when using known concentrations of solutions.[32]

1.8. Rhodamine 6G (R6G) for SERS Detection

R6G is a chemical compound known to have intense fluorescence. The compound itself contains several ring structures with several branching substituents, **Fig 1.7**. R6G is also insoluble in water and can provide extreme toxicity in aquatic environments which leads to the need of a suitable R6G detection system.[33] However the molecule's innate fluorescence is ideal

when studying mechanisms or methods that involve characterization using fluorescence or fluorescent-based analytics. Generally R6G is regarded as a dye, sometimes used in lipstick.[33] It is also an agent used in coordination with super glue adhesive by the local police department for fingerprint analysis. Since the super glue adhesive is naturally clear and leads to low visibility, the R6G component helps the technician have a better view and observation of the fingerprint when handling case work to identify individuals.

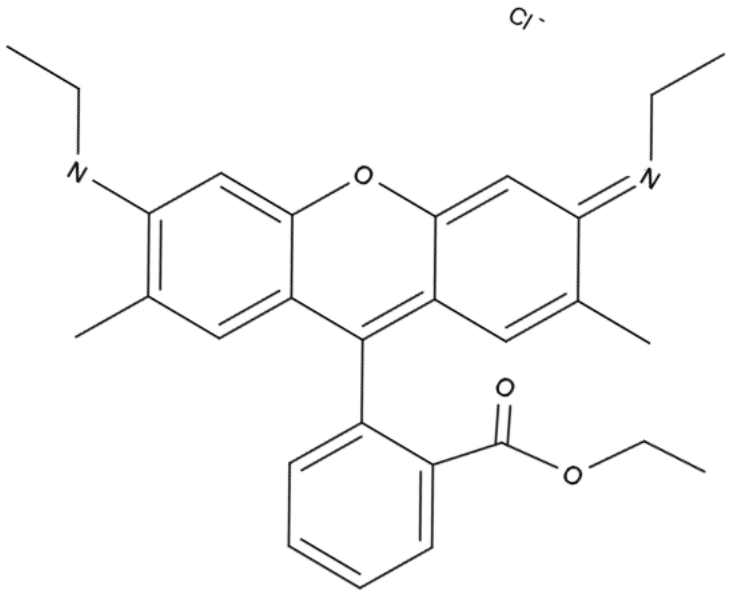

Figure 1.7. Molecular structure of R6G molecule.

SERS methods have been investigated for a plethora of target molecules. Some research focus on biomedical applications, other on environmental, but the possibilities are endless. SERS substrates are a research technique that can be multifunctional; in analytical, forensic, environmental, organic, inorganic, biological – there are existential applications. One molecule of deep interest for SERS application is R6G, because of its ability to help fine tune and create the most ideal sensor with the unique and characteristic peaks. Independently, R6G is incredibly

fluorescent, and will be a bright red-pink when in solution down to 20 mM and beyond. When R6G is paired with a SERS substrate, the molecule's fluorescence becomes quenched.[34] This provides a strong SERS spectrum and a very characteristic one at that.[34] Since R6G has a unique spectrum that is helpful in identifying if a substrate is efficient, the molecule has become a useful tool in SERS research development, **Fig 1.8**.

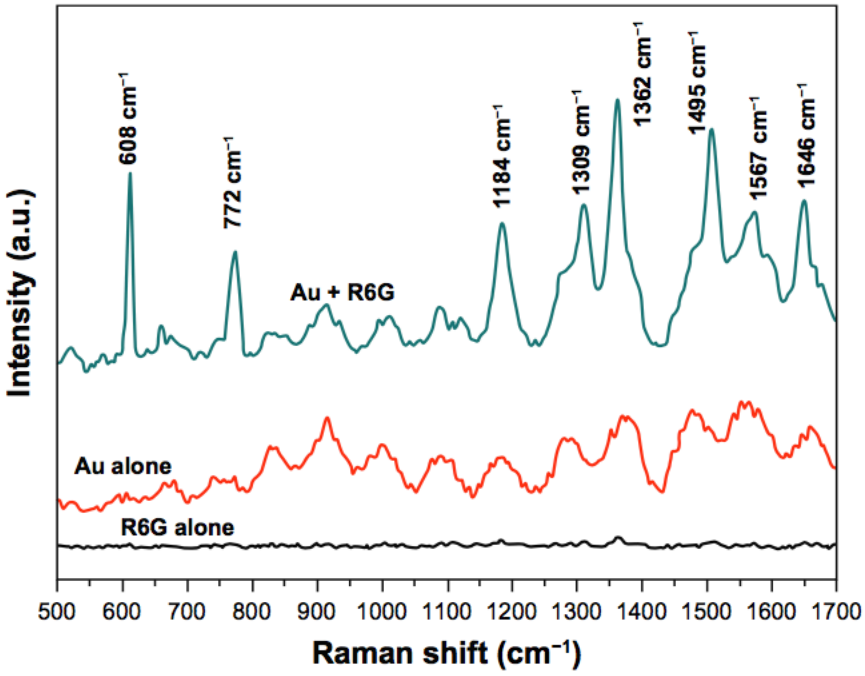

Figure 1.8. Raman spectrum overlap of R6G, gold nanoparticles, and R6G on gold nanoparticles performed by Zhang *et al* in 2011.[35]

From the work performed by Zhang and colleagues, it was apparent that R6G has a uniquely identifiable Raman spectrum.[35] Although this spectrum can only be obtained from SERS; when the R6G is deposited on top of a nanometallic structure the characteristic R6G peaks are visible. Using this spectrum is helpful in determining the efficiency from the metal nanostructures, such as which metal is best in terms of SERS.

R6G is a refining tool in regards to SERS research. Due to the unique spectrum and ability to quench its innate fluorescence, it guides the research project. There have been various research projects performed using R6G as the target analyte. Ultimately the goal remains to make the most sensitive, selective, and competent sensor.

1.9. Fluorescence-Based Sensors

Chemodosimeters are another synthetic method proven useful in detection capabilities. A chemodosimeter, or chemosensor, is a material that is capable of detecting chemical sample.[36] When the targeted molecule is present, the chemical signal can be optical which would generate a positive result. The sensor is comprised of both a fluorophore and a binding site with contact that information can be passed through when referring to a fluorescence-based chemosensor specifically, **Fig 1.9**.[37] Figure shown below depicts the connection between fluorophore and receptor or binding site, where a spacer could be integrated between the two as well so long as the communication can still be passed from fluorophore to receptor.

Figure 1.9. Design of fluorophore and binding site connection.

Although there are many methods that could be used to detect signal, fluorescence is a popular one. This is mainly due to the high sensitivity fluorescence presents. When measuring absorbance, the light source has to be taken into account to properly represent the sample.[38] However with fluorescence this is not the case.[38] A reference beam does not exist and allows for the sample measurements to be taken directly.[38] Lack of a reference beam also helps create a

darker environment which will allow for more subtle measurements to be recorded.[38] Ultimately, fluorescence can measure lower concentrations than absorbance can physically allow for.[38]

When the targeted molecule is present, it will bind with the receptor. [39] In the case of a fluorophore, this could either initiate or quench fluorescence. The result will depend on the type of sensor as well as the type of material being detected and used. Although this dissertation discusses the results using fluorescence, chemosensors could be used to report both optical and electronic changes as well.[39]

An important property of a chemodosimeter is the synthetic advantages. The efficiency of the sensor is high with repeatability and accuracy maintained.[39] Additionally, they are easily fabricated while maintaining low costs.[39] In current research, the chemosensors are primarily focused on anion detection.[39] Several mechanisms exist that are applicable when fabricating a chemosensor. The variety of mechanisms aids in the selectivity and overall efficiency for detection which will yield better results.

Chemosensors have the ability to sense in an assortment of ways. Some of these methods include; photoinduced electron transfer (PET), fluorescence resonance energy transfer (FRET), intramolecular charge transfer (ICT), excited-state intramolecular proton transfer (ESIPT), and through-bond energy transfer (TBET).[39, 40, 41] All of these methods are derived from ratiometric sensing, designed to spike a signal to noise ratio, which will be discussed in further detail in **Chapter 2 Literature Review**. However, **Fig 1.10** displays the concept of both FRET and TBET fluorescence sensors, two mechanisms that are popular for fluorescence probe design.[40] Essentially, the electrons will flow from the receptor to the fluorophore when the target molecule is not present forming a complex that will dismiss all fluorescence. However when the target molecule is present, it will bind the receptor breaking the complex and allowing for the fluorescent signal. The leeway in mechanism design allows for a much more specific

chemosensor and ultimately the detection of target molecules. This is responsible for a large jump in chemosensor research to design sensors that have capability in a wide array of sample testing.

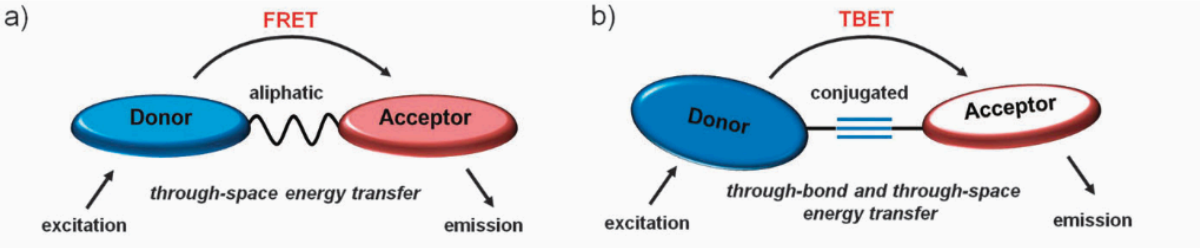

Figure 1.10. Concept of mechanism for a) FRET fluorescence and b) TBET fluorescence.[40]

There has been a significant increase in ionic contamination, which has resulted in a rise of chemosensor research for ionic detection. This led to the need for feasible detection of potentially hazardous ions in samples like water and soil from populated areas. In today's society, there are infamous accounts of metro areas with contaminated water, such as Flint, Michigan. There are also potentials of hazardous waste leaking into natural water sources via soil. Keeping this in mind, many researchers have set out ways to develop the most economic and adequate substrates that could detect these types of ions.

Originally, when chemosensors were first developed, the ideal candidate for detection were metallic particles.[37] It remained this way due to ease of selectivity when creating a sensor that had the capability of binding metallic species from water samples.[37] Now that there are methods that exist that prove sensing capability of ionic and neutral samples, the derivation in chemosensor research has significantly increased.[37]

Sensors have the potential to test among widespread applications, from environmental to in vivo. Specifically testing samples taken directly from human patients would be incredible in both time management and efficiency. This development is not just held to ionic sampling. From

here, specific ions or organics or whatever may be the case, can be sensed to detect pathological illness or disease. Here is where the chemosensors delve into biological and biomedical research.

Sheini *et al.* developed a sensor that could detect carboxylic acids and their derivatives from both water and urine samples .[42] The main difference in this line of research was the signal transducer. This sensor was colorimetric, yielding a visible color difference when target molecule was present. However, this is expanding research upon a well-known and performing chemical application. Although this research field has grown, there is a vast variety of applications these studies are suitable for.

Detection of anionic species and dyes such as R6G are important to ensure safety measures of public water systems, environments, or even cosmetic products. Although there are current marketed products that can achieve detection of these agents, there is a need for a sensor that is; higher in sensitivity, selective, easily fabricated, user-friendly, while also lowering fabrication costs. The research outlined in this dissertation will focus on achieving two functional sensors for anionic species and R6G respectively.

CHAPTER II: LITERATURE REVIEW

2.1. Introduction

The need for testing analytes has risen considerably in recent years. There are more toxic components available to society that were once thought to be safe, and cause communities to back track and check if levels are considered safe by today's standard. For example, lead was once often used, as there were no known side effects or toxic contributions. However, today it is known how detrimental lead ingestion can be, and has caused communities to rip out old lead piping that delivers drinking water in Flint, Michigan, or remove lead-based paint in New York City apartments.

Sensing has always been a functional response chemical processes that holds interest of researchers worldwide. Specifically, fluorescence sensors are of primary focus due to their incredible sensitivity, selectivity, application to in vitro/in vivo studies, ease of use and quick responses.[1, 43] With their ability to be highly selective as well as efficient, fluorescent probes are ideal when it comes to sensing. Fluorescent probes are seen throughout various research as well as on the market. They are capable of detecting a myriad of analytes, and are proving helpful in environmental as well as medical research. Some current research focuses on utilizing fluorescent probes to detect metallic ions, cations, and can be applied to photosynthesis studies.[1, 43, 44, 45]

Fluorescence is generally pursued for detection research due to its enormous sensitivity. It is also favored compared to absorbance due to optical detection capabilities. When measuring absorbance, it is difficult to accurately measure a small amount of light that is absorbed.[38] Absorbance tends to be 1000 fold less sensitive than fluorescence because a more concentrated sample is required for adequate measurements.[46] However with fluorescence, at the same small

measurement, it is easily read due to the sample being measured versus a low light background.[38] These details make fluorescence a recommended sensor when it comes to chemical detection of different arrays.

It remains of utmost importance to create sensors that can detect hazardous substances to keep individuals safe from situations that could otherwise prove fatal. For this reason, research is continually focused on fluorescence detection systems capable of sensing metals and chemical molecules. By enhancing the library of fluorescently detectable reagents, the community is more likely to have an easier time isolating contaminated areas or materials and ultimately producing a much safer environment for human use/consumption. This review will focus on a specific class of chemical compounds suite for environmentally friendly fluorescence-based sensors and the various mechanisms to synthesize such probes.

2.2. Coumarin Compounds in Fluorescence Sensing

A myriad of compounds can serve as a fluorescent sensor, however there are some that are preferred. Coumarin and coumarin-derivative compounds, of the benzopyrone class, are widely used due to their innate fluorescent nature as well as their ability to react to the environment via polarity, pH and viscosity, etc.[47] The cyclic coumarin parent compound is shown in **Fig 2.1**. Coumarin compounds or derivatives exhibits intense fluorescence upon illumination, is easily soluble, and has the ability to permeate cells.[44] These factors make coumarin highly sought for sensing because of their application in various environments. Depending on the functionalization of coumarin, the effect and sensed analyte can vary, making them versatile and easy to manipulate.

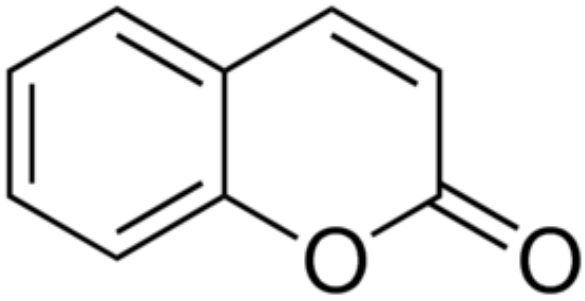

Figure 2.1. Molecular structure of Coumarin.[48]

Coumarin's fluorescent sensing mechanism can be achieved via various methods. These methods include but are not limited to; "internal charge transfer, excited-state intramolecular proton transfer, fluorescence resonance energy transfer, through-bond energy transfer, and monomer-excimer formation."[40] The previously mentioned detection methods are results of what is termed as ratiometric fluorescence sensing. Under the umbrella of ratiometric fluorescence mechanisms, the targeted analyte can alter two or more emission intensities which the probe will then measure and report.[40] This review will focus on the multiple variations of coumarin based fluorescent probes and their applications in current research methods.

2.3. Ratiometric Sensing

The mechanism of a ratiometric fluorescent sensor is identified by a spike in signal to noise ratio.[49] Ratiometric sensing is ideal due to the lack of dependence on the sensor's concentration. Instead, this method relies on the ratio of fluorescence intensity measured at separate wavelengths, either an emission or excitation wavelength.[50] Using ratiometric sensing, it is possible to measure concentration of a present cation, due to absence of sensor dependency.[50] In **Fig 2.2**, emission of the free BAPTA molecule versus emission of BAPTA bound to calcium

can be used in ratiometric measurements to identify the emission shift and concentration.[51] Concentration can be measured by using

$$[Ca^{2+}] = K_d \ (R - R_{min})/(R_{max} - R)\cdot(F^{\lambda 1}{}_{max}/F^{\lambda 1}{}_{min}) \qquad \textbf{Equation 1}^{51}$$

where K_d is dissociation constant, F is fluorescence, R is fluorescence ratio, R_{min} is minimum ratio value, R_{max} is maximum ratio value and $F^{\lambda 1}{}_{max}/F^{\lambda 1}{}_{min}$ is a scaling factor.[51] These factors make a ratiometric fluorescent sensing probe a valuable candidate in sensing research.

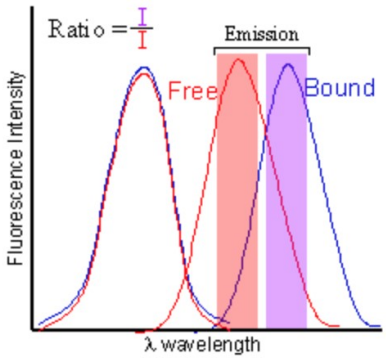

Figure 2.2. Emission spectrum of BAPTA unbound versus bound to calcium for ratiometric measurement.[51]

2.4. Internal Charge Transfer Ratiometric Sensing

Of the several ratiometric methods, internal charge transfer, or ICT, is a branch of sensor probes that use what is referred to as a "push-pull" system.[40] The push-pull system is comprised of an electron-donating and an electron-accepting unit that are responsible for pushing and pulling an electron to and from the excited state.[40] This method in particular is popular for cation specific sensing.[40]

In 2007, Jiang *et al.* synthesized a novel probe that could be used to identify the presence of thiophenols using the intramolecular charge transfer (ICT) pathway.[52] When the human body

is exposed to thiophenols over a period of time, it can prove fatal while also causing rapid breathing, deterioration of the central nervous system, and muscle deficiency.[44] Although novel in theory, the sensor still had obstacles to overcome; feeble intensity measurements, involvement of organic cosolvent, and high pH.[44]

Li *et al*. (2007) recommended a plan to create a thiophenol fluorescent probe using coumarin functionalized with both a N,N-diethyl group to serve as electron donating and a 2,4-dinitrobenzenesulfonic amide group serving as the electron withdrawing group.[44] Utilizing these two functional groups on the same compound created a "push-pull" system that had the capacity to eliminate the fluorophore's, 4-amino-7-nitro-2,1,3-benzoxadiazole, exhibited fluorescence, **Scheme 2.1**.[44]

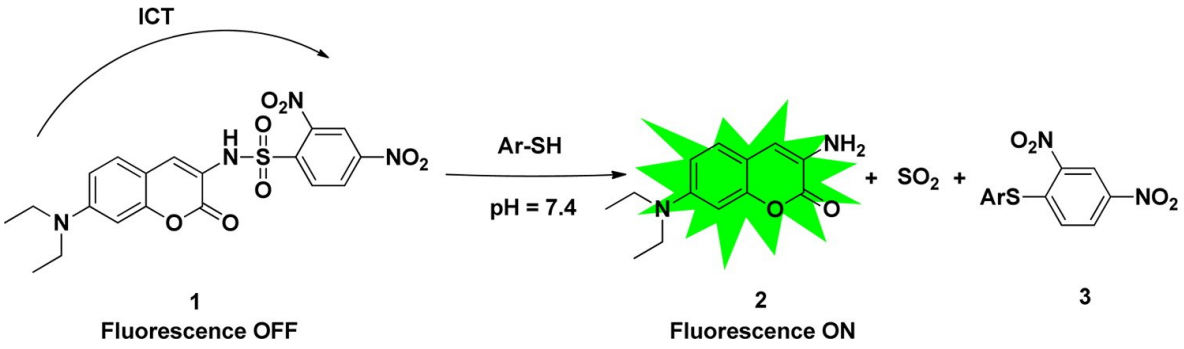

Scheme 2.1. Schematic of Off-On coumarin based fluorescence probe detecting thiophenols.[44]

Two different experiments were conducted to test the feasibility of this sensor; living cell imaging and cytotoxicity, as well as measuring thiophenol in water samples.[44] This allowed to observe how the sensor would work in cell permeation as well as under environmental and practical daily measurements. Ultimately, 20 uM of probe 1 when added to the cells and left to incubate, yielded a bright green fluorescence indicating the probe does indeed permeate the cells.[44] This also gave promise to thiophenol detection in biological samples or living cells, under aqueous conditions at biological pH.[44]

With only Probe 1 introduced to the water samples, no fluorescence was detected. However, when thiophenol was added at concentrations of 0.05, 0.5 and 5 uM, thiophenol was reclaimed at least 92%.[44] These results show promise in accurately detecting thiophenol in water samples with both large recovery percent as well as accurate detection.[44]

To conclude, Probe 1 had a large Stokes shift, high selectivity towards thiophenols, the ability to permeate cells, and prove to have low cytotoxicity.[44] From current research, this Probe 1 seems to have significant abilities in detecting thiophenols in various functioning systems.

The ICT ratiometric fluorescent system is helpful in detection of thiols, but is typically unable to specifically detect glutathione (GSH) from both cysteine (Cys) and homocysteine (Hcy).[53] He *et al*. (2015) decided to develop a bromoketo coumarin sensor that would conduct a turn-on fluorescence.[53] When examining the subtle differences between GSH, Cys, and Hcy, it was found that GSH has a wider gap presented between the amido group and sulfhydryl group.[53] This difference was exploited and it was theorized that the bromide from the probe would be replaced with the sulfhydryl group, and the amido group would interact with the carbonyl group of Cys and Hcy but not of GSH due to the distance.[53] Ultimately this method was successful in GSH specific detection using the ICT concept in biological studies.[53]

ICT based coumarin fluorescent probes can also be utilized in sensing of hydrogen sulfide, an in vivo signaling enzyme that plays a role in multiple diseases including diabetes and liver cirrhosis.[54] To enhance the quenching of the fluorophore, fluorescence resonance energy transfer (FRET) which I will further discuss in section 2.2, was used in addition to ICT to result in dual quenching of 7-notro-1,2,3-benzoxadiazole and (dinitrophenyl)ether respectively, displayed in **Scheme 2.2**.[54] Dual quenching is an advantageous result because it will reduce any background fluorescence while simultaneously increasing the fluorescence when in contact with the targeted analyte.[55] Now that the dual quenching had been applied, this allowed for a more

selective and sensitive coumarin-based fluorescent probe that could create the on-off effect for hydrogen sulfide sensing.[54]

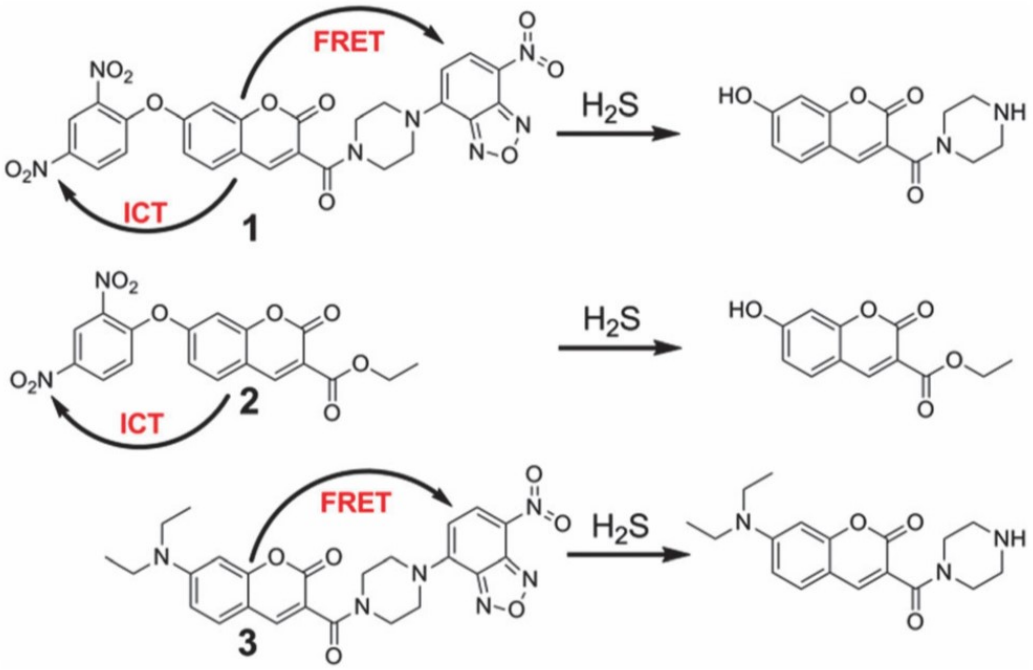

Scheme 2.2. Chemical structures of fluorescent probes **1-3** and their reactions with H_2S.[54]

2.5. Fluorescence Resonance Energy Transfer (FRET) Ratiometric Sensing

Fluorescence resonance energy transfer (FRET) is a method of sensing that can be comparable to or sometimes more effective than ICT. It is common for the intense absorbance peak to overlap with the two emission bands, where with ICT probes it can be impossible to report an accurate ratio of the two peaks. However, with FRET probes, the absorbance intensity will be adjusted but the location of the peak will remain the same.[56] Excitation in FRET will be transferred from the donor to the acceptor compartment, but the result will be dependent on the distance between these two compartments.[57] When the metal ion is introduced, the fluorophores

are adjusted and shift closer to one another closing the distance gap and ultimately creating excitation and eventually fluorescence, **Fig 2.3.**[57]

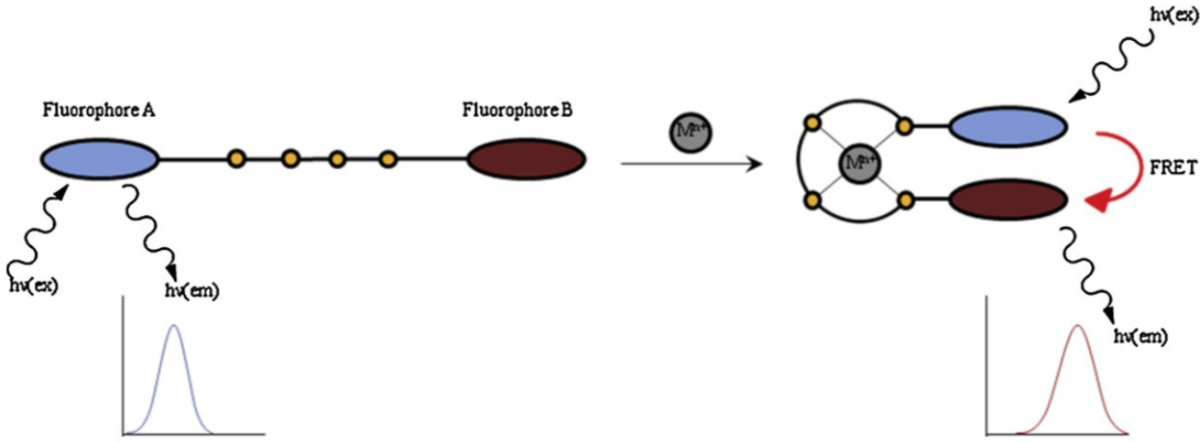

Figure 2.3. FRET mechanism when metal ion is introduced.[57]

A sensor was developed to incorporate the coumarin fluorescent probe linked with M-phenylenediamine and rhodamine as the acceptor.[56] This sensor was used in detection of intracellular Hg^{2+}, which can prove hazardous when in the body. When the Hg^{2+} was in the presence of the coumarin sensor, it caused the ring of rhodamine to break open. The emission band at 478 nm, due to the energy transfer from fluorophore to rhodamine, decreased and a new emission band at 587 nm grew due to the Hg^{2+} addition, indication successful sensing.[56]

FRET sensors are capable of biological sensing and externally controlled by either an "exogenous guest or by an exogenous host molecule" due to new research.[58] In work performed by Hossain *et al*. (2003) at the Tokyo Institute of Technology, a FRET peptide probe was engineered. Ideally, FRET peptide probes are more advantageous compared to single dye labelled probes, discussed in this review, due to the absence of dependability on dye concentration.[58] Unfortunately, a FRET peptide probe proves more difficult in skill to build, due to the peptide's natural helix conformation when it is subjected to aqueous solution

environment.[58] When in helix form, the donor and acceptor compartments become closer in location which will result in a quenching of fluorescence.[58] Cyclodextrin was chosen to host a pyrene and coumarin donor/acceptor group due to the stability it presents when coupled with coumarin.[58]

2.6. Through-Bond Energy Transfer Ratiometric Sensing

Through-bond energy transfer, TBET, is the occurrence where a donor and acceptor are present and conjugated with one another.[40] Although like a FRET based sensors, the appearance of conjugate(d) bonds can help deliver more seamless energy transfer while preventing any spectral overlap from occurring, **Fig 2.4**.[40] This method differs from FRET due to FRET's dependence on the donor emission and the acceptor absorbance band overlapping.[59]

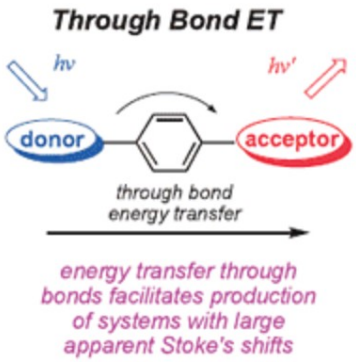

Figure 2.4. Through-bond energy transfer mechanism for fluorescence.[60]

To capitalize on TBET, Lin *et al*. (2010) developed a coumarin based fluorescent sensor that utilize the TBET mechanism by incorporating an enhanced Pseudo-Stokes shift.[59] Pseudo-Stokes shifts are defined as complete energy transfer efficiency with a differential between the acceptor's emission wavelength and donor's absorbance wavelength.[59] Rhodamine was

conjugated with coumarin via a phenyl derivative such as 3-(diethyl-amino)phenol, to develop the TBET based sensor.[59]

A further test was conducted to identify the efficiency of the coumarin-rhodamine sensor. Coumarin did not display its distinctive emission band, however rhodamine's emission band was detected which led to the conclusion that it was a near 100% efficient in terms of energy transfer (~99.9%).[59] These results were positive, but it was important to stack the results against a FRET based sensor. Typically, it is sought to have the energy acceptor, with the donor absent, have a lesser intense fluorescence than the acceptor group when the excitation wavelength of donor absorption is applied.[59] Using this theory, the experiment was applied and it was observed that the coumarin-rhodamine sensors exhibited a much larger fluorescence enhancement factor than the donor, even more so than a FRET based sensor.[59]

From the conducted work, it was proven that a TBET based coumarin-rhodamine sensor could perform just as well, if not better, than a FRET based sensor. Using this sensor, it was also determined to be cell-membrane permeable which could be of use in biological, biomedical, and biochemical research.[59]

2.7. Excited-State Intramolecular Proton Transfer (ESIPT) Ratiometric Sensing

The excited-state intramolecular proton transfer, or ESIPT, is a method of interest due to a significant rise in the Stoke's shift.[41] ESIPT occurs when enol in the excited state is transformed to keto.[41] This transformation takes place due to the relocation of the hydroxyl proton to the electronegative component, which could comprise of a carbonyl oxygen or imine nitrogen, then creating an intramolecular hydrogen bond.[40, 41] The keto then relaxes to ground state, the enol undergoes reverse proton transfer allowing for it to prove ready again.[41]

ESIPT sensing probes can be synthesized for apoptotic, enols, and ionic detection.[40] Wu *et al*. (2007) delved into designing a sensor that was capable of selectively detecting biologically present anions.[61] By incorporating fluoride ions, the hydroxyl proton will become deprotonated resulting in a halt of the ESIPT mechanism which will cause a blue shift in the emission measurement.[61]

Cyclic molecules are useful probes for ESIPT as they contribute a π-conjugated skeletal structure.[62] When chelated with a heteroatom, this provides either a donor/acceptor which greatly emphasizes the compound's polarizability.[62] Utilizing this knowledge, Shreykar and Sekar (2017) synthesized a pyrazole based ESIPT dye that was combined with electron acceptors. The electron acceptors contain different π conjugation distance which will affect the red shift absorption and emission.[62]

2.8. Schiff Base Probes

A Schiff base is derived by either a nitrogen or oxygen atom that will work as a donor.[63] Donor atoms of this nature are able to bind with metallic ions while forming a stable complex, making Schiff bases useful in fluorescence probe work.[63] Majority of the research performed using Schiff base fluorescent probes access the turn on/turn off mechanism.[63] However, when the detected concentration saturates, it causes aggregation-induced quenching, which hinders the ability of the probe.[63] Knowing this, researches have set out to determine if there is a way to overcome the quenching and improve detection.

Aluminum can be found in drinking water due to the natural presence in soil, but it needs to be maintained at low levels as to not cause any severe effects. This led the research group Sheet *et al*. (2017) to explore a possible sensor that could detect the presence of Al^{3+} in an

environmental and physiological setting.[43] Aluminum is the first metal following the transition metals on the periodic table, and Al^{3+} is clarified as a hard-acid which is ideal with a hard-base donor to coordinate.[43] Schiff bases that contain either a nitrogen or oxygen donor coordinate well with Al^{3+} while also resulting in either a lack or absence of fluorescence independently.[43] In previous literature, the exact "turn-on" mechanism of fluorescence due to the "chelation of Schiff base probes by inhibiting the C=N bond" was idealized and led to the interest of using a coumarin derivative as the fluorescent probe for Al^{3+} detection in this work.[43]

The probe design included a Coumarin/Schiff base compound that would be effective in Al^{3+} sensing due the chelation enhanced fluorescence (CHEF) method.[43] Chelation enhanced fluorescence is the mechanism that occurs due to the chelation of one or more donor atoms with the central metal ion.[64] With the new complex formed, the fluorescence intensity is increased by 1000 fold compared to the un-chelated ligand.[64] Along with fluorescence, the stability increases as well once the chelated complex has been formed due to the chelate effect.[64]

To examine the selectivity and efficiency of the HMC probe with various cations, the solutions were tested via UV-Vis and fluorescence spectroscopy. Using a 90% MeOH/HEPES solution (9:1 v/v, pH 7.4), the HMC probe was diluted to concentrations of 50 uM and 10 uM and the metal ions were diluted to concentration of 10 mM in water.[43] For aluminum detection, HMC was immersed with Al^{3+} in a 1:5 ratio via the tetra-n-butyl ammonium salt.[43]

First, the selectivity and sensitivity was implored. Cations tested via HMC probe included; Na^{+}, K^{+}, Mg^{2+}, Ca^{2+}, Mn^{2+}, Co^{2+}, Ni^{2+}, Cu^{2+}, Zn^{2+}, Pb^{2+}, Ag^{2+}, Cd^{2+}, Hg^{2+}, and Al^{3+}.[43] Absorbance of Al^{3+} was observed to increase 425 nm with addition of 0-3.5 equivalents, however decreased with the same additions at 370 nm.[43] These findings indicated that UV-Vis spectroscopy would not be the most ideal method of Al^{3+} detection via HMC probe.

Due to the lack of confidence in detection via absorbance, fluorescence spectroscopy was investigated. Using the same cations, excitation wavelength has established at 410 nm. HMC probe individually contributed weak fluorescence at 520 nm, but was confirmed to be due to the C=N isomerization previously discussed with the amino group of the coumarin derivative.[43] Aluminum contained the ability to coordinate with the Schiff base probes that the other cations did not. When coordinate, the complex became rigid in nature and inhibited the C=N isomerization which led to fluorescence, **Scheme 2.3**. The cations were added at 5 equivalents to the HMC probe at a time, however no fluorescence contribution was observed, with exception of Al^{3+}. Following the 5 equivalent Al^{3+} immersion, intensity increased 7-fold at 520 nm as well as exerting green fluorescence when exposed to UV light (which was not observed when HMC probe alone).[43]

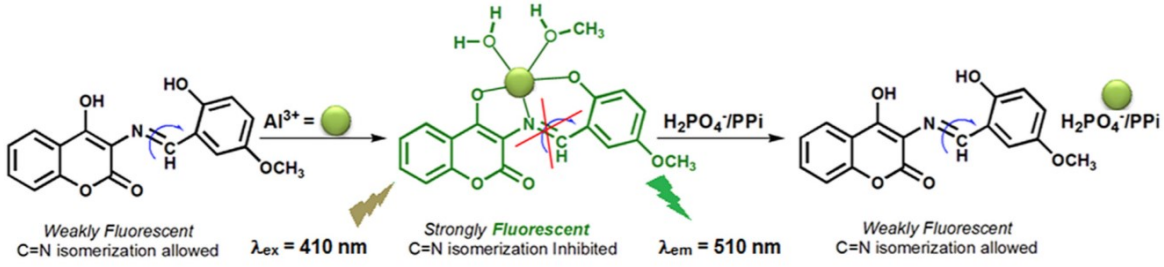

Scheme 2.3. C=N isomerization inhibition due to selective coordination with Al^{3+}.[43]

Though no other cation resulted in detection, Al^{3+} was productive due to the reaction between the cation and HMC probe of deprotonating hydroxyl groups.[43] The C=N isomerization that initially gave HMC slight fluorescence was physically rendered because of the formed complex which ultimately gave rise to a much more significant fluorescent result.[43]

2.9. Chemodosimeters

Chemodosimeters are typically defined as both an off/on sensor and as an irreversible reaction.[57] Irreversible description considers that prior to reaction, chemodosimeters are non-emissive but post reaction is emissive.[57] For example, oxidation could cause a chelated complex to undergo this irreversible reaction where fluorescence is exhibited, **Fig 2.5**.[57]

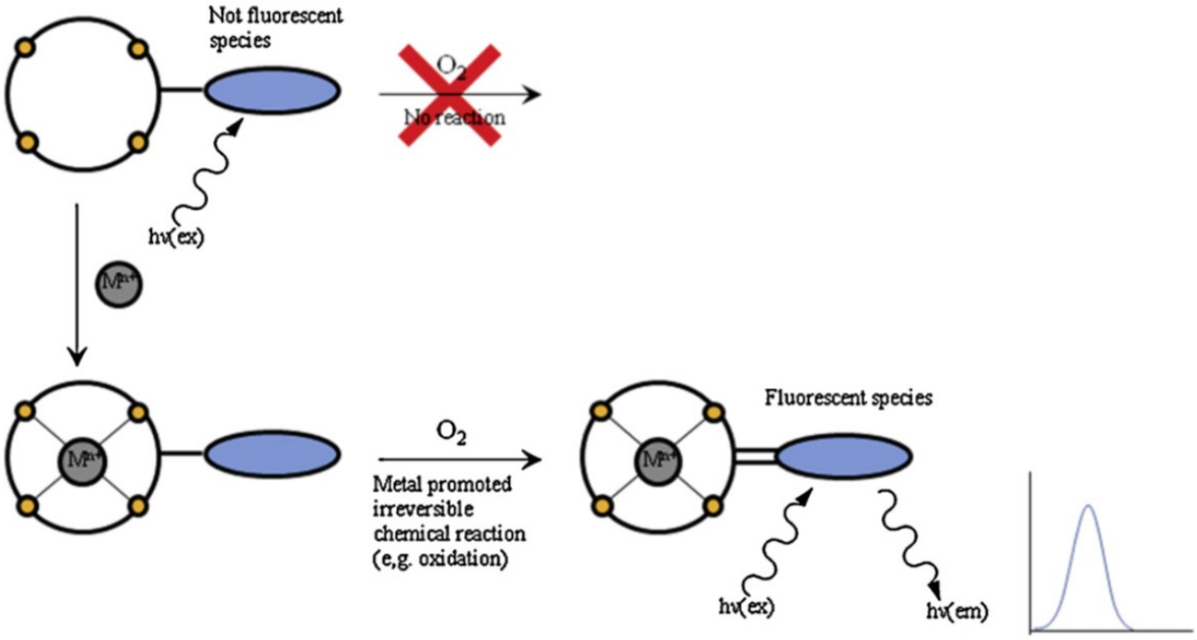

Figure 2.5. Chemodosimeter irreversible oxidation reaction takes place to create fluorescence.[57]

Fluorescent probes also exhibit strength in anionic detection. As previously discussed, fluorescent sensors can be extremely sensitive and prove useful when it comes to detection anions in both biological and environmental studies. To use a probe to identify anions, there are three different methods that can be applied; "binding site-signaling subunit", displacement approach, or "chemodosimeter" approach.[65] Guo *et al*. (2015) decided to advance the chemodosimeter approach, as it is more selective and can detect an independent reaction ultimately causing a variation of fluorescence or colorometry.[66]

In this case, Guo *et al*. (2015) were interested in the detection of phosphate anionic species in a living cell system. More specifically, they were intrigued by the detection of inorganic phosphate (Pi) that is yielded from adenosine triphosphate (ATP) and pyrophosphate (PPi) via hydrolysis, where Pi is typically not the focus of detection.[66] Chemodosimeter approach again seemed to agree with the project's alignment as Pi is fairly hard to detect due to the involvement of other anions that are structurally analogous.[66] To overcome this obstacle, a sensor was designed that would initiate a Pi reaction without the involvement of ATP, AMP, or PPi and would thus only be selective to Pi, designated as Chemodosimeter 1.[66]

Chemodosimeter 1 utilizes an oxalate linked to a coumarin derivative via an ester bond.[66] The idea was that the ester bond would be cleaved due to the interaction of Chemodosimeter 1 and Pi and freeing the coumarin fluorophore creating a fluorescence that could be detected indicating Pi's presence.[66] When Pi was introduced to Chemodosimeter 1, the solution immediately turned to a light blue hue from its previous uncolored solution, indicating some sort of reaction took place.[66] However, all other anions rejected a color change and remained uncolored. When Pi was added, an absorption shift took place from 325 to 387 nm, an absorption shift that was absent from the other anions tested.[66]

Fluorescence spectroscopy was used to further investigate the effect and results of the sensor with these anions with fluorescence occurring at 460 nm. Though Chemodosimeter 1 was very slightly fluorescent on its own, when Pi was introduced a 780-fold escalation of intensity occurred.[66] Of the other anions tested, GMP and UMP both exhibited a very small increase in intensity (less than 6-fold for both), where the remaining anions exhibited no raise in measurement.[66]

From the data, Chemodosimeter 1 was proven to be effective in detecting inorganic Pi through both colorimetric as well as fluorescence. The reaction with Pi that causes the cleaving

of the ester bond and freeing coumarin is responsible for selective fluorescence via the coumarin fluorophore.[66] Beyond the quantification of Pi via UV-vis, it also proved helpful in detection of both exogenous and endogenous Pi in vivo.[66] Specifically, Pi could be detected in cells were "apyrase catalyzed ATP hydrolysis" occurred.[66]

2.10. Summary of Coumarin Compounds as Fluorescence Chemosensors

There are a variety of methods to search and detect for analytes in today's scientifically advanced community. However, majority of these methods are destructive, time consuming, and/or costly. There is a need for development in creating a path for detection that could bypass these obstacles while also providing an efficient and qualitative measurement.

Coumarin has been a part of chemical research as early as the 1800's. However, it's recently developed a large role when it comes to synthesizing fluorescent probes that detect anything from environmental ions to in vivo biologically significant ions. It was known that coumarin already attained a sensitivity to several environmental factors including pH, researchers thought to improve on this and develop future sensors that could provide a sensitivity like that of pH.[47]

The more difficult aspect is deciding which pathway is ultimately the best route to make a coumarin-based fluorescent probe with the highest efficiency, selectivity and sensitivity, and these advantages/disadvantages can be visualized in **Table 2.1**. Some of the ways described in this review include; ICT, ESIPT, TBET, FRET, Schiff base and chemodosimeter probes. Some of these mechanisms proved to be an obstacle for particular sensors; such as in the case of utilizing the rhodamine probe sensor via TBET over FRET.[59]

Table 2.1. Advantages and disadvantages of each type of coumarin sensor.[40, 41, 67, 68]

	TBET	ICT	FRET	ESIPT	Schiff Base	Chemodosimeter
Independent of environmental factors	--	No	Yes	--	--	--
Ratio of two emissions easily readable	Yes	No	Yes	Yes	--	--
Spectral overlap	No	Yes	Yes	No	--	--
Irreversible mechanism	No	No	No	No	No	Yes
Proton Transfer	No	No	No	Yes	No	No
Deprotonation	No	No	No	No	Yes	No
Results based on coordination	No	No	No	No	Yes	No

Whichever method is applied, coumarin-based sensors are expanding daily with a wide range of detectable analytes. Some sensors work well in aqueous solutions, others in vivo work involving biological sensing or a biomedical application. In this review, coumarin-based probes were found capable to detect; Al^{3+}, Pi, F^-, Hg^{2+}, H_2S, GSH and thiophenols.[43, 44, 53, 54, 56, 63, 66] These are only some of the target analytes that coumarin based probes show capability of detecting, while there are still many others that exist.

Coumarins as a chemical class is described as broad due to the copious derivatives available for synthesis. When taking them into account as a chemical sensor, the opportunities only expand. The sensor and result will entirely depend on the compound used, ligating system if present, and the mechanism involved. Three factors such as these described earlier, play a crucial role in developing the sensing system and the overall efficiency, selectivity and sensitivity.

This review discussed TBET, ICT, FRET, ESIPT, Schiff base and chemodosimeter functions between sections **2.1** and **2.10** as a possible route of coumarin based sensors. Some specific examples of research on each were introduced where coumarin was the primary complex used and how a derivative or mechanism could ultimately change the way the sensor worked.

There is still a great deal of research to be performed to overcome obstacles such as quenching or spectral overlap, however this research is heading in the ideal direction. Environmentally friendly, nondestructive, and easily fabricated sensors have and can be made from these materials. These sensors are capable of increased sensitivity and effectivity which can reduce cost, ultimately making environmental testing more feasible and attainable while overall improving community health and awareness.

2.11. Literature Review of Surface Enhanced Raman Spectroscopy Introduction

Raman spectroscopy has been a phenomenally useful analytical tool to identify molecular structure. Sir C. V. Raman first came about the technique in 1928.[69] Using a laser source, a photon causes excitation to the sample which then exhibits inelastic scattering that can be detected and reported to the user. This ultimately gives a unique spectrum to the sample where rotation and vibration modes can be determined.[69]

Though Raman is incredibly useful on its own, a relatively new technique known as Surface Enhanced Raman Spectroscopy (SERS) has become of greater interest. Using the same application of Raman, a metallic nanoparticle is used to better adhere target analyte. The Raman technique is applied to the surface of the nanoparticles (where the analyte is bound or adsorbed to) which causes a significant increase in enhancement compared to without the nanoparticles, **Fig 2.6**. [70]

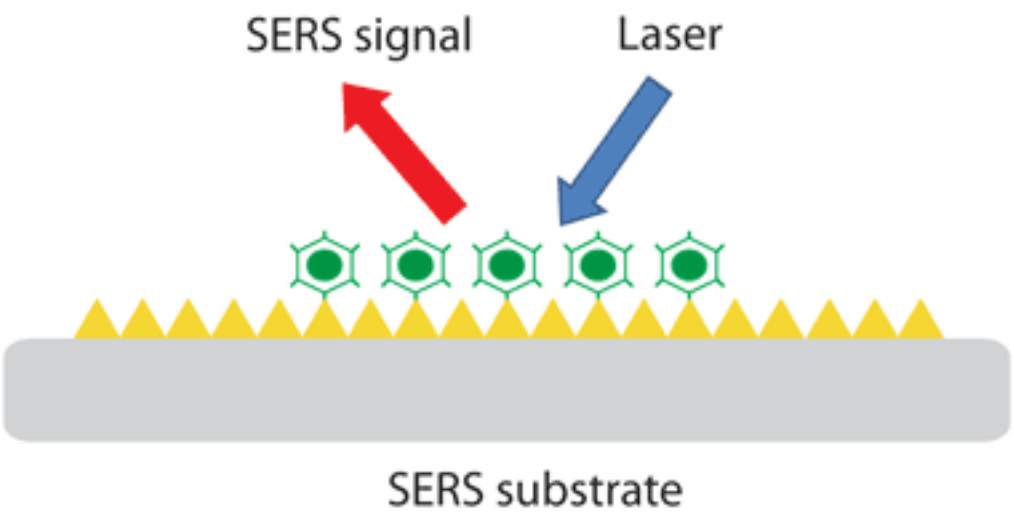

Figure 2.6. SERS signal mechanism.[71]

Due to the presence of metallic nanoparticles, a localized surface plasmon resonance (LSPR) occurs because of metal's conductive electron property.[72, 73] The LSPR is also responsible for creating "hot spots" which are known as areas on a sample with stronger Raman scattering than other locations.[74] Ultimately this means that the electromagnetic field that is created is restricted to the metal nanoparticle surface which can coax dipole moments in molecules that encounter the nanoparticles.[72, 73] This results in an enhanced Raman effect which allows for lower limits of detection.

Three typical metals that are used when investigating SERS include; silver, gold, or copper nanoparticles.[73, 75, 76] Although originally SERS was applied using "roughened" metallic surfaces, the method has now been persuaded in the direction of metallic nanoparticle surfaces.[16, 17, 18] It's now been several decades since this technique was first uncovered, however the method and explanation has not yet been fully identified. Many researchers believe the phenomenon occurs for two different reasons; an electromagnetic mechanism and/or a chemical mechanism.[16]

2.12. Electromagnetic Mechanism

As previously stated, the electromagnetic mechanism is believed to play one of the more functional roles in how and why the SERS method works in such a way. It is believed that the electromagnetic field created and carried by the surface metal (whether roughened metal or metallic nanoparticles) can excite any nearby "localized surface plasmons".[16] This creates a large shift in enhancement of Raman and is one of the primary ways SERS is believed to function, **Fig 2.7**.[16] However, a chemical mechanism is also thought to exist, and divides researchers on what the ultimate mechanism is behind SERS and the existential enhancement factor that is seen.

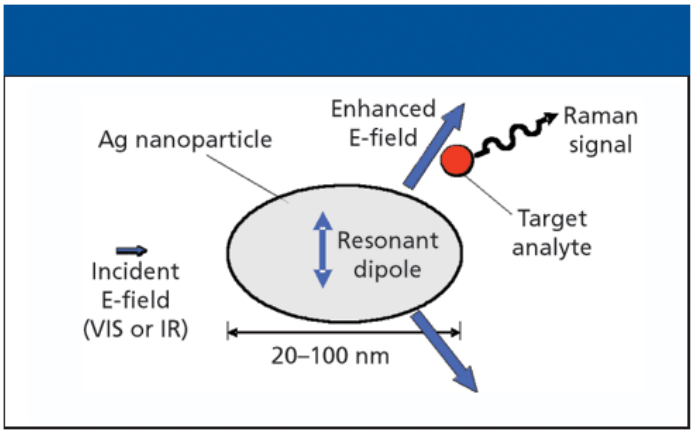

Figure 2.7. Schematic of electric field enhancement due to metallic particles presence creating SERS active material.[77]

2.13. Chemical Mechanism

For SERS mechanism, there are two schools of thought on why and how SERS works the way it does. This doesn't necessarily mean one independently works to create enhancement with Raman or that they don't work hand in hand. However, the chemical mechanism is based solely on the relationship that exists between the surface (metal) and target analyte. Essentially,

coupling occurs when the target analyte bonds with the metallic surface and creates Raman scattering.[78] Some scientists believe that the enhancement of Raman comes from the coupling mechanism rather than the electromagnetic field produced by the metal. If this is true, then the enhancement factor relies solely on the material used as both substrate and analyte and could simply be due to which molecules are chosen for compatibility.

2.14. SERS Research Investigations

Research has been conducted to attempt manipulation into either mechanism, to identify if greater enhancement could be potentially possible. Morton and colleagues investigated the possibility of creating a selective photoswitch which would be able to turn on and off the chemical mechanism of SERS. Through the research, they understand that the electromagnetic factor does play a role in the compatibility and success of the SERS active substrate.[78] However, they also note that resonant charge transfer as well as a non-resonant chemical mechanism can take place between metal and analyte.[78]

A dithienylcyclopentene molecule bonded with two *p*-benzenethiol linkers were chosen as the photoswitch when adsorbed to surface gold.[78] The reasoning in choosing this photoswitch was due to the resulting reversible photocyclization when a specific wavelength is irradiated, **Fig 2.8**.[78]

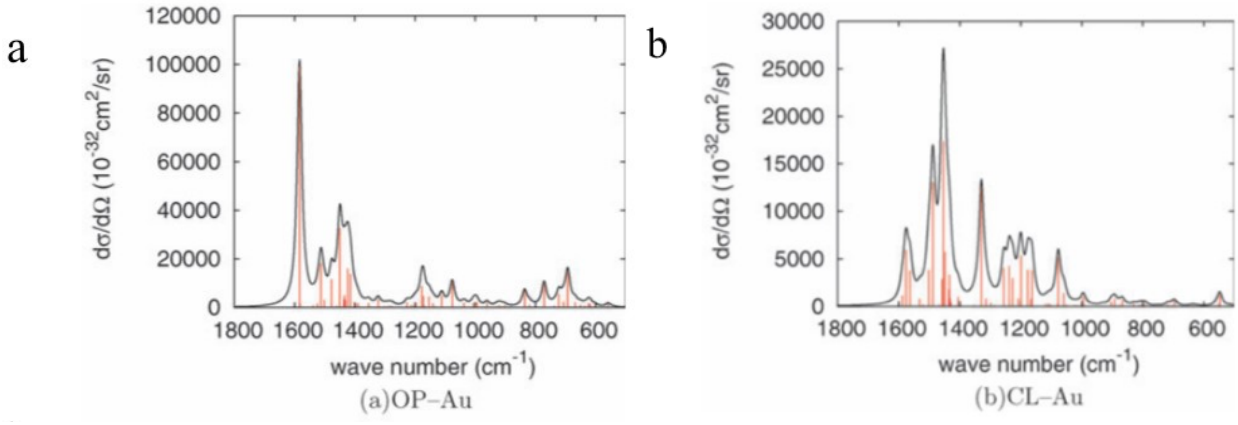

Figure 2.8. A) Raman spectra of openswitch-Au_{19}^{+} and b) closed photoswitch-Au_{19}^{+}. [78]

From the research Morton *et al.* conducted, it is apparent that the chemical mechanism behind SERS can be controlled. When the photoswitch is "open" the enhanced Raman spectrum is visible.[78] However, when the photoswitch is "closed", it results in a noticeable decline in intensity.[78] This indicates that the photoswitch is successful in controlling the chemical mechanism while also maintaining reversibility.[78]

2.15. Summary

As new of a technique as SERS is, it has come to the forefront in terms of investigation due to its feasibility, ease of use, and ability to manipulate enhancement. Raman spectroscopy on its own can be incredibly useful resulting in unique spectrums of molecules. With the addition of metal, the variation of analyte, and further manipulation spectrums can result in a much larger enhancement factor. Ultimately, these characteristics make SERS active substrates of high interest when focusing on molecule detection, concentration, and identification.

CHAPTER III: MATERIALS AND METHODS

3.1. Materials

All reagents and solvents used throughout this dissertation are listed below in **Table 3.1.**

Table 3.1. Reagent tables listing companies purchased from and reagent grade.

Reagent or Solvent	**Chemical Formula/Short Name**	**Purity**	**Purchased From**
2,2[1]-Azobis(2-methylpropionamidine) dihydrochloride	NA	97%	Sigma Aldrich
4-(2-hydroxyethyl)-1-piperazineethanesulfonic acid	HEPES	NA	Bioland Scientific
Dimethyl sulfoxide	C_2H_6SO	≥99%	Sigma Aldrich
Ethanol	C_2H_5OH	200 Proof	Koptec
Ethyl-4-chloroacetate	$ClCH_2CO_2C_2H_5$	98%	ACROS
Hexadecyltrimethylammonium bromide	CTAB	≥99%	Sigma Aldrich
Hydrochloric acid	HCl	12M, 37%	VWR Analytical
Hydroxylamine solution	NH_2OH	50% wt	Sigma Aldrich
Ligroin	NA	NA	Fischer Scientific
Methanol	MeOH	99.8%	VWR Analytical
Methyl chlorooxoacetate	$ClCOCOOCH_3$	96%	Sigma Aldrich
Methylene chloride	CH_2Cl_2	≥99.8%	Sigma Aldrich
Methyl methacrylate	$C_5H_8O_2$	99%	Sigma Aldrich
Nylon Membrane Filters, 13 nm diameter, 0.1 um pore	NA	NA	Tisch Scientific
Ocean Optics Ag SERS Substrate	NA	NA	Ocean Optics
Potassium bromide	KBr	≥99%	Sigma Aldrich

Potassium hydrogen sulfate	$KHSO_4$	97%	Alfa Aesar
Resorcinol	$C_6H_4(OH)_2$	98%	ACROS
Reusable polycarbonate filter holders	NA	NA	Whatman
Rhodamine 6G	R6G	95%	Sigma Aldrich
Silver nitrate	$AgNO_3$	99%	Arthur P. Thomas Company
Sodium acetate	$NaCH_3COO$	99%	Fischer Scientific
Sodium borohydride	$NaBH_4$	≥98%	Sigma Aldrich
Sodium chloride	NaCl	≥99%	Fisher Biotech
Sodium citrate dihydrate	$C_6H_9Na_3O_9$	99-101%	Fischer Scientific
Sodium citrate tribasic dihydrate	$C_6H_5Na_3O_7.2H_2O$	≥99%	Sigma Aldrich
Sodium hydroxide	NaOH	NA	Mallinckrodt
Sodium iodide	NaI	≥99%	Fischer Scientific
Sodium nitrate	$NaNO_3$	≥99%	Spectrum
Sodium nitrite	$NaNO_2$	99.6%	Baker Analyzed
Sodium phosphate dibasic	Na_2HPO_4	≥99%	Fischer Scientific
Sodium phosphate monobasic	NaH_2PO_4	99%	Fischer Scientific
Sodium phosphate tribasic dodecahydrate	Na_3PO_4	99%	Sigma Aldrich
Sodium sulfate anhydrous	$NaSO_4$	≥99%	Fischer Scientific
Sulfuric Acid	H_2SO_4	18M	VWR Analytical
Tetraethyl orthosilicate	TEOS	≥99%	Sigma Aldrich
Triethylamine	$C_6H_{15}N$	≥99%	Fischer Scientific

3.2. Methods

Raman Spectroscopy was performed using a Horiba XploRA Plus. Filters were placed on a microscope slide and excited using a 785 nm laser. A filter of 10% was applied (15 mW) and

acquisition was set to 1 s for 5 accumulations. The spectral slit and hole width was set to 100 μm and 500 μm, respectively. Data was recorded using a spectral range of 100 to 1700 cm^{-1}.

Atomic Force Microscopy (AFM) was performed using a Bruker Innova SPM AFM in tapping mode. Samples were used as is on thin films without further preparation.

Tunneling electron microscopy (TEM) was performed at University of Delaware's Delaware Biotechnology Institute. Imaging was achieved on a Zeiss LIBRA 120 Transmission Electron Microscope. The system utilized a Köehler illumination set up that used an accelerating voltage of 80 to 120 kV.

Some Scanning Electron Microscopy (SEM) imaging was performed using the FEI Quanta 250 FEG Scanning Electron Microscope. Samples were made more conductive using a conductive carbon tape before images were taken. Images were obtained between the 6000X and 130000X magnification. SEM imaging was also obtained from University of Delaware's Delaware Biotechnology Institute using a Hitachi S4700 Scanning Electron Microscope system.

Nuclear Magnetic Resonance (NMR) was provided from a JOEL ECX-400 MHz NMR. The NMR instrument was used for both ^{1}H and ^{13}C NMR in a variety of solvents, mainly focusing on DMSO. NMR properties were determined based on samples.

To examine infrared spectrums, Fourier Transform Infrared Spectroscopy (FTIR) was used via a Shimadzu IRPrestige-21. Pellets were made using potassium bromide in a 50:1 ratio with sample. The powder was subjected to a hydraulic press to form a pellet which was then used as the sample and further underwent purged conditions via argon. Both transmittance and absorbance methods were examined.

Fluorescence was detected via a Shimadzu RF5300pc using a 1cm quartz cell. The excitation and emission slit widths were both set to 1.5 nm. Excitation wavelength was set to 385 nm and an emission range of 400 to 600 nm was used. These characteristics may vary from

sample to sample and were manipulated based on samples taken to provide the best and most accurate results.

UV-Vis, or Ultraviolet-Visible Absorption Spectroscopy, was often used to determine the suitability of the silver prior to substrate use. This was performed on a Shimadzu UV-3600 Plus via a quartz cuvette in solution form.

Inductively Coupled Plasma Mass Spectrometry (ICP-MS) was used in a latter part of the dissertation. The model used was an Agilent ICP-MS 7900. Matrix used was water, as the element examined was insoluble under typical acidic conditions. Calibration standards were prepared using a sodium phosphate dibasic solution in the ppb range. Internal standards and tuning solutions were purchased from Agilent.

3.3. Silver Nanostars

Silver nanostars were synthesized by adding 10 mL of hydroxylamine solution with 10 mL of NaOH in a 100 mL RB and left to stir for 4 minutes at RT using the method developed by Garcia-Leis *et al.* originally and reported again by Oliveira *et al*.[79, 80] In a separatory funnel, 75 mL of H_2O was added with 6 mL of a 5 mg/mL $AgNO_3$ and added to the hydroxylamine solution all at once and stirred for 5 minutes. At this point, 2 mL of a 1.5% citrate ion was added and solution was stirred for 14 minutes. The product was transferred into dialysis tubing where it was submerged in 1.8 L of H_2O with stir for 15 minutes. Product was then transferred to 50 mL falcon tubes were it was stored at 4 ^oC in the dark. Absorbance peak for product was recorded at 373 nm.

3.4. MSN Stellate Material

MSN material was synthesized by adding 480 mL of H_2O and 7 mL of 2M NaOH solution in a 1L RB with vigorous stir, according to previously reported methods.[81, 82] As the solution temperature was raised to 80 ºC, 2.0 g CTAB was added to solution to stir. Once at 80 ºC, 10 mL of TEOS was added and left to react for two hours. The material was placed through a vacuum filtration system and washed with excess H_2O. A final rinse was performed with MeOH. The material was left to vacuum filter to dryness for one hour before being transferred to vacuum oven overnight. Once dried, 1.50 g of material was collected and subjected to an acid wash of 9 mL HCl in 160 mL of MeOH and refluxed for 20-24 hours. The material was again washed thoroughly and dried overnight prior to use.

3.5. MSN-AgNS SERS Substrate

To prepare the substrates, both MSN and AgNS are required to be incubated together. A solution is produced of a 1:1:0.075 ratio of 5 mM NaCl:AgNS:MSN of which the MSN is prepared as 8.3 mg of acid washed MSN per 2 mL of water. The MSN is probe sonicated to prevent aggregation. The solution then underwent gentle rocking for 10 minutes prior to use. A membrane filter was then pre-wet in a 1:1 H_2O:EtOH solution and placed subsequently into a filter holder. Using a syringe, 0.5 mL of 1:1:0.075 solution is drawn and the solution is pushed dropwise through the filter. Filter is immediately removed and left to dry where 5 mL of concentrated R6G solution is then pushed through the filter dropwise. Measurements were obtained once the R6G deposition was complete.

3.6. Silver Nanoparticles (Spheres)

This method was adapted from Gao *et al*. which was further modified from Yu *et al.* of the Lee-Miesel Method.[83, 84, 85] To 100 mL of ultrapure H_2O, 18.0 mg of silver nitrate was added and vortexed for five seconds. A separate solution was made containing 1 mL of H_2O and 27.0 mg of sodium citrate dihydrate and vortexed for five seconds. The silver nitrate solution was then transferred to a conical flask where it was vigorously stirred and heated to 350 ^oC. Once the solution began boiling, the sodium citrate dihydrate solution was added immediately and the solution was left for approximately 20-22 minutes until the solution had turned a dark greenish brown. Following the color change, the solution was removed from heat and left to stir until RT with a constant color observed. The final solution was diluted to 100 mL with ultrapure H_2O and stored in at 4 ^oC in the dark.[83, 84, 85]

3.7. PMMA Synthesis

A 25 mL RB was used for 16 mL H_2O and 3 mL methyl methacrylate under inert gas. The solution was under vigorous stir and subjected to a 70 ^oC water bath. Approximately 0.0172 g of 2,2[1]-azobis(2-methylpropionamidine) dihydrochloride was then added and left to stir for forty minutes. This solution, referred to as unpure, was used to create inverse opal films. A 28.6 wt% TEOS solution was made using 0.1 M HCl, TEOS and EtOH. The solution was left to stir for one hour prior to inverse opal solution use. In a 50 mL beaker, 110 µL of unpure solution was added to 20 mL of H_2O and 150 µL of the 28.6 wt% TEOS solution. A clean glass substrate (microscope slide) was vertically suspended into the solution, which was placed in a box furnace at 65 ^oC for 24-36 hours. The slide developed an opalescent material thin film with little

cracking. The PMMA synthesis was adapted from Schroden *et al.* and the inverse opal synthesis was adapted from Lisensky *et al*.[86, 87]

The inverse opal substrates were then used for further silver SERS development. AgNPs and AgNSs were attempted by spray coat, spin coat, dip coat, and direct deposition. On these silver based inverse opal films, R6G was deposited on the surface area. Results were carried out using Raman Spectroscopy.

3.8. Chemodosimeter PSP 281 Synthesis, Adapted from Guo *et al.* [66]

A solution of triethylamine (0.2 mL) in 15 mL of anhydrous DCM was added to 176 mg of 7-hydroxy-4-methylcoumarin at 0 ^{o}C. Another solution containing 0.2 mL of methyl chlorooxoacetate and 5 mL of CH_2Cl_2 was added to the original solution dropwise with constant stir for a time frame of 30 minutes. Solution was then brought to room temperature and continued to stir overnight where it was then further diluted with 30 mL of CH_2Cl_2, washed with brine twice (30 mL) and dried with anhydrous Na_2SO_4.[66]

3.9. Chemodosimeter Synthesis – PSP 286, 287

The first step in synthesizing and functionalizing the chemodosimeter material required synthesizing 4-chloromethyl-7-hydroxycoumarin via methods adapted from Zagotto *et al*.[88] This involved 10.0 g of 1,3-dihydroxybenzene in 100 mL of concentrated sulfuric acid at 0 ^{o}C. A 10 mL aliquot of ethyl 4-chloroacetatoacetate was added and the solution was left to stir for ten hours at RT. The solution was added to 500 mL of water and left as is overnight. A precipitate product was collected via vacuum filtration, washed with excess H_2O, and crystalized out using a 4:1 ethanol-ligroin solution, yielding PSP 286 or 4-chloromethyl-7-hydroxycoumarin.[88]

The next step required 543 mg of PSP 286 with 30 mL DI H_2O refluxing overnight.[89] After the solution was cooled, crystallization occurred to produce 7-hydroxy-4-(hydroxymethyl)-2H-chromen-2-one, referred to as PSP 287. This is the main product worked with in the Pi sensor project.

3.10. Fluorescence Chemodosimeter Procedure

Originally, the method of chemodosimeter solution was adapted from Guo *et al*.[66] The procedure used a 9:1 V/V HEPES-DMSO solution (0.02 M). This solution contained a $4.68x10^{-3}$ M chemodosimeter with a $2x10^{-3}$ M ion for detection, both in final concentration. The DMSO was unsuccessful from this adaptation. Due to this logic, DMSO was subtracted from the experimental procedure and all reagents were prepared directly into a 0.02 M HEPES buffer solution.

A solution was first prepared of chemodosimeter in 0.02 M HEPES buffer of a concentration which would give the final concentration of $4.68x10^{-3}$ M when added to the anion in a 9:1 volume. From the chemodosimeter, 10 mg was added to 10 mL 0.02 M HEPES buffer and dissolved. Of this solution, 2.7 mL was taken and added with 300 μL of a $2x10^{-3}$ M stock, or less depending on concentration being sought. A 3 mL sample was prepared into a quartz cuvette after allowing 30 minutes of proper dispersion at RT. Anionic stocks ($2x10^{-2}$ M) were prepared fresh daily and HEPES buffer solution was stored at 4 ^{o}C.

Background measurements were obtained by using solely chemodosimeter without anion present. Essential samples were made using 2.7 mL of a 10 mg/10 mL chemodsoimeter with 300 uL of HEPES buffer in place of an anionic species. Samples were subjected to

spectrofluorometry using the conditions as stated above. This allowed for the examination of what, if any, fluorescence was provided solely by the chemodosimeter or solution.

When concentration quantification studies were performed, all samples made were prepared at the same time. They were left to sit for 30 minutes and all prepared in the same manner. Observations were done based on concentration of chemodosimeter, anion, type of anion, time left, and solvents used.

CHAPTER IV: RESULTS OF THE COUMARIN-BASED PHOSPHATE SENSOR

4.1. Methods Adapted from Guo *et al.*

Coumarin is a chemical known to work for fluorescence sensing. However, there are endless coumarin derivatives that could also prove useful. This research will delve into some different variations of coumarin that could potentially have use in chemical sensors. Using prior research along with new techniques, this dissertation will investigate chemodosimeters that show potential in the detection of phosphate as well as other ions.

Originally, it was the hope to start this project in reference to Guo *et al.* (2015) work. Research results from this group showed a sensor that was specific for inorganic phosphate (Pi), **Scheme 4.1**. Mostly this research was pursued to identify endogenous phosphate. However, it was thought that a different variant of coumarin may be able to yield similar results.

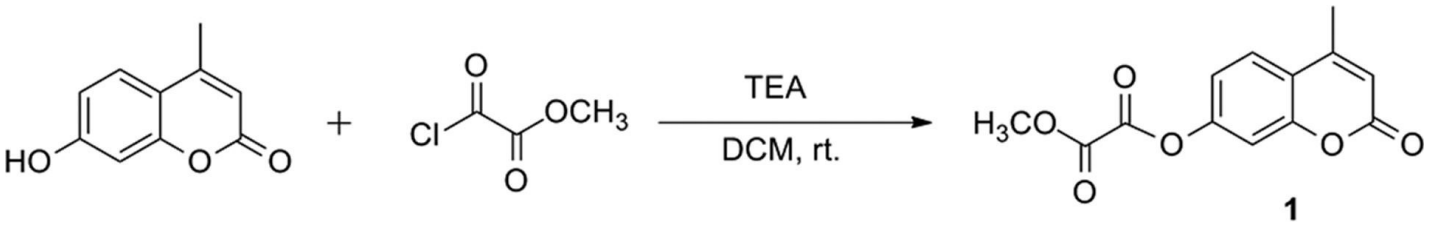

Schematic 4.1. Synthetic route of Guo *et al.* chemodosimeter used to detect phosphate.[66]

Though successful, there was no mentionable selectivity for inorganic phosphate specifically, suggesting all phosphate in whatever form could be detected this way with no distinction. Though their mechanisms indication hydrogen phosphate species there is no mention of other tested species or variability. In their investigation of the sensor, the solution used contained a 9:1 (V/V) DMSO:HEPES (0.02 M, pH 7.4). Since this method seemed to work for the sensing of phosphate, it was decided to try the same methodology using a variation of the

chemodosimeter. The hope was that the same mechanism could be applied using a variation of the chemodosimeter which could then be further modified to enhance the selectivity.

At first, to better understand the mechanism, this method was pursued using a coumarin based derivative with a small range of phosphate ion. With exception to the exact chemodosimeter molecule, all methods would remain the same. Guo *et al*. had success using the 9:1 DMSO/HEPES (V/V) method, but this method was only investigated under the chemodosimeter molecule with the oxalate moiety.[66] It was questioned if this method would have similar success when the coumarin compound was functionalized variably.

4.2. Chemodosimeter PSP 286 Synthesis

The precursor material was synthesized using a method created by Guo *et al.* in 2015 but manipulated to form a derivative. [66] Using coumarin, a couple of derivatives were synthesized to identify which functionalization would give the best result in detection of phosphate ion present in miscellaneous samples. However, this research focused on creating a functionalized coumarin compound that would have to capability to selectively detect differing phosphate species. The ultimate goal was to create a more specific and selective sensor than current methods.

This led to a series of synthetic steps that would yield the specific phosphate sensor used in the remaining portions of the experiments. From this, the first molecule synthesized was 4-chloromethyl-7-hydroxycoumarin or PSP 286, **Fig 4.1**.[88] To ensure that the correct molecule was synthesized, both FTIR and ^{1}H NMR were observed, **Fig 4.2** and **Fig 4.3** respectively. The FTIR displayed a peak correlating to the alcohol functional group around 3300 cm^{-1} and a peak indicative of chlorine between the 600-800 cm^{-1} mark.[90] ^{1}H NMR (400 MHz, DMSO-d6) δ: 4.95 (s, 2H); 6.42 (s, 1H); 6.75 (d, 1H); 6.82-6.85 (dd, 1H); 7.66-7.68 (d, 1H); 10.67 (s, 1H). It is

important to note that the DMSO peak at 2.50 ppm shows some impurity along with a water peak at 3.32 ppm due to residual water in the NMR solvent.[91]

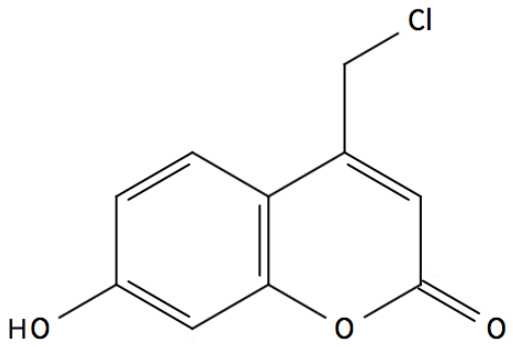

Figure 4.1. Molecular structure of 4-chloromethyl-7-hydroxycoumarin, PSP 286.

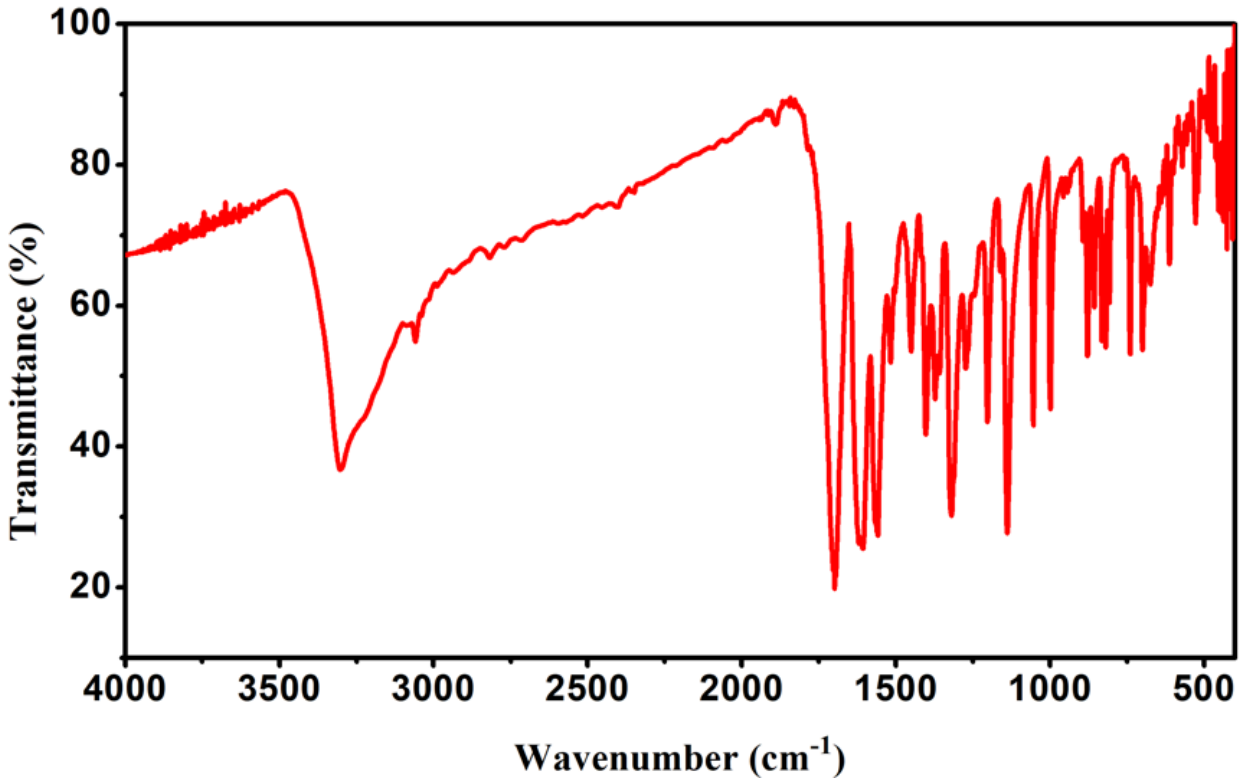

Figure 4.2. FTIR spectrum of PSP 286.

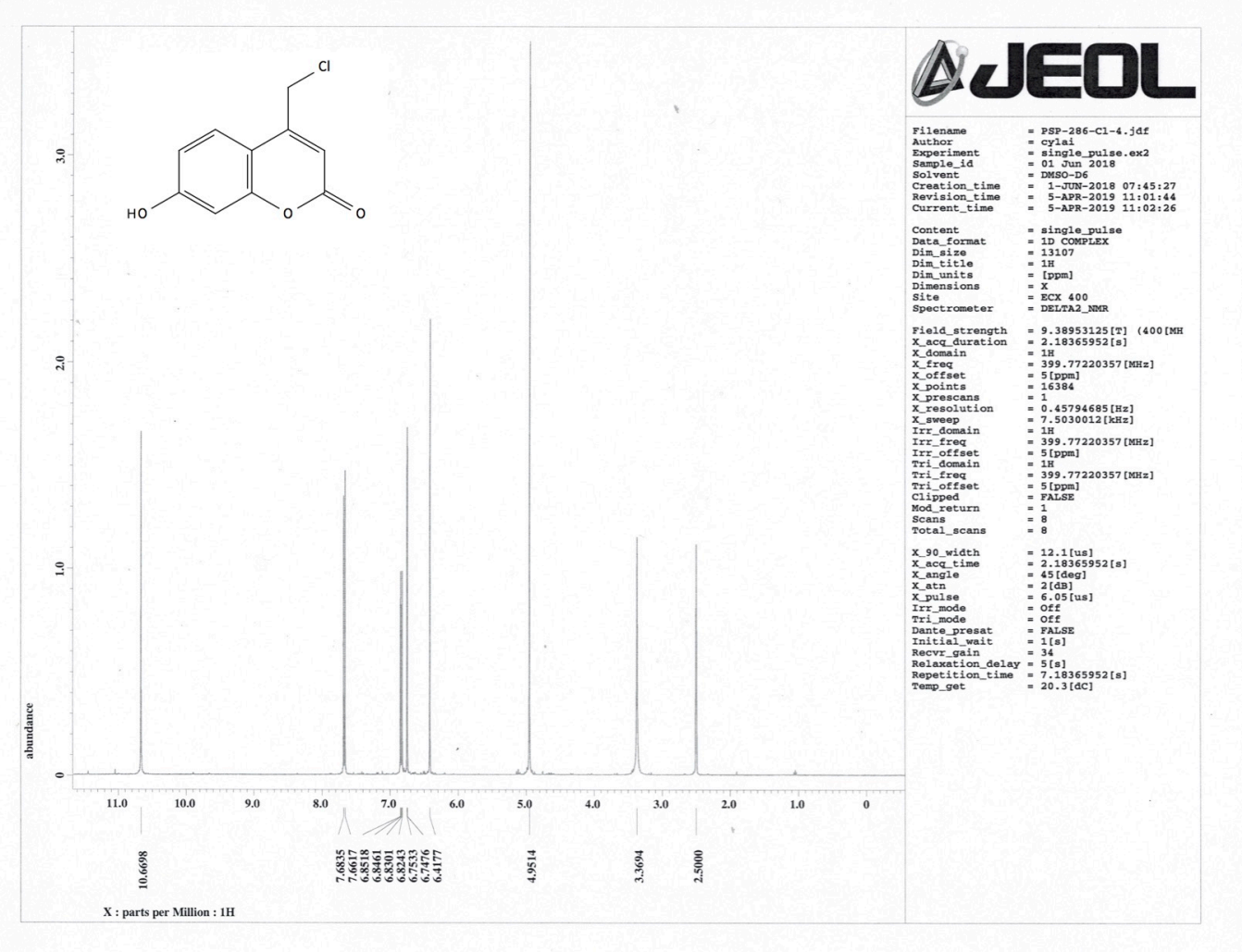

Figure 4.3. ^{1}H NMR spectrum of PSP 286.

4.3. Chemodosimeter PSP 287 Synthesis

Now that the precursor had been synthesized, the first functionalization step could begin. The chlorine at the third position would be replaced with a hydroxyl group, **Scheme 4.2**. This synthesis was performed by refluxing 4-chloromethyl-7-hydroxycoumarin with water.[89] Excess water was removed to allow for recrystallization to occur. Once collected this would be the secondary product known as 7-hydroxy-4-(hydroxymethyl)-2H-chromen-2-one or PSP 287.

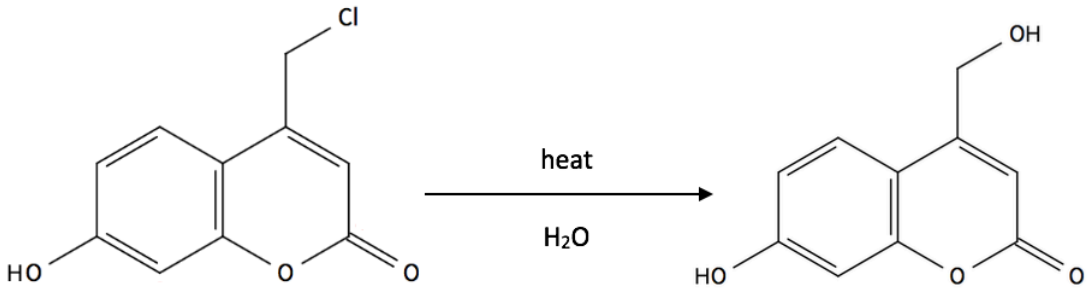

Schematic 4.2. Synthesis of 7-hydroxy-4-(hydroxymethyl)-2H-chromen-2-one, PSP 287, from 4-chloromethyl-7-hydroxycoumarin, PSP 286.

The second hydroxylation would allow for an addition of hydroxy in hopes of forming a more ideal sensor. Identification of this molecule was pursued under various characterization methods. Once the molecule had been synthesized and purified, the chemodosimeter was in good standing to pursue phosphate selectivity testing.

4.4. Characterization of PSP 287

Since the compound was in crystalized form, it was ideal for FTIR sampling. The crystals were ground down to a powder substance and examined under FTIR via pellet formation, **Fig 4.4**. The broad peak displayed at 3446 cm^{-1} is distinctive of the two hydroxyl functional groups present in the molecule, where alcohols are known to demonstrate broad peaks from 3200-3600.[90] As for the peak at 1631 cm^{-1}, this is characteristic of alkenes. The slightly broad peak at 1089 cm^{-1} is most likely do to the ester C-O stretching.[90] There are two very small peaks near 2800 and 2900 cm^{-1} indicative of sp^3 hybridized carbons.[90] The peak around 1090 cm^{-1} is the C-O stretch of the alcohol functional group, which usually presents a strong peak between 1050 and 1150 cm^{-1}.[90] From the FTIR, the functional groups could be observed but the molecule could not

be positively confirmed solely from this.

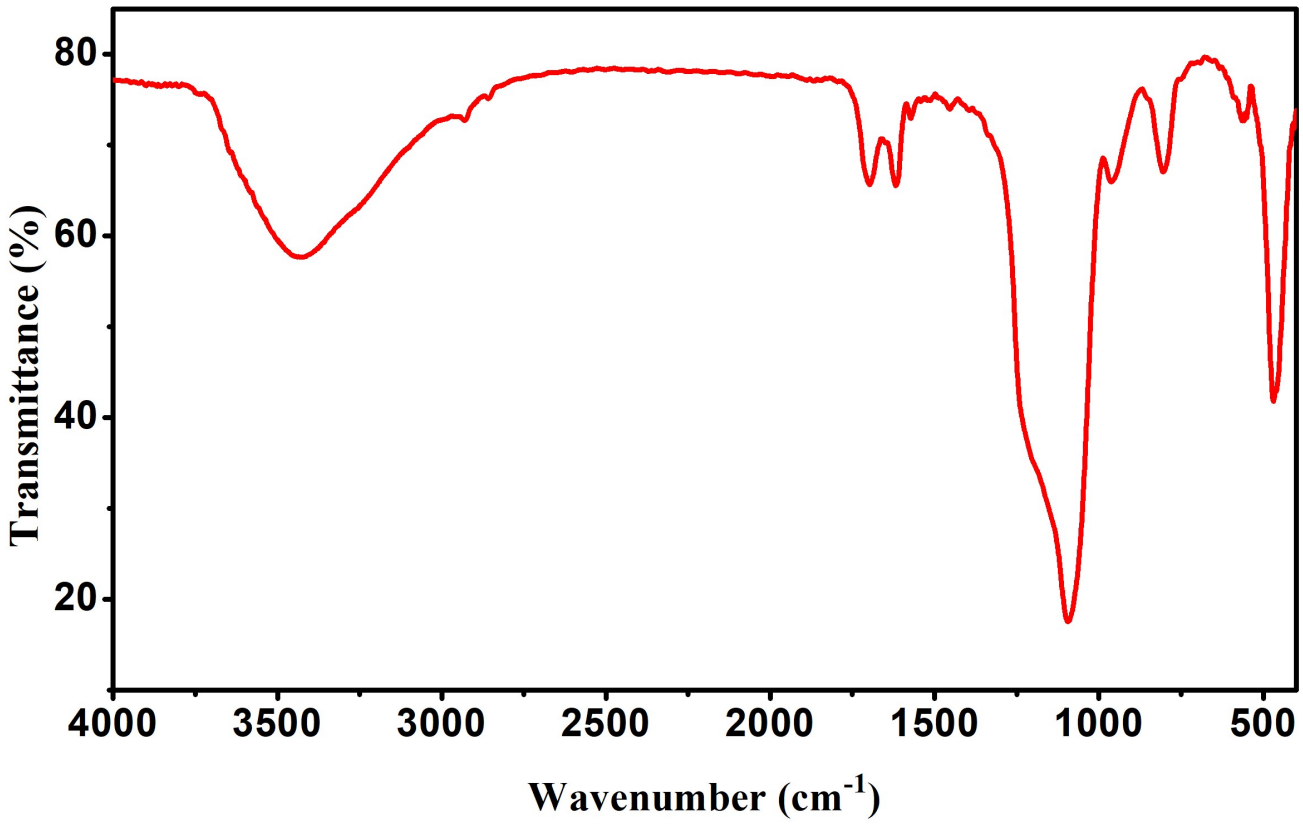

Figure 4.4. FTIR spectrum showing transmittance of PSP 287 precursor material.

To further analyze and characterize the precursor material, ^{1}H NMR was performed. **Fig 4.5**. displays the molecule labeled as to be shown in NMR spectrum and the coordinated NMR spectrum. From the NMR spectrum, chemical shifts were derived; ^{1}H NMR (400 MHz, DMSO-d6) δ: 4.70 (s, 2H), 5.59 (s, 1H), 6.23 (s, 1H), 6.72 (d, 1H), 6.75-6.78 (dd, 1H), 7.50-7.52 (d, 1H), 10.55 (s, 1H). It was concluded that the peak at 3.34 ppm was due to residual water present in the DMSO which was used as the solvent. Using coumarin data, as well as chemical shift knowledge, all protons were properly assigned and accounted for concluding the identification of 7-hydroxy-4-(hydroxymethyl)-2H-chromen-2-one, PSP 287.

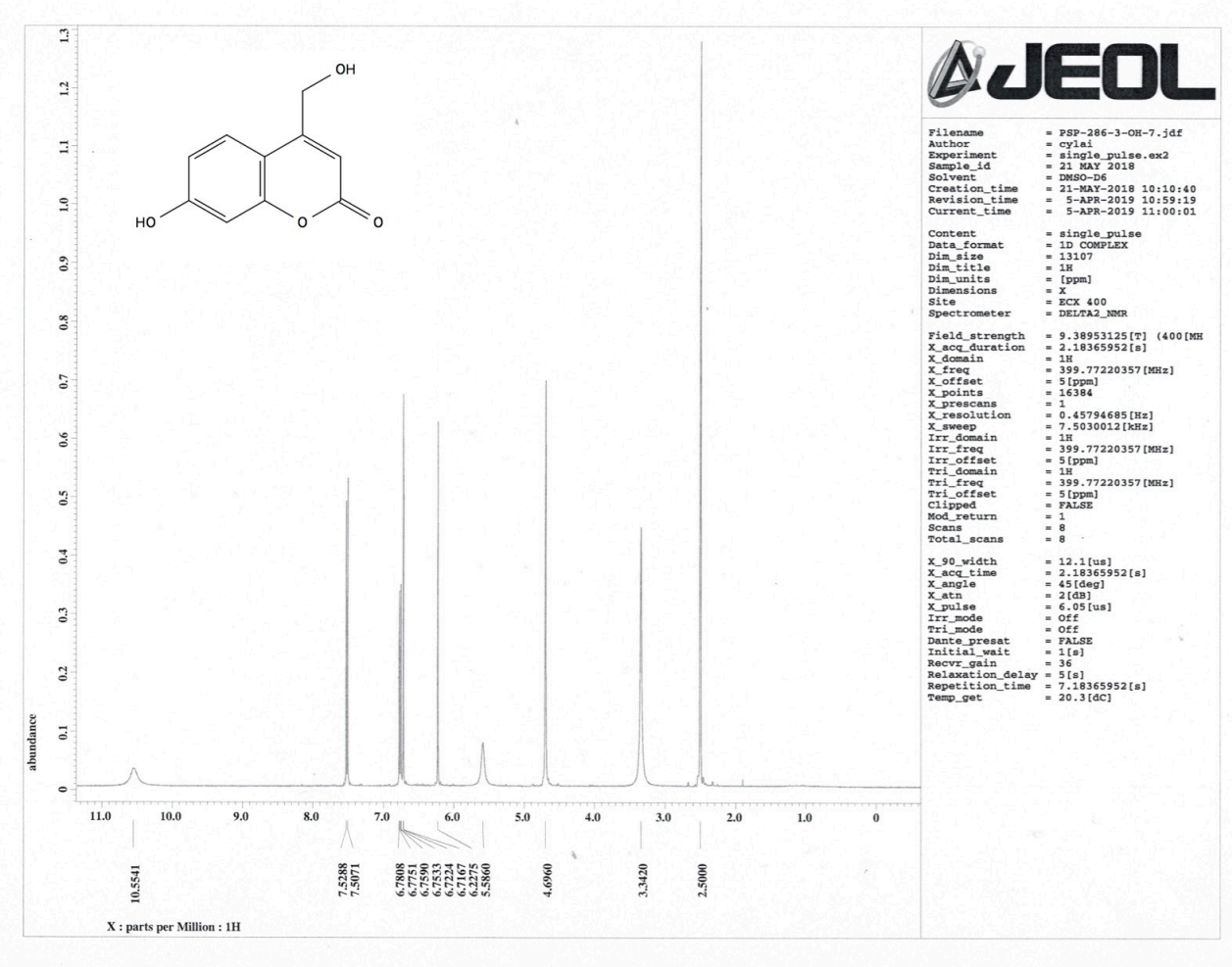

Figure 4.5.[1]H NMR spectrum of PSP 287.

Aside from a proton NMR being performed, a [13]C NMR spectrum was also obtained. From the [13]C spectrum, the correct molecular structure could be confirmed in addition to having the [1]H spectrum, **Fig 4.6**. The chemical shifts were; [13]C NMR (400 MHz, DMSO-d6) δ: 161.98 (s), 160.69 (s), 155.84 (s), 151.54 (s), 127.11 (s), 113.61 (s), 111.60 (s), 109.88 (s), 103.04 (s), 41.90 (s). DMSO d6 presented a peak at 39.62, as was expected. Due to the nature of the carbon NMR, the residual water present in the solvent did not cause trouble in this spectrum.

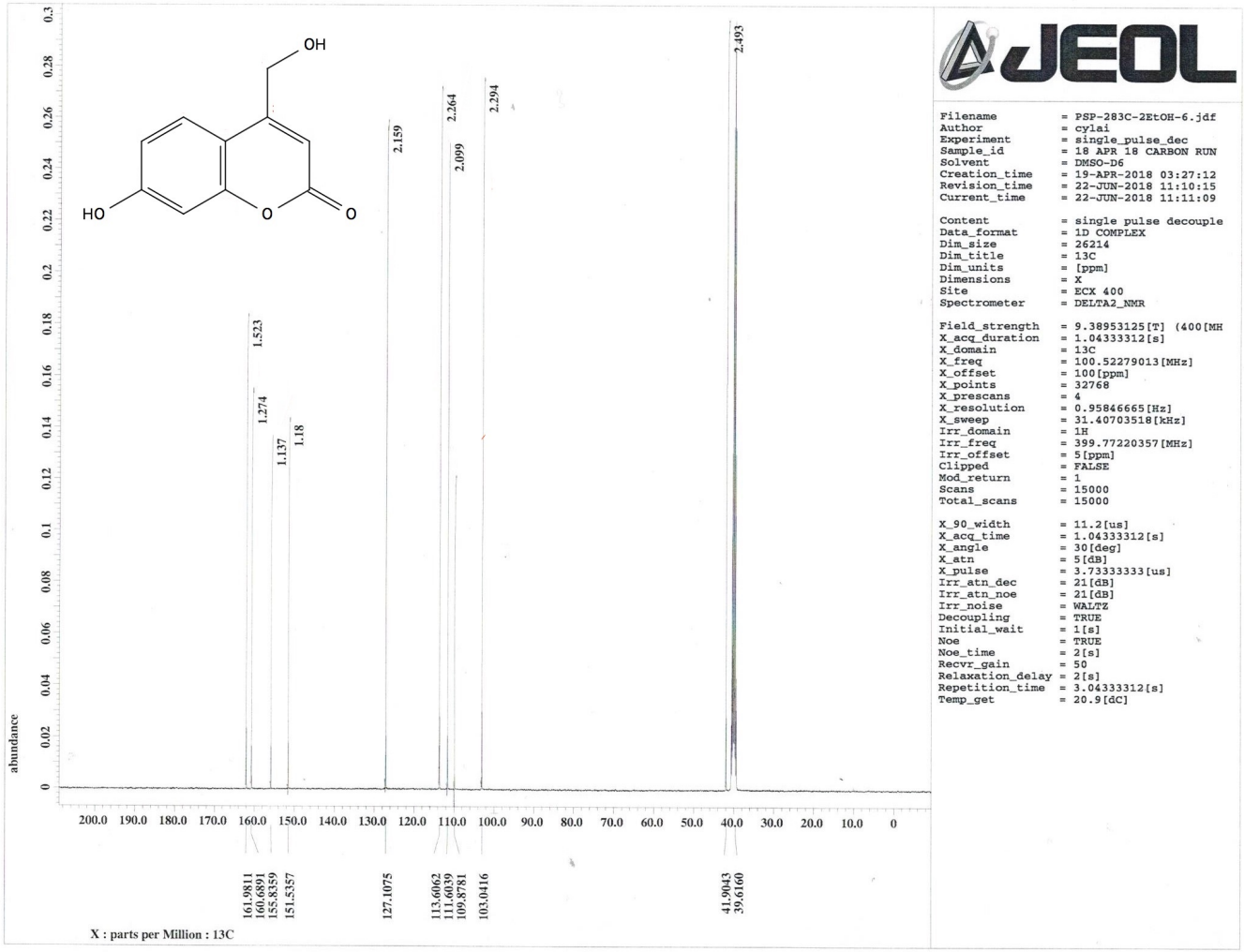

Figure 4.6. ^{13}C NMR spectrum of PSP 287 with labeled molecule.

From the different characterization methods recorded, PSP 287 was purified and consisted of the two hydroxyl groups. Again, PSP 287 differed from Guo *et al.* chemodosimeter which consisted of an oxalate moiety.[66] PSP 287 material was used to determine if it was a suitable chemosensor for phosphates in particular.

4.5. Phosphate Detection Using Methodology Developed by Guo *et al*. via PSP 287

A full range work up was performed to examine how $2x10^{-3}$ M of Pi would differ from lower concentrations and background results, **Fig 4.7**. Guo *et al*. examined ion concentrations in terms of equivalents, where 100 eq of an ion was equal to $2x10^{-3}$ M. For the remainder of this work, concentrations will be in terms of molarity but are the same concentrations as used in the published methods. From the work of Guo *et al.*, it was idealized that using the DMSO-HEPES solution method should work rather well in the detection of Pi even when using a variant chemodosimeter.[66] From their work, Pi was not specified as to which form of the ion, so it can be assumed that the selectivity stops at Pi in general rather than delving into which protonated form is being used. Throughout the research, it was decided to focus on the HPO_4^{2-} form in this particular instance to decide if using DMSO-HEPES as solvent would be effective. Using the knowledge provided through Guo *et al.* phosphate work, a similar procedure was developed and carried out using the newly synthesized chemodosimeter material; 7-hydroxy-4-(hydroxymethyl)-2H-chromen-2-one, which will be referred to as PSP 287 from here on out.[66]

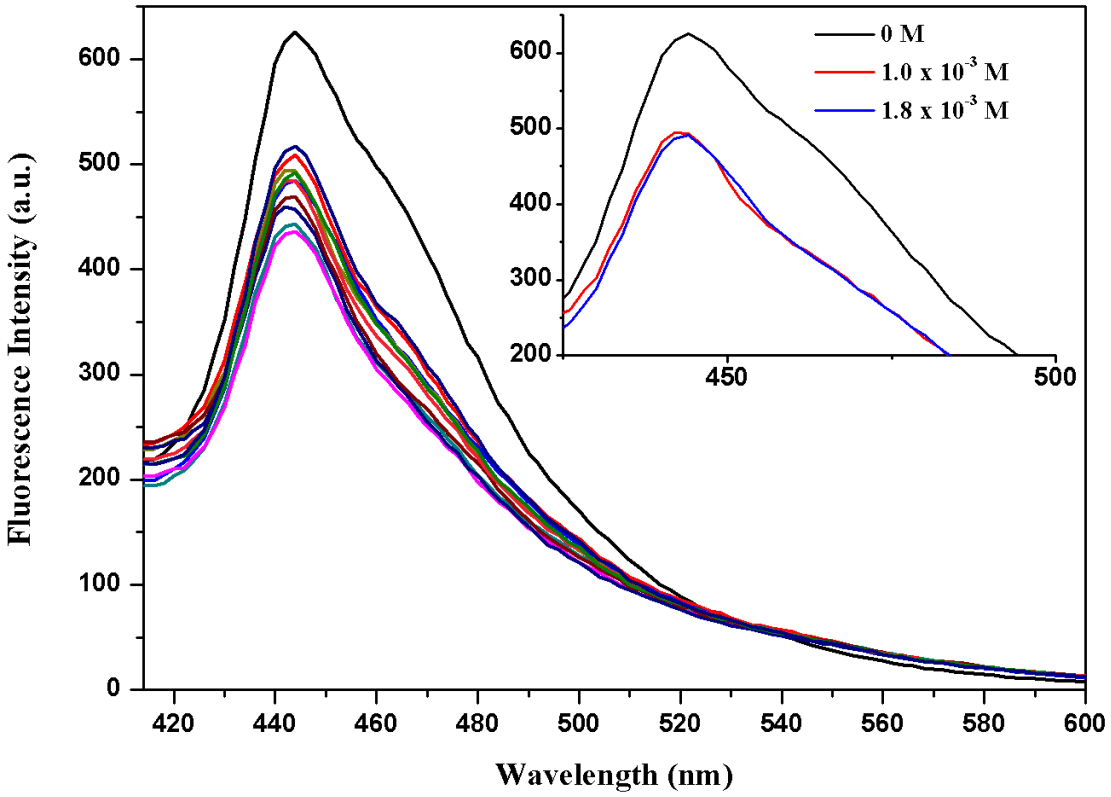

Figure 4.7. Fluorescence spectrum of coumarin derivative PSP 287 sensor detecting 0 M to $2x10^{-3}$ M of HPO_4^{2-}.

From these results, it was concluded that quenching had occurred when HPO_4^{2-} ion was present at any concentration. However, these were not the same results seen when DMSO was used in Guo *et al.* research, where there was a fluorescence increase that directly correlated to increasing concentrations. In this case, from the results observed it was evident that there was no direct correlation between concentration and fluorescence as the concentration increase gave no indication of a pattern in terms of fluorescence. Concentrations tested included 0 M up to $2x10^{-3}$ M and was increased by $2x10^{-4}$ M increments. In the close up image of **Fig 4.7**, it can be seen that there was no difference in fluorescence between the $1.8x10^{-3}$ M and 1.0×10^{-3} M concentrations, indicating that this method was ineffective in terms of quantifying concentration

from fluorescence intensity. This data would not be useful when trying to determine concentration, though possibly helpful in detecting if ion is present based solely on the quenching of a signal produced without quantification. Ultimately, this procedure proved lacking when compared to a sensor that is multi selective and also sensitive enough to distinguish between similar ions.

4.6. HEPES Solution Method Incubation Study of PSP 287

It was theorized that the presence of DMSO was ultimately hurting the signal and could be responsible for why the signals were not improving with ionic presence. After toying with the volumetric ratio of DMSO to HEPES, it was decided to attempt measurement with complete absence of DMSO. Instead of adding material to a DMSO-HEPES solution, 10.0 mg of PSP 287 material was added to 0.02 M HEPES buffer solution (pH 7.4) in addition to $2x10^{-3}$ M PO_4^{3-} (final concentration), **Fig 4.8**.

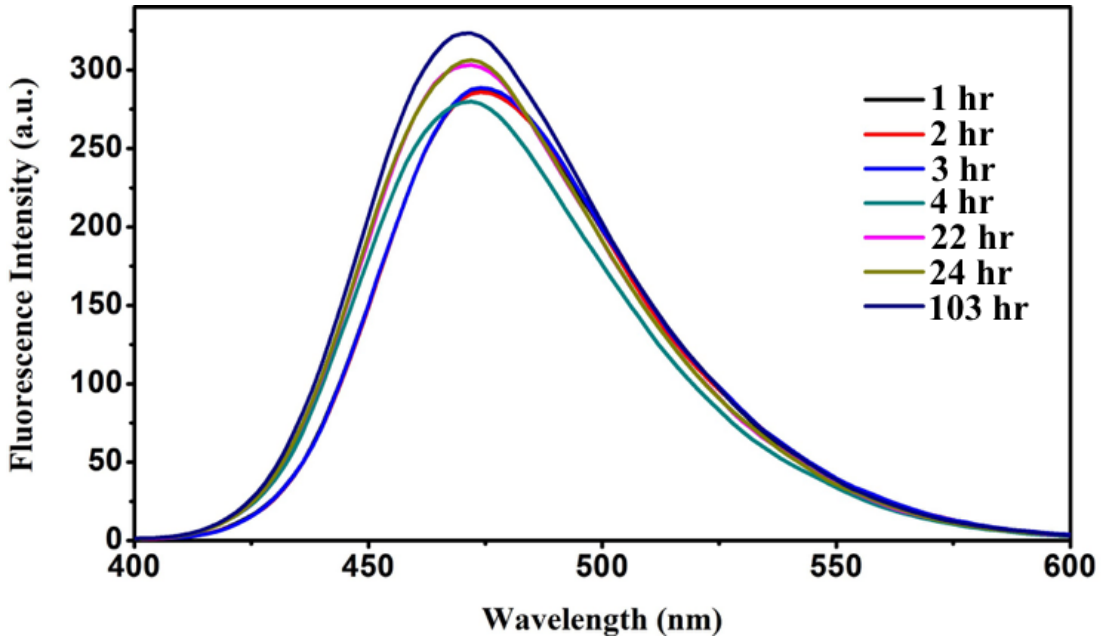

Figure 4.8. $4.68x10^{-3}$ M Chemodosimeter PSP 287 with $2x10^{-3}$ M (final concentration) PO_4^{3-} in 0.02 M HEPES buffer (pH 7.4) at 35 °C at multiple time points to observe fluorescence shift.

Measurements were observed at various time points after incubation at 35 °C to examine stability and accuracy of fluorescence intensity of the material. It appeared that as time progressed, the precursor material remained stable with only small fluorescence changes for the detection of the PO_4^{3-} ion. Over a period of time ranging in 1 to 103 hours, some fluorescence increase did occur but proved that this material was stable and unwavering in terms of the results, **Fig 4.9**. As long as measurements were obtained consistently time wise, this sensor could be stored prior to use with up to 103 hours of promised stability. Ideally, the sensor material would still be taken with 'background' measurements prior to use to positively identify how much fluorescence is being contributed by the sensor PSP 287 material itself.

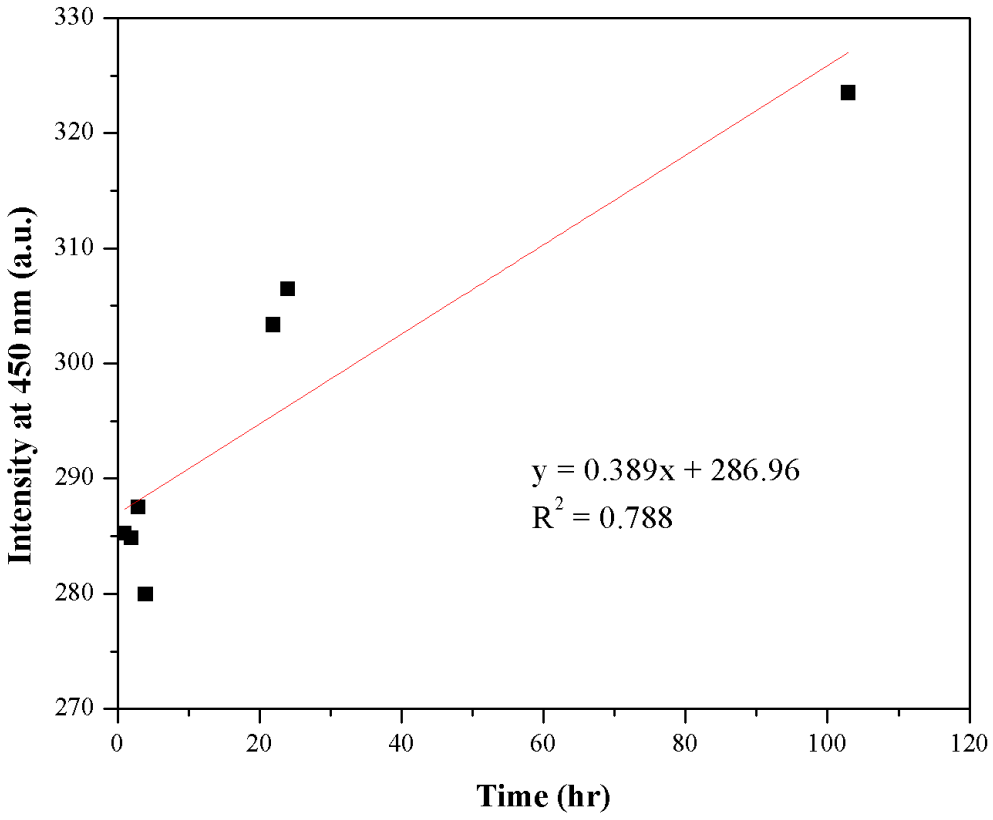

Figure 4.9. Stability plot of fluorescence intensity at 450 nm versus time of measurements of PSP 287 with $2x10^{-3}$ M PO_4^{3-}.

4.7. PSP 281 Incubation Study and Characterization

Another derivative further explored included PSP 281, according to the method of Guo *et al.*, **Fig 4.10**.[66] The chemodosimeter as reported proved capable of detecting phosphate ions versus other ionic compounds. This material was further investigated to examine if there were any distinguishable differences between PSP 287 material and this PSP 281 sensor. Since prior research performed included DMSO as a large component in the solvent, it was wondered how the material would fare when under new conditions such as solely 0.02 M HEPES buffer solution.

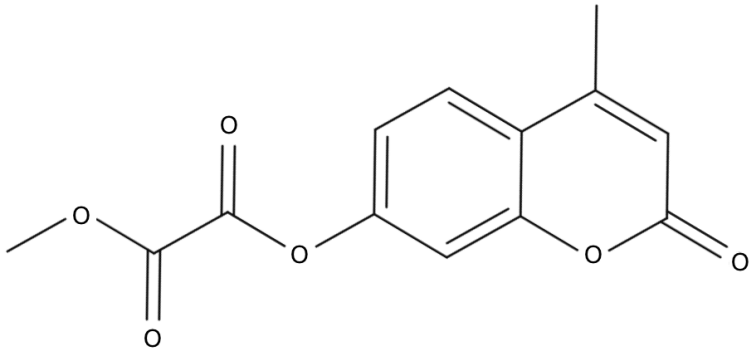

Figure 4.10. Chemical structure of PSP 281, the chemodosimeter material as synthesized by Guo *et al*.[66]

A proton NMR confirmed the material as reported by previous literature with exception to some shifting occurring, **Fig 4.11**.[66] ^{1}H NMR (400 MHz, DMSO-d6) δ: 2.56 (s, 3H), 3.96 (s, 3H), 6.48 (s, 1H), 7.35-7.37 (dd, 1H), 7.42-7.43 (d, 1H), 7.92-7.94 (d, 1H). Functional groups present play an important role in the selectivity, as they are sometimes more compatible with target analytes than others. This led to the investigation of which derivatives with various functional groups proved most efficient and selective when detecting phosphate ions specifically.

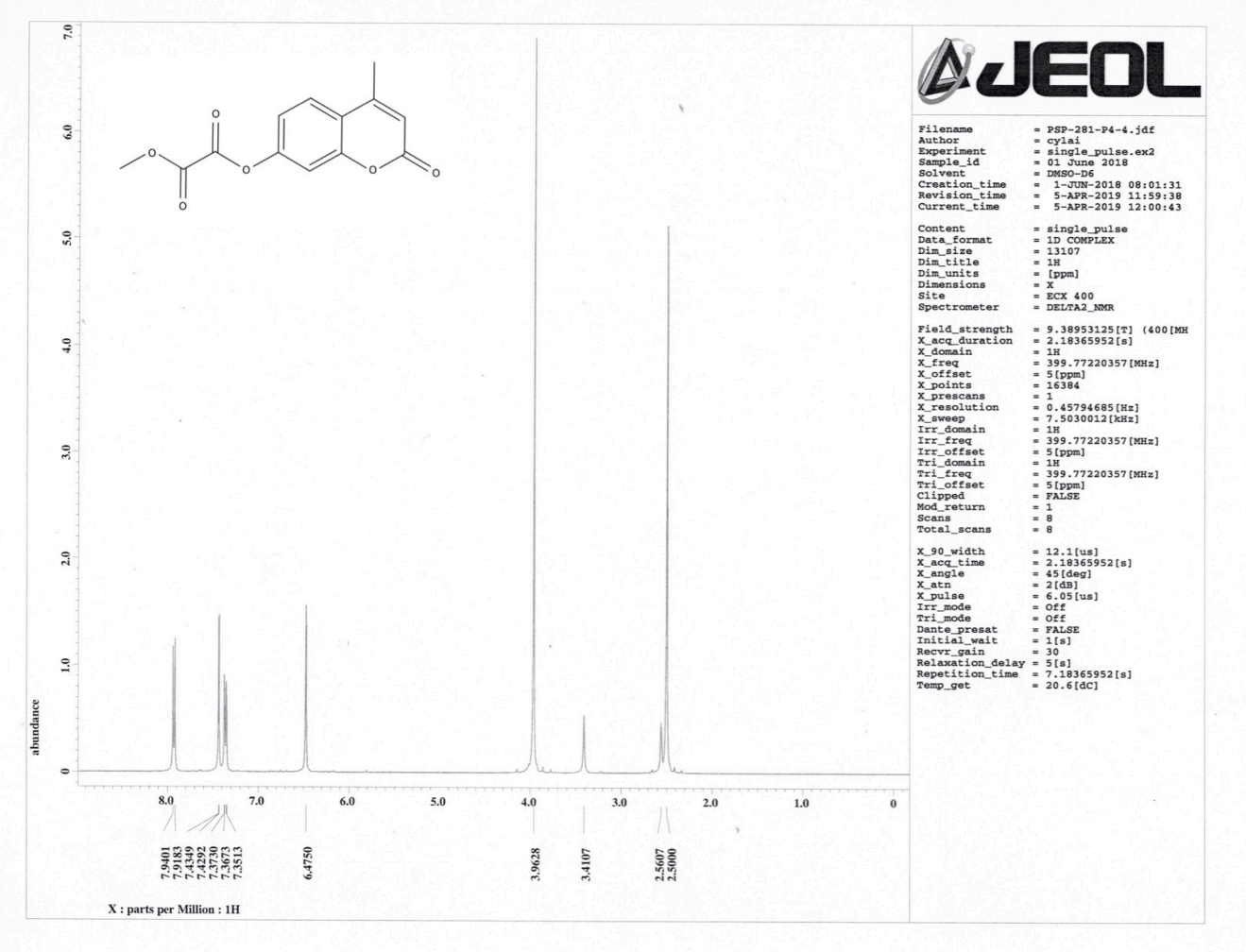

Figure 4.11. ^{1}H NMR spectrum of PSP 281, synthesized as reported by Guo *et al*.[66]

First, an incubation study was performed to determine the stability of this material when in solution for prolonged periods of time. The chemodosimeter PSP 281 as reported by Guo *et al.* was added at concentration of 4.68×10^{-3} M to 2×10^{-3} M of PO_4^{3-} in 0.02 M HEPES buffer (pH 7.4). Material was kept under constant stir in 35 ^{o}C and measured throughout various time points to determine if any loss or rise of fluorescence had occurred, **Fig 4.12**. This experiment would help further determine how stable the material was when in solution compared to the

chemodosimeter material PSP 287. Incubation study performed on PSP 281 was done with 0.02 M HEPES buffer solution in absence of DMSO.

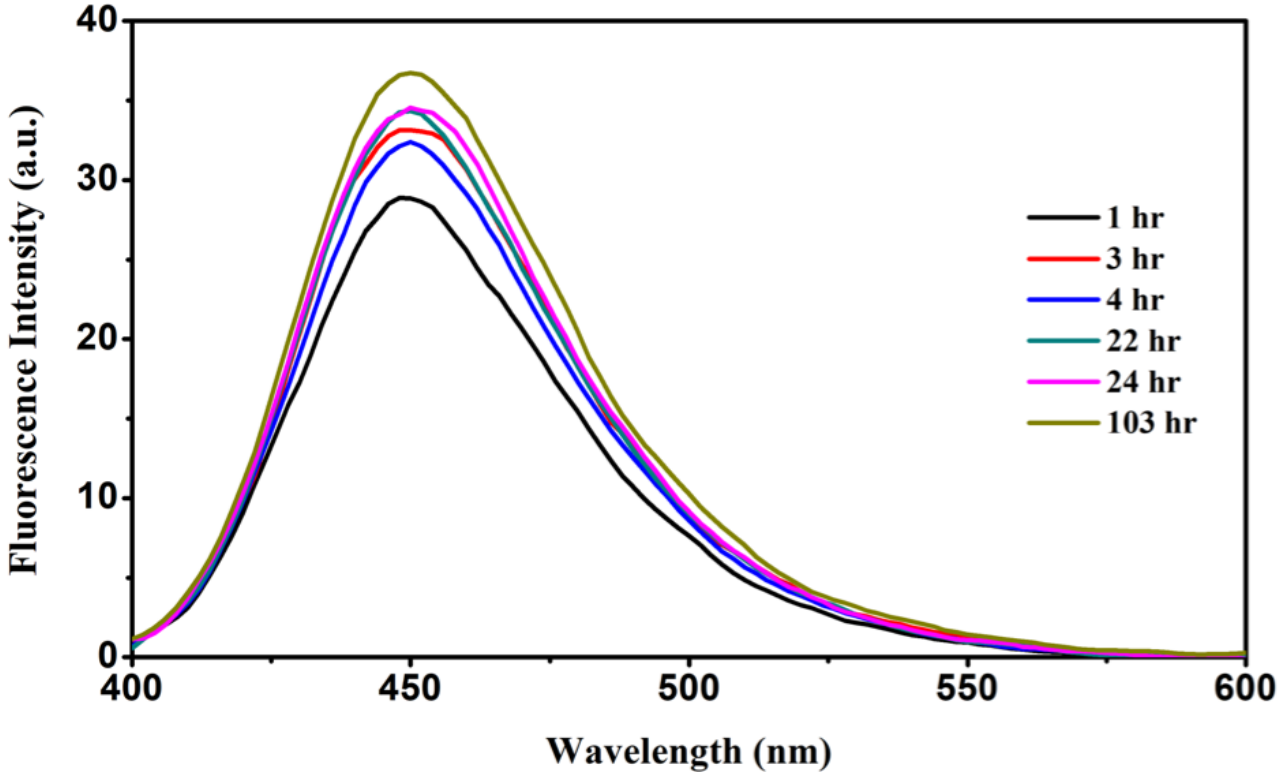

Figure 4.12. Fluorescence spectra of PSP 281 at various time points throughout being incubated at 35 ^{o}C with 2x10^{-3} M (final concentration) PO_4^{3-} in a 0.02 M HEPES buffer (pH 7.4)

From the **Fig 4.12**, it was shown that chemodosimeter PSP 281 was indeed stable. However, it is noted that the concentration of PO_4^{3-} detected when using PSP 281 in this method resulted in minimal fluorescence intensity compared to the PSP 287 material. Peak fluorescence occurred at roughly 37 a.u. which resulted from small increases over the 103 hour time frame. This is not worrisome as long as the measurements of detection tests are performed at the same time as individuals measure their calibrations. This experimental procedure determined that the PSP 281 material was stable over time when in solution and exposed to a concentrated ionic species, **Fig 4.13**.

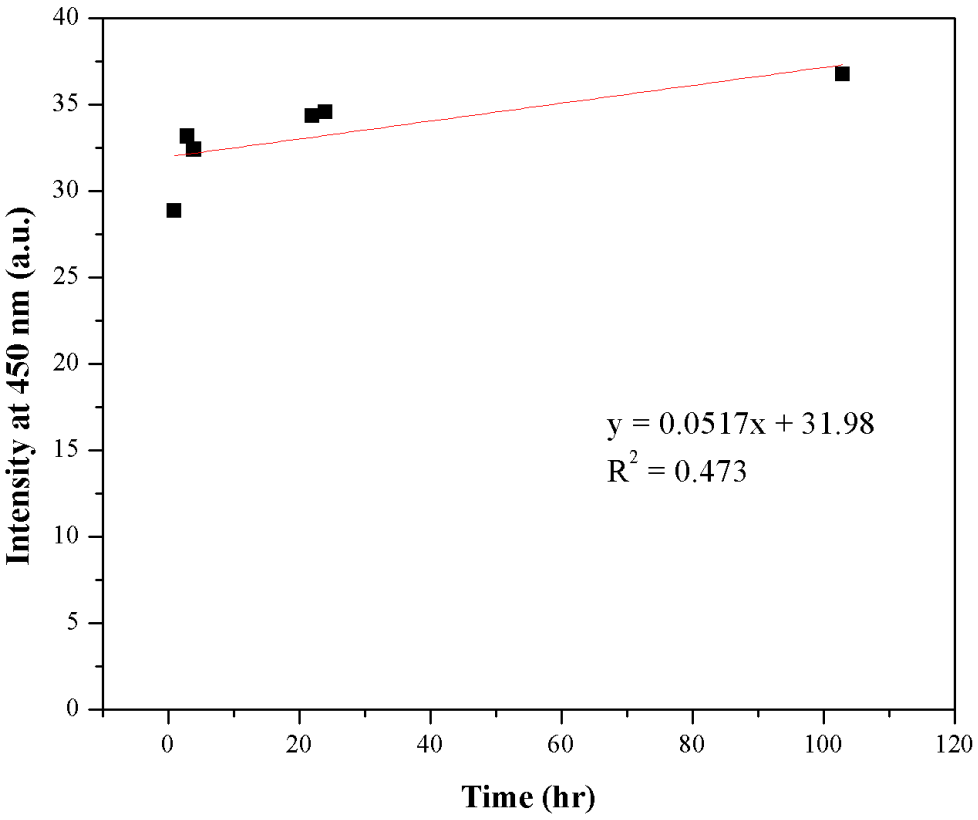

Figure 4.13. Stability plot of fluorescence intensity at 450 nm versus time of measurements of PSP 281 with $2x10^{-3}$ M PO_4^{3-}.

Ultimately, it was encouraging that the PSP 281 material remained stable when in solution, particularly a solution containing a phosphate ion. On the other hand, the fluorescence that occurred from "high" concentration of the phosphate ion was lacking and would not be useful in quantifying samples for phosphate, as the fluorescence gradient would be very minute and difficult to quantify. This led to the conclusion that a variant compound with larger fluorescence potential would need to be synthesized for sensor precursor material, as PSP 281 was not ideal when working with HEPES solution.

Since the PSP 287 material proved stable and sufficient when incubated, it was decided it would be worth further investigation of some other aspects of PSP 287. Specifically, when PSP

281 material was used in presence with PO_4^{3-}, very little fluorescence was observed. In this case, when the chemodosimeter was swapped from PSP 281 to PSP 287, using the same target analyte of PO_4^{3-} and concentrations, there was a significant enhancement in fluorescence from the incubation study with better relative stability of signal. This led to the belief that this analyte may be more selective than the PSP 281 precursor material examined for PO_4^{3-}.

In the prior work, it is suggested that the fluorescence detection is due to the phosphate species cleaving the ester bond.[66] Once the bond is cleaved, a fluorescence shift is the result as the coumarin compound is isolated.[66] However, this work presents an alternative method without the use of an oxalate moiety. It can be suggested that the same concept is applied, however rather than attacking a functional group, the phosphate species are attacking a proton, still leaving the isolated coumarin compound which results in fluorescence when phosphate is present.

4.8. Ionic Detection Methodology using PSP 287

Experimental set up was conducted to test the PSP 287 material with a multitude of ions. For detection purposes, the mixture was sonicated for 15 minutes, then manually shaken every 5 minutes to ensure solubility and dispersion stayed consistent. Various ions were selected for differential testing, including; Pi, NO_3^-, NO_2^-, I^-, Br^-, Cl^-, HSO_4^-, SO_4^{2-}, and CH_3COO^-. For Pi, three ions were tested; PO_4^{3-}, $H_2PO_4^-$, and HPO_4^{2-}. The hope remained that the sensor material would not just be effective, but also selective in the ions it was able to detect for and some of these anions would not be suitable. Beyond selectivity of these eleven ions, it was specifically investigated if the sensor could distinguish detection between all three phosphate ions, rather than solely testing “positive” for Pi as a general category. Since it had already been discovered that the precursor exhibited slight fluorescence, it remained of utmost importance to measure the

background each time a trial was conducted to discount the innate fluorescence the chemodosimeter PSP 287 possessed. This would help determine that if an ion did display any fluorescence that it was the ion material in presence of the chemodosimeter rather than solely the sensor.

All ions were prepared at $2x10^{-2}$ M stock in 0.02 M HEPES buffer solution (pH 7.4) to further investigate what, if any, selectivity was present. Chemodosimeter PSP 287 ($4.68x10^{-3}$ M) was combined with a particular ion in a 9:1 V/V, respectively, and tested at $2x10^{-3}$ M (final concentration) first to identify sensor specificity, **Fig 4.14**. Refer to **Fig 4.15** (bar graph) for better visualization on spectrum of ions with background removed.

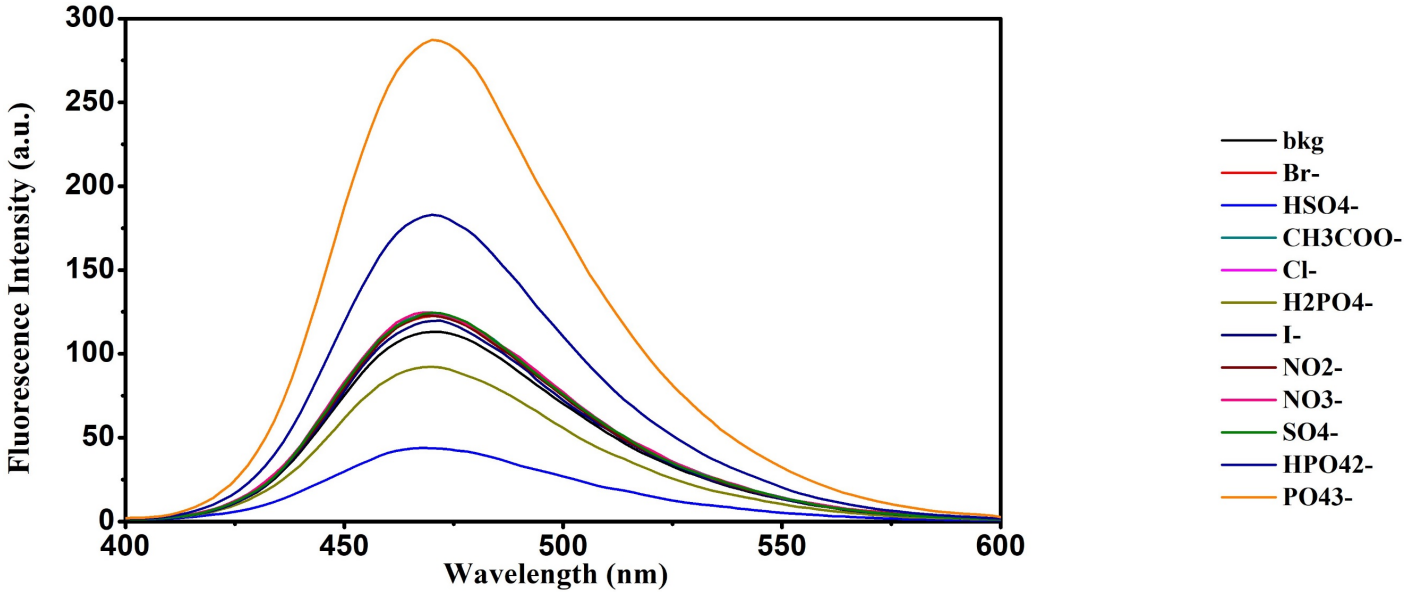

Figure 4.14. Fluorescence observations of $2x10^{-3}$ M various ions with chemodosimeter PSP 287.

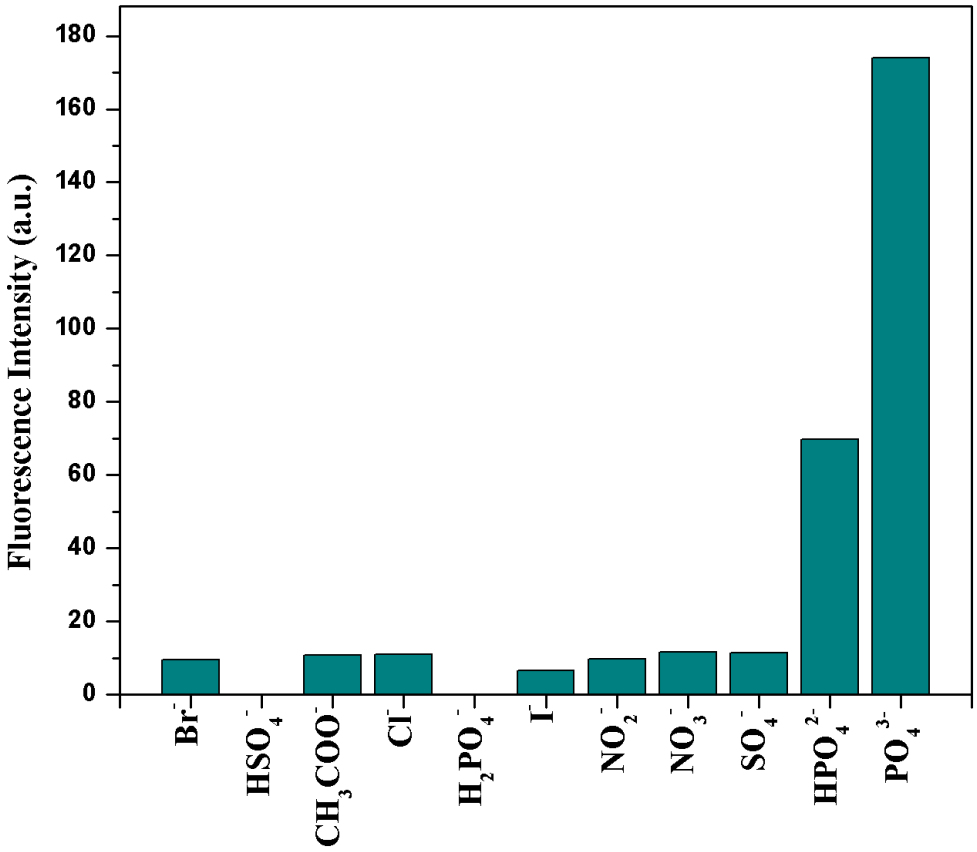

Figure 4.15. Bar graph displaying all ions tested at $2x10^{-3}$ M with PSP 287 innate fluorescence removed.

Prior to measurements being recorded, the solutions were allowed to sit for up to 30 minutes. This ensured proper adherence and allowed for accurate fluorescence to be observed after proper solution mixing had occurred. HEPES buffer does not exhibit fluorescence on its own, however in addition to the chemodosimeter PSP 287, fluorescence is displayed indicating innate fluorescence of the chemodosimeter material. When ions were added, background was discounted (background being PSP 287 in HEPES buffer) to account for actual ion dependent fluorescence. It was concluded that there was indeed selectivity of ionic presence detection when using this method with PSP 287 material.

4.9. Ionic Selectivity of PSP 287 Chemodosimeter

It was determined from **Fig 4.14** and **Fig 4.15** that both PO_4^{3-} as well as HPO_4^{2-} ion resulted in large increases in fluorescence intensity. The protonated phosphate species provided a less intense increase that directly correlated to concentration versus PO_4^{3-}, **Fig 4.16**. Though the intensity escalation was small, there was an obvious correlation between intensity and concentration of the sodium dibasic phosphate ion, **Fig 4.17**.

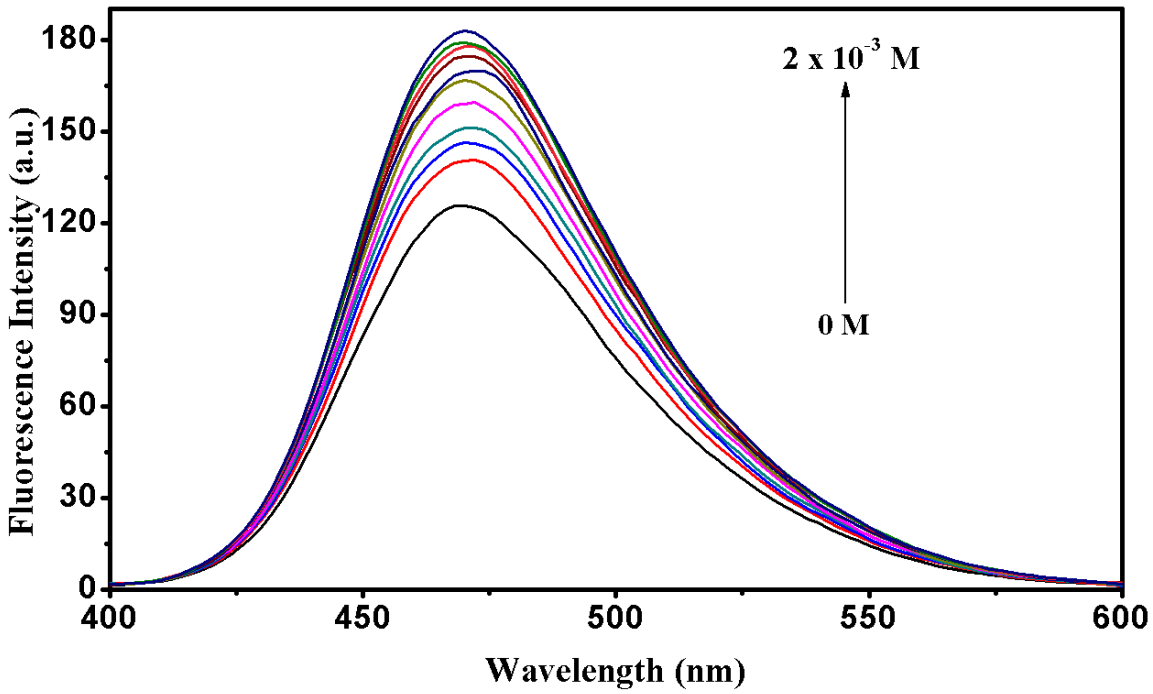

Figure 4.16. Fluorescence spectrum of HPO_4^{2-} at increasing concentration from 0 M to $2x10^{-3}$ M in solution with chemodosimeter PSP 287 ($4.68x10^{-3}$ M) in 0.02 M HEPES buffer (pH 7.4).

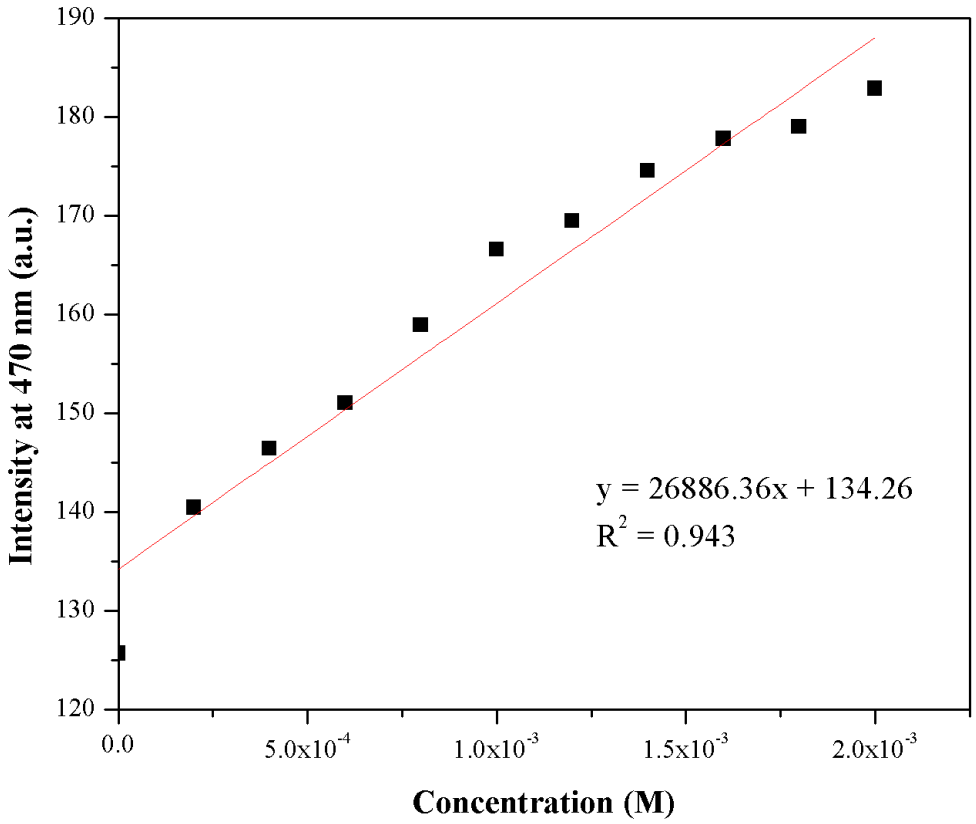

Figure 4.17. Calibration curve of fluorescence intensity at 470 nm for PSP 287 detection of HPO_4^{2-}.

Using PSP 287 in addition to varying concentrations of HPO_4^{2-}, it was confirmed that not only detection, but quantification were achievable. The calibration curve in **Fig. 4.17** also confirmed the correlation between concentration of the ion and fluorescence intensity. Using the equation of $3\sigma/k$ (where σ is the standard deviation of 6 blank-PSP 287 with no ion fluorescence readings, $\sigma = 6.2243$) and k is the slope of the calibration curve, limit of detection could be calculated. In this case, the limit of detection in regards to PSP 287 detection of HPO_4^{2-} was 6.95×10^{-4} M.

The PO_4^{3-} ion yielded a 2-fold increase in intensity when compared to the HPO_4^{2-} ion at the 2×10^{-3} M measurement. To compare the results, the same experiment was performed with the PO_4^{3-} ion to observe the correlation of concentration gradient with intensity. To a solution of

chemodosimeter PSP 287 and HEPES buffer, PO_4^{3-} was subjected to the solution at increasing concentrations where fluorescence was observed, **Fig 4.18**. Using the same concentration gradient between $2x10^{-3}$ and $2x10^{-4}$ M, the fluorescence intensity increased as the concentration also increased, **Fig 4.19**. It was also noted that the fluorescence scale for this ion was larger than the HPO_4^{2-} ion. The $2x10^{-3}$ M of PO_4^{3-} saw fluorescence that nearly doubled that of the $2x10^{-3}$ M HPO_4^{2-} when in solution with PSP 287. Applying the same equation for limit of detection observation of $3\sigma/k$, it was calculated to be $2.41x10^{-4}$ M. In this case, this is a lower LOD than the HPO_4^{2-} ion.

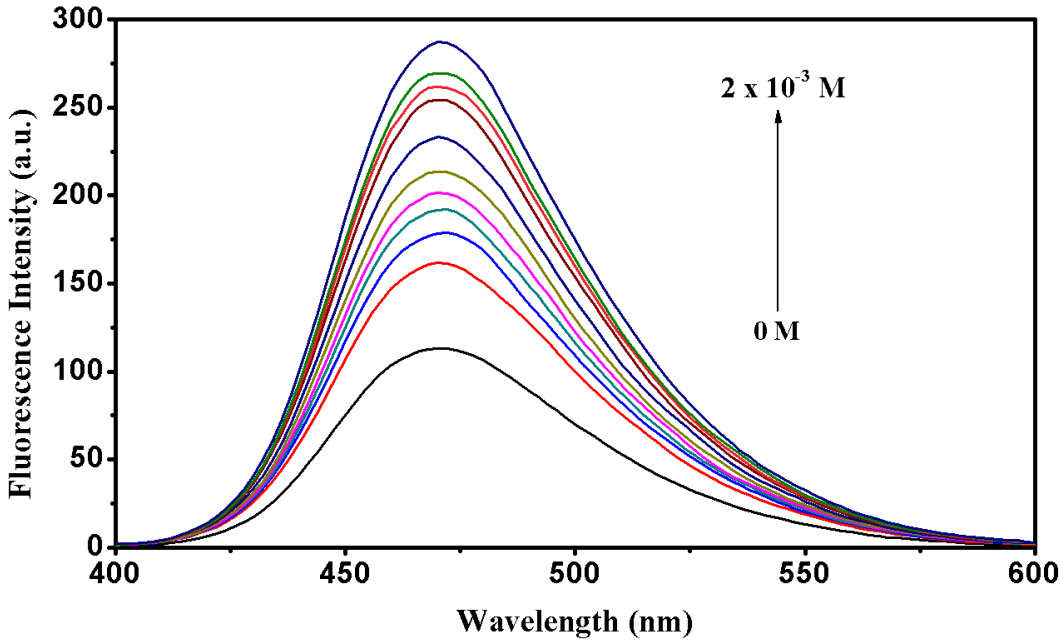

Fig 4.18. Fluorescence spectrum of PO_4^{3-} at increasing concentration from 0 M to $2x10^{-3}$ M in solution with chemodosimeter PSP 287 ($4.68x10^{-3}$ M) in 0.02 M HEPES buffer (pH 7.4).

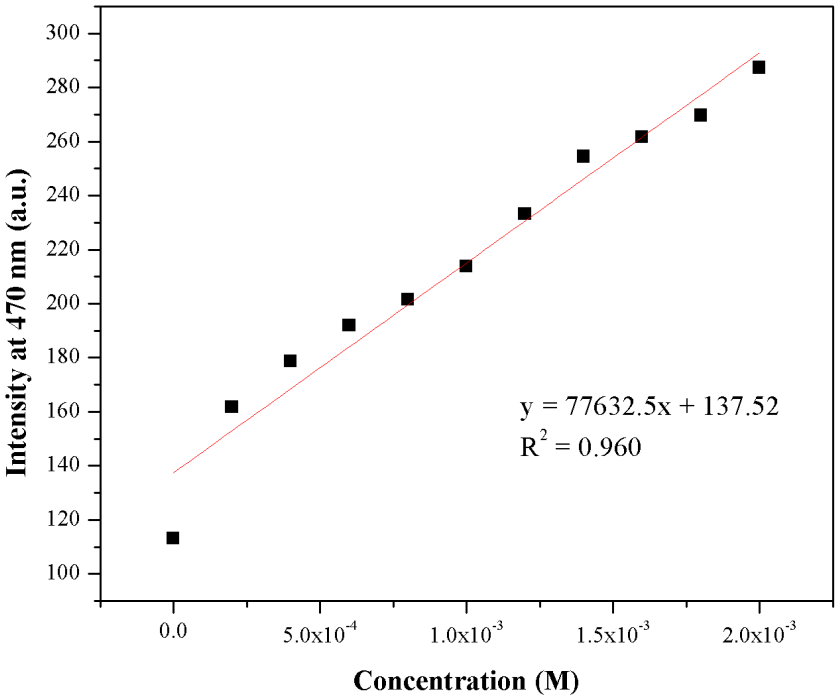

Figure 4.19. Calibration curve of fluorescence intensity at 470 nm for PSP 287 detection of PO_4^{3-}.

Although a similar result was presented between these two ions, they can be independently useful. HPO_4^{2-} gave fluorescence intensity that ranged between 150 and 180 a.u. where the fluorescence range increases to 150 to ~280 a.u. when examining the PO_4^{3-} ion using the same concentration gradient. This concludes that there is a distinctive difference between the two ions, and that overall the sensor is specific between HPO_4^{2-} and PO_4^{3-}.

Referring back to **Fig. 4.14** and **Fig 4.15**, it was observed that there were two ions which resulted in quenching of signal. It was identified that the sulfate and $H_2PO_4^-$ ion quenched any fluorescence, where all other ions either gave some factor of intensity as the background sensor. To further investigate, these two ions were tested at higher concentrations of $2x10^{-4}$, $2x10^{-3}$, and $2x10^{-2}$ M versus background measurement of chemodosimeter PSP 287 in HEPES, **Fig 4.20**.

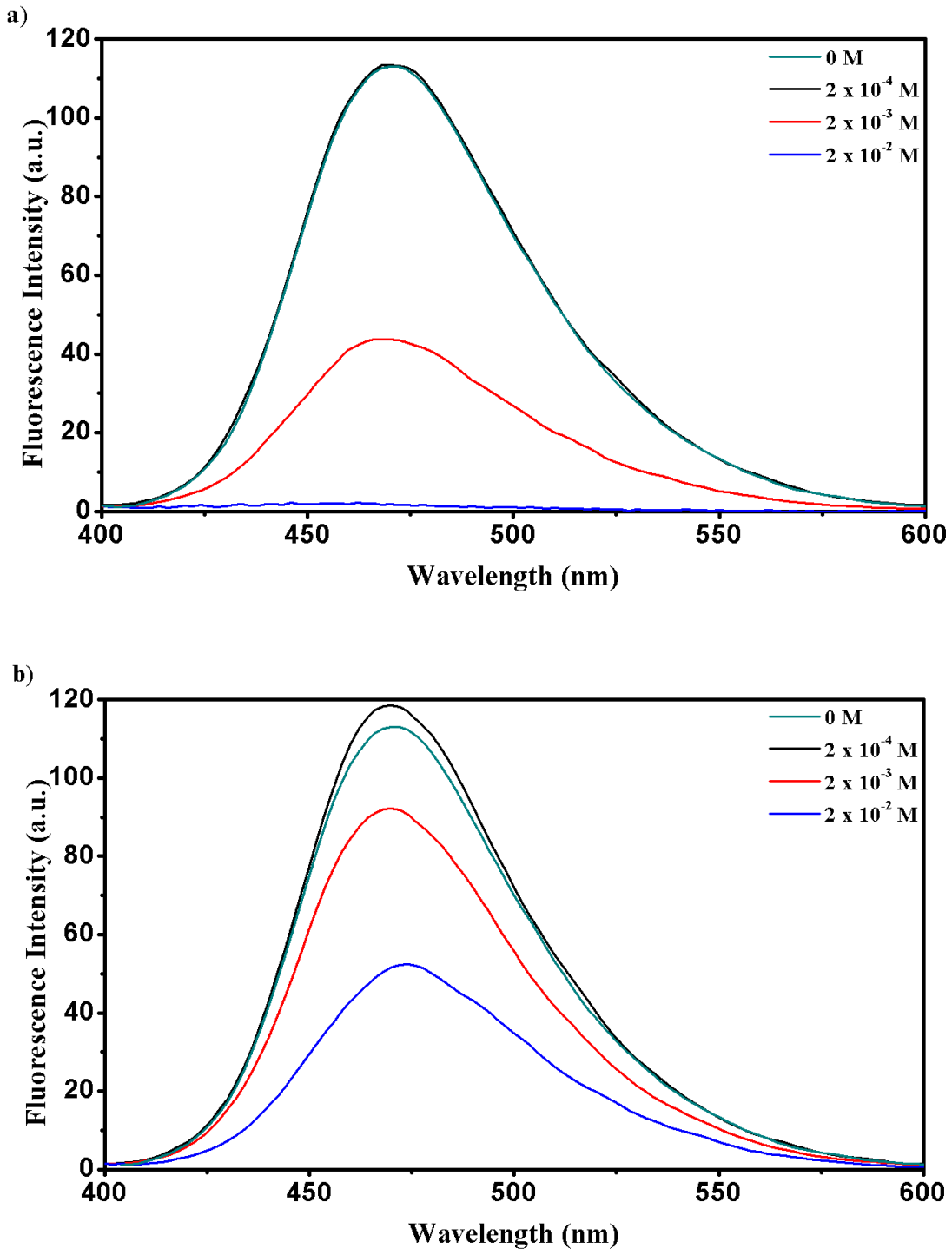

Figure 4.20. a) Fluorescence spectrum of HSO_4^- at 0M, $2x10^{-2}$ M, $2x10^{-3}$ M, and $2x10^{-4}$ M with chemodosimeter PSP 287 ($4.68x10^{-3}$ M) in 0.02 M HEPES buffer (pH 7.4). b) Fluorescence spectrum of $H_2PO_4^-$ at 0 M, $2x10^{-2}$ M, $2x10^{-3}$ M, and $2x10^{-4}$ M with chemodosimeter PSP 287 ($4.68x10^{-3}$ M) in 0.02 M HEPES buffer (pH 7.4).

From the above data, **Fig. 4.20**, it could be confirmed that the $H_2PO_4^-$ and HSO_4^- salts were quenching the fluorescent data. As the concentration of either ion was increased, the signal would respectively decrease. HSO_4^- noted a completely quenched signal at $2x10^{-2}$ M indicating that this was the detection limit. However when observing the $H_2PO_4^-$ signal, $2x10^{-2}$ M still gave rise to a measurement, though significantly lower than 0 M. This indicated that there still is a selectivity between these two ions throughout the concentration gradient, **Fig 4.21**.

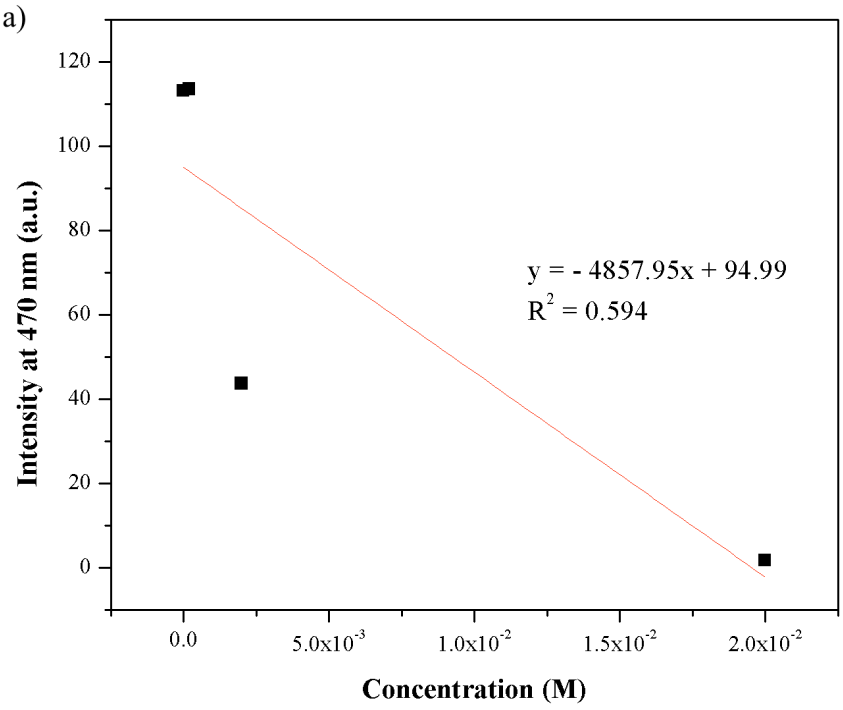

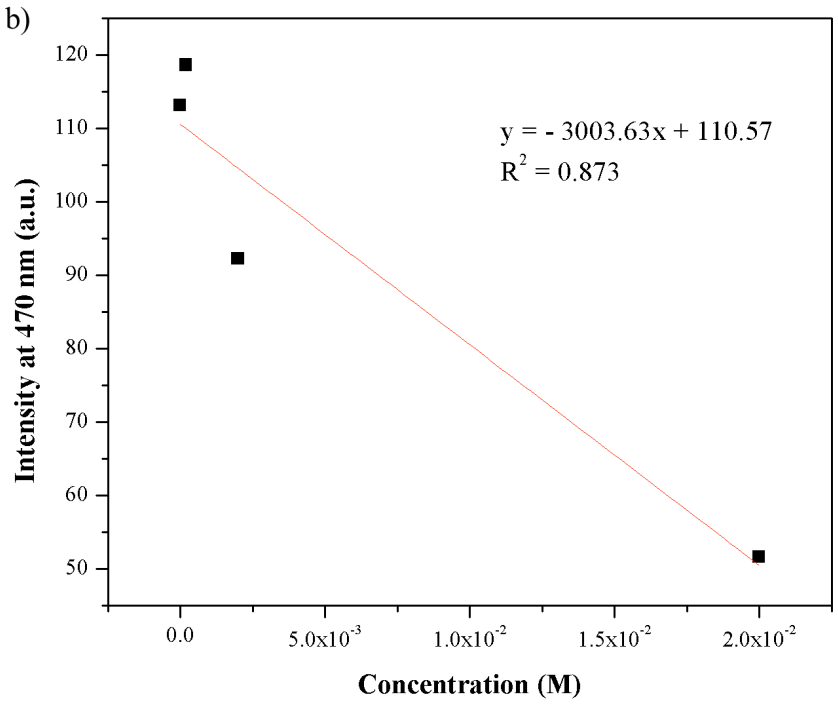

Figure 4.21. Calibration curve of fluorescence intensity at 470 nm of a) PSP 287 quantification and detection of HSO_4^- and b) PSP 287 quantification and detection of $H_2PO_4^-$.

Although the decreased signal was not the original intent, the decrease does correspond to concentration, however in an inverse proportionality. From this data, it could be useful in identification of not just these two ions, but potentially could quantify the concentration based on how far the signal becomes quenched since there is a linear dependence. Ultimately this sensor could be practical in multi-elemental detection.

As for the quenching signals, the sensor is specific between sodium phosphate monobasic and potassium bisulfate. Though the quenched signal was not quite what was expected from this investigation, it could prove useful in future research. Since the $H_2PO_4^-$ did not quench quite as quickly nor drastically as the HSO_4^- did, this can be used to distinguish the two ions in terms of detection. As the only two ions that provided any suppression of fluorescence, we can selectively

test for these two ions and also quantify based on a calibration curve. For bisulfate ion, the detection limit stands at $2x10^{-2}$ M as the highest concentration attainable.

This type of signal, as stated previously, was not expected. However, this could be incredibly useful if testing for selective ions in fieldwork. Quenching of fluorescence is still a signal and in this case it is quantifiable to an extent. With increasing concentration of the ions, the signal was quenched slightly further. These results prove the chemodosimeter PSP 287 is useful on multiple levels of detection, whether it's quenching or increasing fluorescence across four different ions. Although in work performed by Guo *et al*., the chemodosimeter was effective via ester bond cleavage in presence of Pi, this was not the case for PSP 287. Since there was no oxalate moiety, it is suggested that two ions that displayed selective fluorescence were deprotonating one of the hydroxyl groups, if not both, leaving the coumarin compound which has innate fluorescence. As for the two ions that resulted in quenched, signal, it is believed that the ions are bonding to PSP 287, diminishing any fluorescence result.

4.10. ICP-MS Phosphate Quantification

After understanding the context of the selectivity of the coumarin based sensor for phosphate detection, competition was further explored. Of course there are many instruments currently on market that could perform phosphate detection in a variety of sample types. The issue is the reliability, sample preparations, cost effectiveness as well as how user friendly the overall set up is. Some of the instruments currently available include Atomic Absorption, Mass Spectrometry, Fourier Transform Infrared Spectroscopy, Nuclear Magnetic Resonance, and finally Inductively Coupled Plasma Mass Spectrometry. However, these instruments are costly both in purchasing as well as maintaining. Aside from this, they are also bountiful in training and

require skilled technicians when performing analysis. Overall, these instruments are useful in analytical characterization, but miss the mark in both user friendliness, easy sample preparedness, cost effectiveness and portability.

Although the spectrofluorometer used throughout this dissertation was a bench top model and not a portable instrument, there are portable options that can be purchased. This is to be kept in mind for the feasibility of the new phosphate sensor applicability. Sensitivity was another matter that was to be investigated. Essentially, it was vital to delve into the plausibility of this sensor being reliable and potentially a better fit in certain sample testing facilities. Of course there will always be situations where using a larger, costlier, and more complicated instrument is the correct choice for detection. For primary detection confirmation however, this phosphate sensor seems to be very ideal.

The first step in determining the phosphate sensing chemodosimeter's future was to compare against current in-market methods. Instrument of choice in this phase was the ICP-MS, Agilent 7900 model. ICP-MS is known for being ultra-sensitive with quantified results that are reproducible short of user error. Once a technician is trained on the instrument it is of relative ease to use. However, it is a large, bulky bench top instrument that requires a fair amount of calibration and maintenance. In comparison, spectrofluorometers do not require the same attention with exception to replacing bulbs every so often. It takes roughly 15 minutes to warm up the bulb prior to sample detection and requires no calibration other than creating a calibration curve to properly quantify the results obtained. On the other hand, ICP-MS takes approximately 35 minutes to warm up before analysis can be performed.

Typically when creating a calibration curve for ICP-MS samples, a calibration verification standard is purchased from the same company providing the instrument. In this particular set of circumstances, this standard was not used. The logic was the standard did not

provide phosphate as one of the included ions, and therefore would not quantify the phosphate present in given samples. To bypass this, calibration standards were made using Sodium Phosphate dibasic in water. Again, this differs from normal ICP-MS operating procedure. Most samples as well as calibration standards are acidified to properly disperse sample, decrease turbidity and prepare the ions for detection. In this case, phosphate is not soluble in nitric acid, the acid that is most commonly used for ICP-MS detection. The only acid that phosphate is soluble in is hydrofluoric acid. This being said, the matrix was chosen as DI H_2O rather than an acidified solvent, due to the lack of HF on hand and the high solubility in water alone which can serve as a low matrix.

Using DI H_2O works fine as a low matrix and is generally used for the Environmental Protection Agency method as well if turbidity standards are met, which is typically the case in drinking water samples. Acidifying samples is more worrisome when regarding waste water or samples that have plentiful contamination. With this in mind, all calibration standards were made using the DI H_2O matrix with the phosphate dibasic ion, which was one of the ions that showed selectivity in quantification, though at a lower level than the tribasic ion.

To explore the ICP-MS method feasibility in detection and selection of phosphate ions, water samples were retrieved from five local water sites that were of the same common water source; Silver Lake of Dover, DE 19904. Water was collected from local vicinity sites; Site 1 located at latitude 39.1756 and longitude -75.7508, Site 2 of latitude 39.1611 and longitude -74.5188, Site 3 of latitude 39.1727 and longitude -75.5263, Site 4 of latitude 39.1756 and longitude of -75.5308, and lastly Site 5 of latitude 39.1689 and longitude -75.5229.

At each five sites, approximately 100 mL of water was removed for further sampling at the laboratory. Water sites were tested for salinity as well as pH, DO (dissolved oxygen), ORP (oxidation-reduction potential) and temperature to regard what the differences were within the

samples from the same source but in different locations, **Table 4.1**. Samples were diluted to form ICP-MS samples at a 10X, 50X and 200X dilution. Though it was quickly realized that the 200X was too dilute and unquantifiable for further studies. This led to the quantification of both a 10X and 50X dilution to understand that low detection capabilities when utilizing ICP-MS instrumentation.

Table 4.1. Water sampling locations and data acquired while sampling from Silver Lake in Dover, DE 19904.

	Site 1	***Site 2***	***Site 3***	***Site 4***	***Site 5***
Latitude Coordinates	39.1756	39.1611	39.1727	39.1756	39.1689
Longitude Coordinates	-75.7508	-74.5188	-75.5263	-75.5308	-75.5229
Salinity	0.07	0.03	0.00	0.06	0.00
Water Temperature	21.05 ^{o}C	22.17 ^{o}C	23.48 ^{o}C	21.06 ^{o}C	22.57 ^{o}C
pH	6.9	7.7	8.0	7.6	7.8
DO%	29.3	91.9	94.5	74.9	84.8
ORP	215.8	146.8	254.4	239.7	143.5

Over the course of several months, data was collected using the sampling method described above on several occasions. Most data was collected using the EPA 200.8 requirements. This allowed for a higher threshold and to obtain the most accurate and precise results possible. Originally, samples were run under no gas mode with only Argon as a purge gas and disregarding Helium gas, **Table 4.2**. However, the helium gas would negate any excess collisions and provide a more accurate measurement opposed to operating under no gas mode exclusively and under quick scan, which would not remove any interferences. The method was

set up to sample from all five sites with each dilution (10X and 50X) of 3 replicates each. This would allow to observe both reproducibility as well as human error in sample preparations.

Table 4.2. ICP-MS results quantifying five Silver Lake sample sites of 10X and 50X dilution replicates under no gas mode.

31 P [No Gas]			
Sample Name	CPS	CPS RSD	Conc. [ppb]
blank	68207.76667	0.2608554	<0.568
1 ppb P	70752.42667	1.4502476	2.710020913
5 ppb P	72074.26667	2.0211316	4.117758702
10 ppb P	79272.12333	0.750596	11.78335729
50 ppb P	118828.72	0.7755603	53.91048004
100 ppb P	162307.0867	2.1428929	100.2142231
500 ppb P	537262.7733	0.7353569	499.5358426
Site1 10X r1	138972.6233	1.4621719	75.36340471
Site1 10X r2	140588.1667	1.3406614	77.08393171
Site1 10X r3	136930.1667	2.9361065	73.18822207
Site1 50X r1	93423.51333	3.7305514	26.85435413
Site1 50X r2	92882.38333	1.7925495	26.27805961
Site1 50X r3	94386.74333	3.6036862	27.88017819
Site2 10X r1	106117.1833	2.3948051	40.37290324
Site2 10X r2	108317.4567	2.1944528	42.71615803
Site2 10X r3	108943.3467	1.6490668	43.38272055
Site2 50X r1	81538.28667	4.0259649	14.19678384
Site2 50X r2	84720.62333	2.2368052	17.58591988
Site2 50X r3	83131.89	4.8911315	15.8939451
Site3 10X r1	66273.97	1.6267689	<0.568
Site3 10X r2	67696.5	5.0773703	<0.568
Site3 10X r3	66068.16	4.2044892	<0.568
Site3 50X r1	66374.77	4.1765464	<0.568
Site3 50X r2	67261.87333	2.2488342	<0.568
Site3 50X r3	65090.78333	1.282058	<0.568
Site4 10X r1	136333.8467	5.3343526	72.55315111
Site4 10X r2	133785.1533	2.4213166	69.83883476
Site4 10X r3	140638.2033	2.9012624	77.13721993
Site4 50X R1	90204.55333	2.8512502	23.42621485
Site4 50X R2	95918.26	0.6472579	29.51121817
Site4 50X R3	102173.5667	0.67873	36.17301656

Site5 10X R1	133656.96	5.2812806	69.70231097
Site5 10X R2	127831.0667	3.0518605	63.4978307
Site5 10X R3	125771.8067	2.0548459	61.30475278
Site5 50X R1	87830.94333	4.0580393	20.89835936
Site5 50X R2	87159.66333	3.8928362	20.18345724
Site5 50X R3	91784.15	4.547821	25.10845923
Site3 10X r1	65305.34	1.2789033	<0.568
Site3 10X r2	62067.80667	1.7479759	<0.568
Site3 10X r3	63130.87667	2.8437442	<0.568
Site3 50X r1	59410.12333	1.0173896	<0.568
Site3 50X r2	59434.11333	2.0569584	<0.568
Site3 50X r3	61231.38	1.5351335	<0.568

Site 3 was tested twice within this batch to determine if the lack of quantification was a batch mistake or rather a lack of phosphate. This particular set of data was observed under the parameter of LOD, limit of detection. The <0.568 ppb signifies that this is the lowest possible concentration that the ICP-MS could theoretically quantify given these calibration standards. It should be noted that a manual tune was not performed prior to the sample collection and internal standard was not supplemented which could affect the instrument's sensitivity in detection.

The calibration standards were chosen from 1 ppb to 500 ppb to aid in the most accurate quantification possible. The data from each replicate was in good agreement with each other detailing that no human error occurred when sample preparations had taken place. From this batch, the lowest concentration detected was that of Site 2 50X replicate one at 14.197 ppb. The highest concentration was from Site 4 10X replicate three at 77.137 ppb. Respectively, these concentrations equated to 100 nM and 543 nM. This particular set of data was obtained without the EPA 200.8 batch method, and instead under individually picked circumstances that were calculating detection limits instead.

In the end there was a very subtle, about 10 ppb difference, in quantification from exclusive no gas mode versus the no gas and helium modes used concurrently. It was also noted

that the Site 3 samples were not quantifiable under this method. This batch did not use the EPA 200.8 operating procedure and instead used a limit of detection method to calculate what the lowest concentration of phosphate detectable was. From this experiment, it was determined to be 0.568 ppb.

Once the helium mode was added in succession, the data did appear a bit cleaner. Unfortunately there was still an error with the Site 3 data. Again, all five sites were used to make three replicates of each dilution factor to attest for repeatability, **Table 4.3**. The grey columns were performed under no gas mode, where the white columns were performed under helium mode.

Table 4.3. ICP-MS Data results of all five sampling sites, 3 replicates per dilution under helium and no gas modes.

	31 P [No Gas]			31 P [Helium]		
Sample Name	CPS	CPS RSD	Conc. [ppb]	CPS	CPS RSD	Conc. [ppb]
0 ppb	13225.15667	27.316681	0	86.666667	40.521745	0
500 ppb	204766.9833	0.6631661	492.4292417	2526.97	5.4888836	489.034546
100 ppb	64654.82333	3.4238712	132.2190156	803.38667	20.007859	143.6300295
50 ppb	36017.85333	1.1277152	58.59707267	430.02333	12.948631	68.80836055
10 ppb	20127.55667	6.1618434	17.7451769	186.67667	11.151185	20.04191212
5 ppb	19136.33333	6.6576626	15.19687002	176.67667	31.173163	18.03792131
1 ppb	15632.05667	3.1599827	6.187828333	160.00667	10.826671	14.69726862
Site1 r1 10X	51701.46333	2.7232203	98.91760377	620.03667	2.7939308	106.886858
Site1 r2 10X	47891.68333	3.6377875	89.12315256	550.03	19.242496	92.8575863
Site1 r3 10X	47921.67	5.6414755	89.2002444	573.37	7.8645321	97.53490086
Site1 r1 50X	23928.07333	6.8157211	27.51581328	243.34333	31.116027	31.39786006
Site1 r2 50X	22052.75667	4.1806049	22.69461689	173.34333	12.008919	17.36992437
Site1 r3 50X	21199.04333	4.387093	20.49983042	226.67667	9.1834154	28.05787537
Site2 r1 10X	39852.96	2.3511703	68.45663546	460.02667	9.9627295	74.82100099
Site2 r2 10X	37043.34	1.3129537	61.23346614	366.68667	20.104534	56.11575074
Site2 r3 10X	36941.59667	6.9775046	60.9718972	463.35667	12.461416	75.48832993
Site2 r1 50X	20075.16	11.129907	17.61047185	233.34333	26.185025	29.39386925
Site2 r2 50X	19757.45667	3.2137467	16.79369771	203.34333	10.237198	23.38189681

Site2 r3 50X	19406.64	4.064917	15.89179347	230.01	11.502766	28.72587231
Site3 r1 10X	15915.73333	4.6684453	6.917124321	153.34	22.905694	13.36127475
Site3 r2 10X	17330.73333	0.6556872	10.55490615	196.67667	7.7666825	22.04590293
Site3 r3 10X	17013.66667	1.3805594	9.739768796	163.34333	9.3516227	15.36593356
Site3 r1 50X	16346.16667	3.9754131	8.023712703	116.67	51.669145	6.012640435
Site3 r2 50X	15965.95667	4.1523504	7.04624201	120.00333	58.336475	6.680637373
Site3 r3 50X	15685.64333	3.6573886	6.325592716	123.34	39.996925	7.349302307
Site4 r1 10X	53567.31333	10.172352	103.7144626	556.7	6.8017086	94.19424817
Site4 r2 10X	53098.13	6.3977055	102.508253	730.05667	13.905224	128.9347649
Site4 r3 10X	51169.94	5.2040971	97.55112609	576.70333	14.124548	98.20289779
Site4 r1 50X	21099.07667	8.6475176	20.24282906	216.67667	29.310276	26.05388456
Site4 r2 50X	21249.23333	0.3813929	20.62886241	176.67333	22.878547	18.03725331
Site4 r3 50X	23822.57	14.246405	27.24457787	196.67667	10.584204	22.04590293
Site5 r1 10X	42960.49667	2.1851064	76.44570997	490.02667	21.20822	80.83297343
Site5 r2 10X	45156.68	5.0032141	82.09181303	510.02667	30.186478	84.84095505
Site5 r3 10X	43478.2	6.7538638	77.77665823	533.36667	9.4375724	89.51826961
Site5 r1 50X	19994.26	2.9439782	17.40248843	160.01	0	14.69793662
Site5 r2 50X	20601.49	4.8852472	18.96359815	243.34333	6.277243	31.39786006
Site5 r3 50X	19984.16	4.9623326	17.37652263	206.67667	15.553523	24.04989374

From the data, it was observed that the three replicates were well relatable between each other. However, Site 3 samples still resulted with odd outcomes. Between the 10X and 50X dilutions there was no difference in concentration, although there should have been. This was identified as a problem since it should have not been quantifiable at all at the 50X dilution range from the concentrations the 10X dilution yielded.

To ensure proper data and that human error did not exist yet again, one last batch was performed using the EPA method of the same sample made freshly, with internal standard added but still missing a manual tune. All samples were prepared day of experimental run (for each ICP-MS results) to ensure proper dispersion of phosphate and other contributing elements. Prior to running ICP-MS, samples were sonicated and warmed to room temperature as water samples were kept at 4 ^{o}C.

It appeared from this trial that all results were quantified between the 10 to 100 ppb range. The Site 3 sample 50X dilution third replicate yielded a concentration of 6.33 ppb. Taking into account the formula weight of sodium phosphate dibasic as 141.96 g/mol and calculating the conversion, it resulted in 6.33 ppb equating to 44.6 nM. Of course, when comparing to the synthesized chemodosimeter, the ICP-MS results are significantly lower in detection. However, they are still in the realm of detection making the synthetic sensor a viable option for in field testing. The largest concentration detected from this sampling was Site 4 10X replicate 1 at 103.71 ppb. This converted into 725.6 nM.

Again, samples were tested on a separate occasion with a refined method; using both internal standard as well as performing a manual tune prior to running the instrument. These initializations should help the instrument be as proficient as possible and yield the most accurate results. With the new method set up, samples were prepared at a 10X and 50X dilution with a calibration curve that ranged from 1 to 500 ppb, **Table 4.4**.

Table 4.4. ICP-MS results from 5 sample site of Silver Lake using replicates at 10X and 50X dilution using No Gas mode.

	31 P [No Gas]		
Sample Name	CPS	CPS RSD	Conc. [ppb]
0 ppb	47135.62		0.049108434
0 ppb	46373		0
1 ppb	56097.65		0.626212704
5 ppb	110661.04		4.139787792
10 ppb	197571.56		9.736335916
50 ppb	829926.32		50.45642189
100 ppb	1602968.57		100.23599
500 ppb	7809812.38		499.9217828
Site1 50X r1	55113.86		0.562862167
Site1 50X r2	57775.94		0.73428513
Site1 50X r3	56304.49		0.639532035

Site1 10X r1	136475.04		5.802064042
Site1 10X r2	134902.6		5.70080776
Site1 10X r3	141259.7		6.110169205
Site2 50X r1	52828.74		0.415713306
Site2 50X r2	52926.18		0.421987893
Site2 50X r3	49144.07		0.178441305
Site2 10X r1	114348.59		4.377245249
Site2 10X r2	119429.26		4.704411789
Site2 10X r3	96759.08		3.244579845
Site3 50X r1	41398.29		<0.000
Site3 50X r2	40506.62		<0.000
Site3 50X r3	40255.56		<0.000
Site3 10X r1	43818.27		<0.000
Site3 10X r2	48022.95		0.10624749
Site3 10X r3	45963.23		<0.000
Site4 50X r1	57839.08		0.73835099
Site4 50X r2	55069.03		0.559975368
Site4 50X r3	55130.85		0.563956228
Site4 10X r1	133432.85		5.606164136
Site5 50X r1	51977.13		0.360874417
Site5 10X r4	124194.21		5.011247739

It was evident that the Site 3 sample site did not produce a quantitative amount of phosphorous. The only exception being a 10X replicate (replicate 2) which yielded a concentration of 0.106 ppb, however the other two replicates were undetectable. This indicates that if phosphorous is present in this specific location, it is at a very minute amount when undiluted. Ultimately, these results were much more accurate than previous trials were, as can be seen in the earlier ICP-MS data such as **Tables 4.2** and **4.3**.

This trial differed from the previous two in the case that every sample detected measured under the 10 ppb mark. In earlier cases, the samples were detected to have up to 100+ ppb. The samples have been kept at 4 ^{o}C in the dark to ensure that algae and bacteria growth mostly does not take place. When samples are prepared manual shaking is performed to ensure proper

dispersion prior to ICP-MS running. It is likely that the manual tune prepared the ICP-MS at a much higher level than when this initialization methods were not taken into account.

All ICP-MS data discussed in this section is under the no gas mode. Helium mode was also performed however did not promote as consistent of results. When examining helium mode, the standard deviations were significantly larger than those from no gas mode. No gas mode provided accurate measurements through all three trials, and can be seen specifically in the last trial where no gas mode resulted in closely related concentrations, **Table 4.5**.

Table 4.5. ICP-MS results from trial 3 of various Silver Lake samples under Helium mode.

	31 P [Helium]		
Sample Name	CPS	CPS RSD	Conc. [ppb]
0 ppb	390.02		<0.000
0 ppb	420.02		0
1 ppb	460.02		0.210049414
5 ppb	1170.09		3.938794094
10 ppb	2240.23		9.558351084
50 ppb	9983.71		50.22118694
100 ppb	18652.27		95.74183558
500 ppb	95797.68		500.8505391
Site1 50X r1	640.03		1.155324288
Site1 50X r2	500.03		0.42015134
Site1 50X r3	540.03		0.630200754
Site1 10X r1	1780.17		7.142467752
Site1 10X r2	1660.15		6.512214486
Site1 10X r3	1530.13		5.829448867
Site2 50X r1	520.03		0.525176047
Site2 50X r2	380.02		<0.000
Site2 50X r3	580.03		0.840250167
Site2 10X r1	1110.07		3.623614948
Site2 10X r2	1350.11		4.88412148
Site2 10X r3	820.05		2.100651674
Site3 50X r1	380.02		<0.000
Site3 50X r2	340.02		<0.000
Site3 50X r3	300.02		<0.000

Site3 10X r1	540.03		0.630200754
Site3 10X r2	340.02		<0.000
Site3 10X r3	390.02		<0.000
Site4 50X r1	640.03		1.155324288
Site4 50X r2	490.03		0.367638986
Site4 50X r3	570.03		0.787737814
Site4 10X r1	1450.12		5.409297527
Site5 50X r1	580.03		0.840250167
Site5 10X r4	1230.09		4.253868214

Although all concentrations detected remained under 10 ppb, there was much more digression between replicates of samples. The accuracy between replicates was much more diminished under the helium mode than the no gas mode. This led to the conclusion that no gas mode may result in more accurate results for the phosphate detection and yield more productive results than strictly adhering to the helium mode – though it cannot hurt to perform simultaneously which is what the EPA labs prefer to. In addition, it is important to note that Silver Lake is generally low in organic nutrient concentration. Other locations may have a larger presence of organic matter which could contribute to matrix effects and potentially alter true quantifications. Silver Lake tends to contain more inorganic nutrients due to fertilizers, soaps, etc due to close proximity with residential areas, which reduces matrix effects.

In the chemodosimeter PSP 287 sensor research, concentration of phosphate was detected linearly from $2x10^{-4}$ to $2x10^{-3}$ M. A stock solution of $2x10^{-2}$ M per ion was created which would be further diluted when added to the chemodosimeter PSP 287 solution. Using this method of chemodosimeter, the detectible concentrations ranged from 200 uM up to 2 mM. Evidently this method is not quite as sensitive as the ICP-MS results were, but they are still viable results in field work.

Another notable point in this research were the consumables. For the chemodosimeter PSP 287 sensor, the materials were easily fabricated, had short synthetic times, safe to use and

were proven to be stable when stored for periods of time. The samples were also 3 mL sample sizes which are ideal for measuring samples when in the field. For ICP-MS, the purchase of the consumables, internal standards, tune solutions, etc. tend to add up. This could be a driving factor behind the chemodosimeter PSP 287 sensor as a useful tool that can be used to pre-quantify. If lower detection is wanted at a later time using a lower sensitivity based instrument (ICP-MS, AA, etc.) then further analysis can be performed on collected samples.

CHAPTER V: INVERSE OPAL SERS SUBSTRATE

5.1. PMMA SERS Substrate

Prior to starting SERS active substrate research, an optical sensor was thought to be ideal. Specifically a photonic sensor that would give a colorimetric response and be very user friendly with little disadvantage. One of the leading techniques in sensors like this include the Poly(methyl methacrylate), or PMMA material. These sensors prove useful in gas detection, where gas comes into contact with the sensor causing a hydrogel swelling.[92] Refractive index changes are resulted from the swelling, giving a visible color shift which would indicate a positive results. Sensors of this nature can be incredibly useful in both environmental and toxic sensing.

This led to the idea that maybe a sensor could be created using the same material, but instead of using a hydrogel to create the colorimetric sensor, material can be supplemented and characterization carried out analytically. Essentially, it was theorized to remove the PMMA template and leave a structure that would still give the opalescent appearance. By pursuing this avenue, this allows room to add in supplementary material that could increase sensitivity and selectivity by further manipulating the refractive indexes of the materials. Ultimately, this would change the way the sensor works, no longer specific for gases with a simple color change. An instrument could be used for detection or detection that may be possible with other physical states observances.

Removing the PMMA template material is commonly referred to as an inverse opal. First, a PMMA template is created onto substrate of choice, generally silica, and the PMMA material is then removed via calcination. Resulting material is a layer of pores from where the PMMA nanoparticles once were layered neatly which are suitable to hold other materials. Using

these pores, substances such as silver or another SERS component could be substituted onto the substrate and used for detection methods. It was theorized that the combination of material with varying refractive index properties (such as opal) when combined with a SERS material, could exponentially increase sensor signals.

5.2. Inverse Opal Synthesis

Prior to forming inverse opals, the template needed to be designed, which included synthesizing PMMA nanoparticles. This technique was adapted from Schroden *et al*. from the University of Minnesota.[86] By altering the size of the nanoparticles, the refractive index would also vary and create colorimetric difference in the opal. Size and diameter of the nanoparticles could be controlled by altering the ratio of solutions used for synthesis. This step began with the polymerization of methyl methacrylate, as described in materials and methods section.

Using this method, the polymerized solution was added to a vial containing water and the 28.6% wt solution of TEOS, HCl, and EtOH. A glass substrate was suspended in the solution and left to evaporate slowly to prevent disturbing the formation of smooth, even layers rather than cracking, **Fig 5.1**. When the substrate was removed, opalescent thin film was visibly apparent that altered color when rotated. In this case, the film was violet/red or a green/yellow depending on the angle of observation.

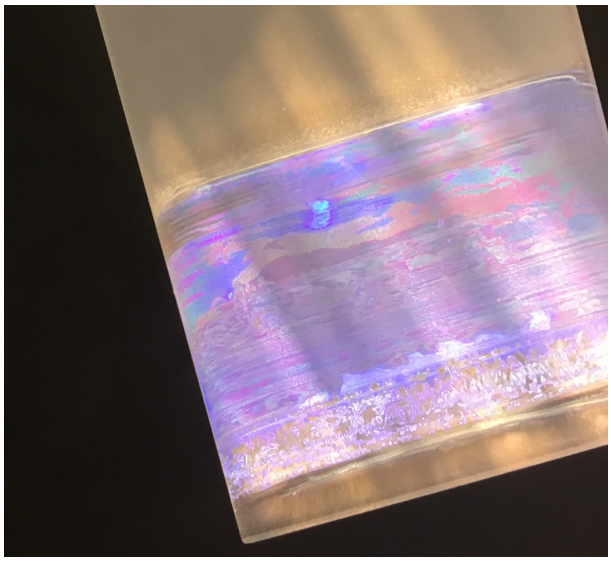

Figure 5.1. Image of inverse opal templated onto a silica substrate.

Removal of the nanoparticles were achieved via calcination at 65 ^{o}C for 36 hours. Pores left behind allow for other chemicals or substrates to be added or functionalized to the template. These indentations from PMMA elimination were uniformly distributed and left organized pores inside. Each pore contained a pattern that resembled a honeycomb visually, **Fig 5.2**. It was ideal that these pores should plausibly hold a SERS material that could be manipulated for detection purposes. Since the inverse opal template already contributed to light manipulation and enhancement, it was idealized that in addition to a SERS active material, the substrate could achieve SERS active substrate status.

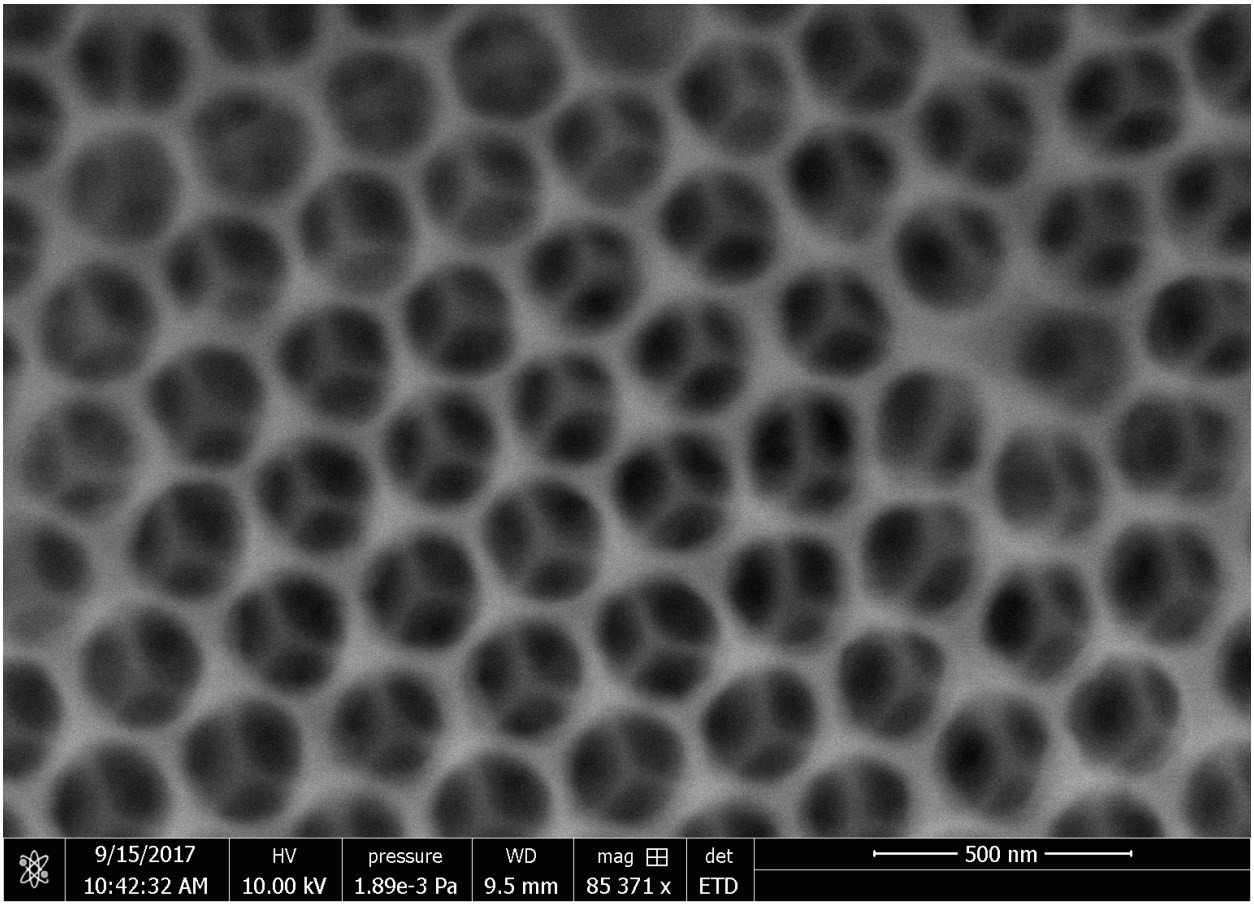

Figure 5.2. SEM image of inverse opal template.

The new template resulted in extreme symmetry between size and shape, as seen in the SEM image. Cross sections from the inverse opal template were achieved to examine the thickness of the substrates and uniformity of layering via TEM, **Fig 5.3**. The uniformity can be seen throughout the layering process as well as the surface, indicating the high order or organization throughout this material.

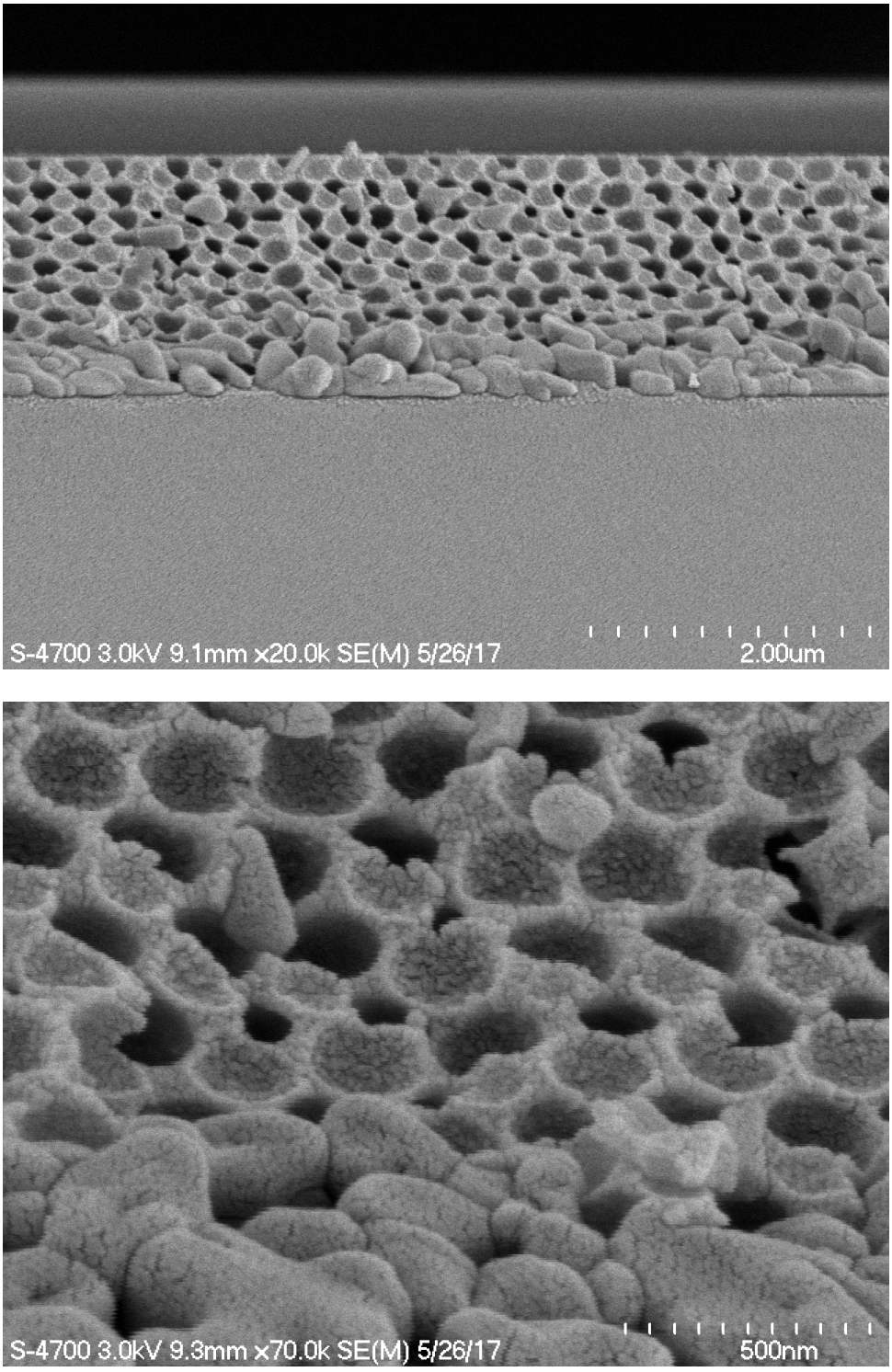

Figure 5.3. TEM images at a) 10.0 k and b) 70.0 k of inverse opal template cross section.

Although the films were rather thin, measurements could still be obtained pertaining to thickness and heights. Using Atomic Force Microscopy (AFM), depth of the pores, distances between pores, and height could be observed, **Fig 5.4**. AFM instrumentation allowed for further characterization of the distances between the uniform pores.

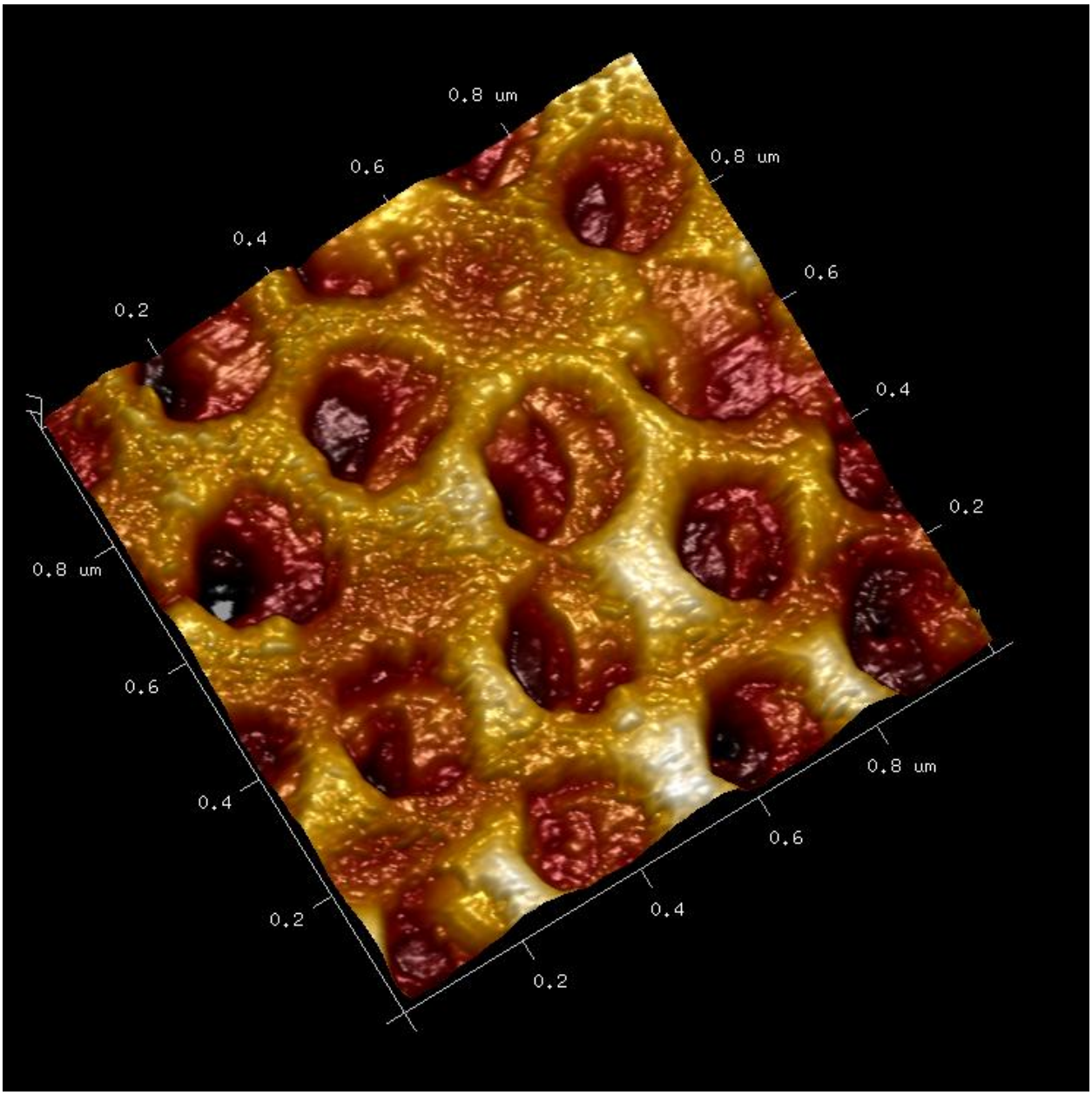

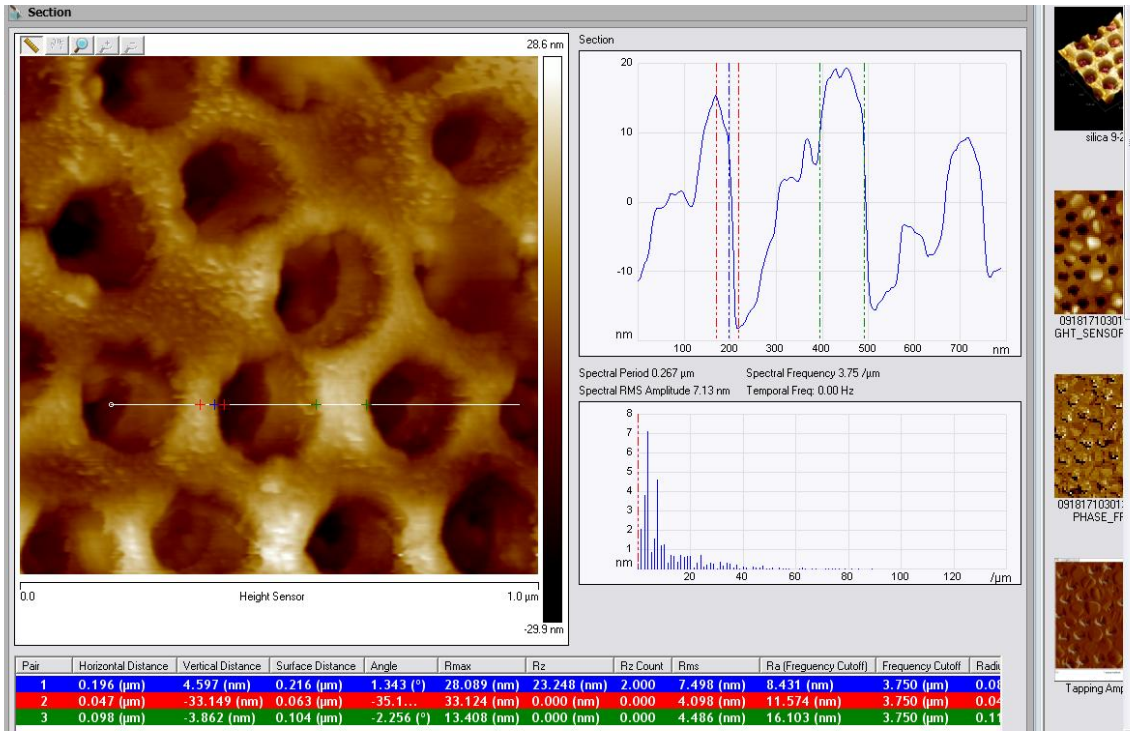

Figure 5.4. a) AFM top view image of inverse opal template and b) AFM top view image with locations of measurements taken using contact mode.

5.3. AgNS-PMMA SERS Substrates for R6G Detection

Knowing that these pores were capable of holding material that otherwise would not be possible with PMMA nanoparticles present, it was investigated if silver would fulfil the gaps left. Once silver was planted, it was idealized that a SERS active substrate was the result. However, silver nanoparticles would not evenly aggregate to the order necessary to fill the diameter of these gaps, which resulted in the theory of application for nanostar silver nanoparticles invested on inverse opal templated substrates, **Fig 5.5**.

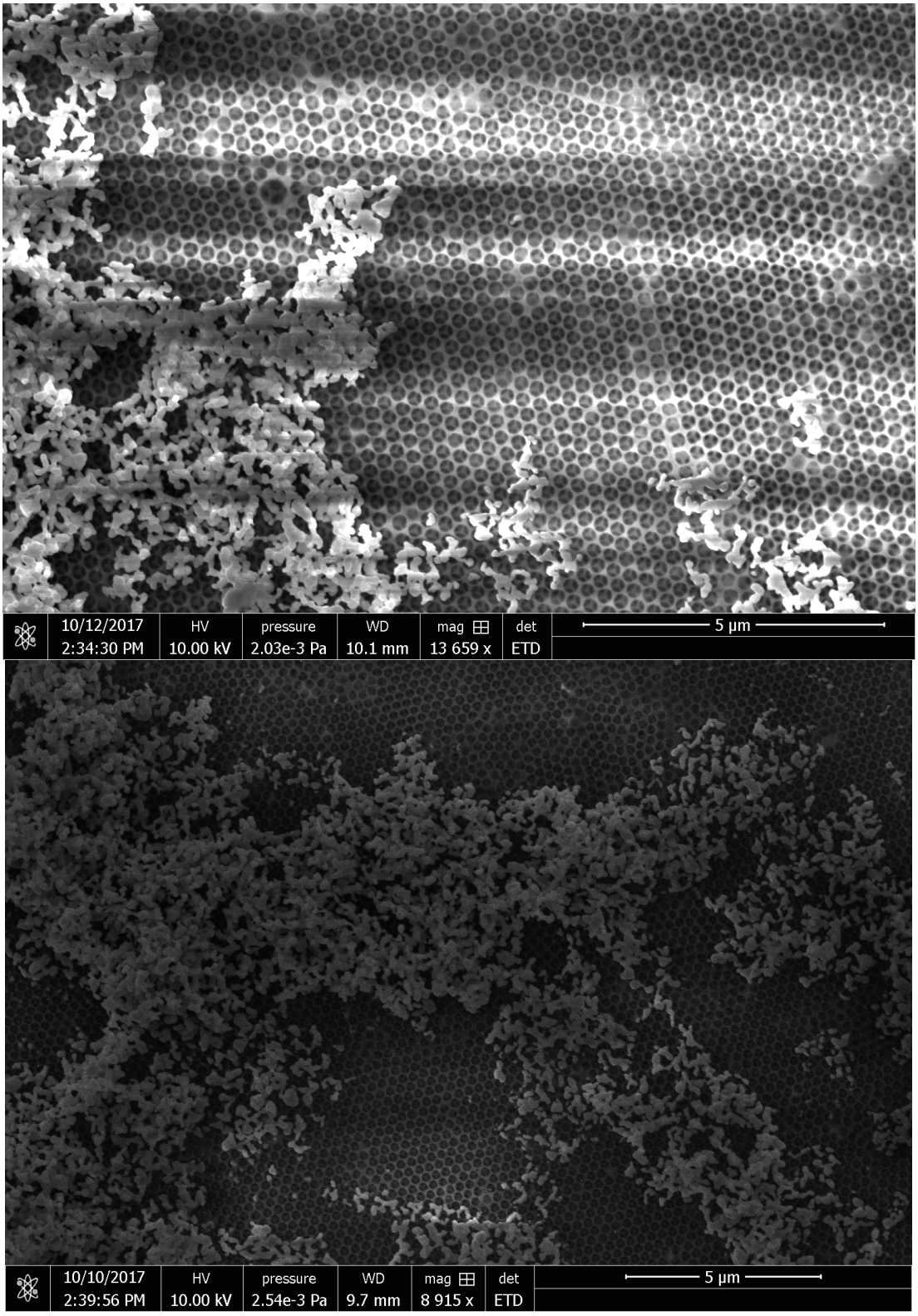

Figure 5.5. SEM image of inverse opal template with aggregated AgNP (spherical) at 13659X and 8915X.

Nanostars are a relatively new type of nanoparticle. Rather than a spherical morphology, nanostars take on a unique 3D shape where they resemble a snowflake, with several symmetrical points. Using the same knowledge of nanoparticles, the size can be tuned and ultimately manipulated through the synthetic methods. For the sake of SERS research, nanostars are preferred over the typical nanoparticles due to their increase in SERS which is correlated to the morphology. The distinct shape of nanostars helps to cause more significant aggregation. When referring to SERS research, aggregation plays a large role in causing hot spots and the overall SERS effect that would be exhibited. In this research, silver nanostars of approximately average 50 nm diameter were synthesized, **Fig 5.6**. The synthesis was adapted from methods by Garcia-Leis *et al.* and Oliveira *et al*.[79, 80]

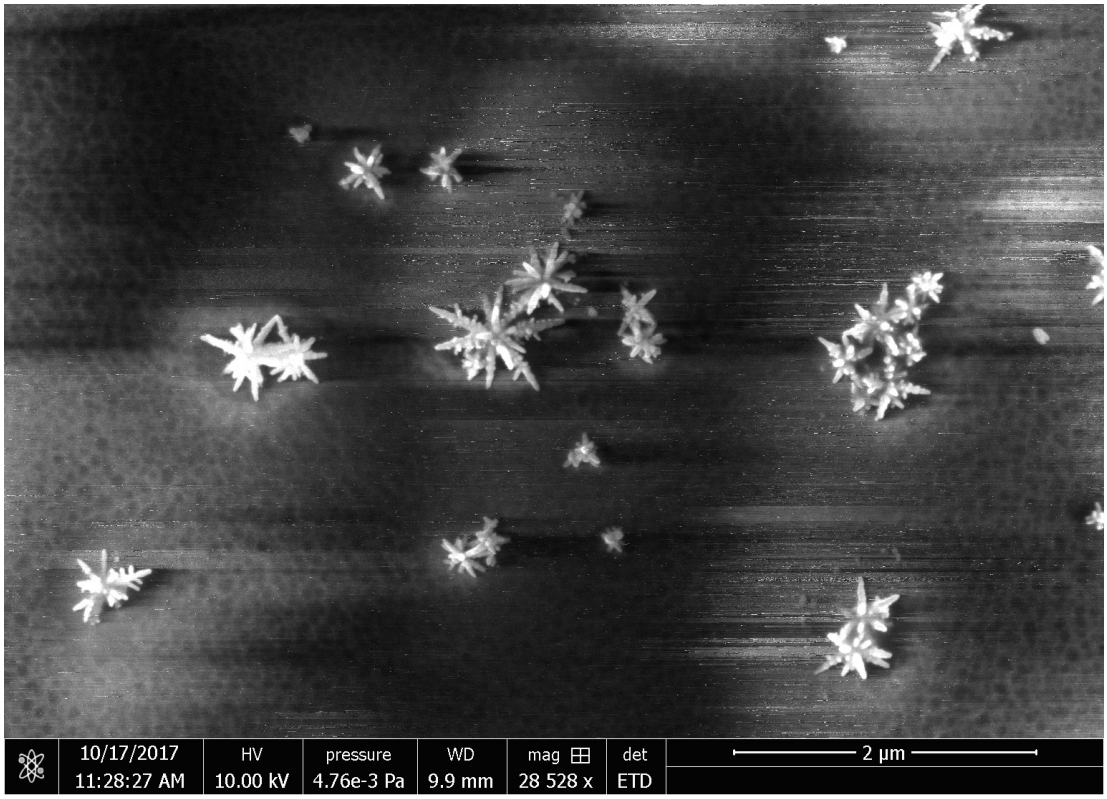

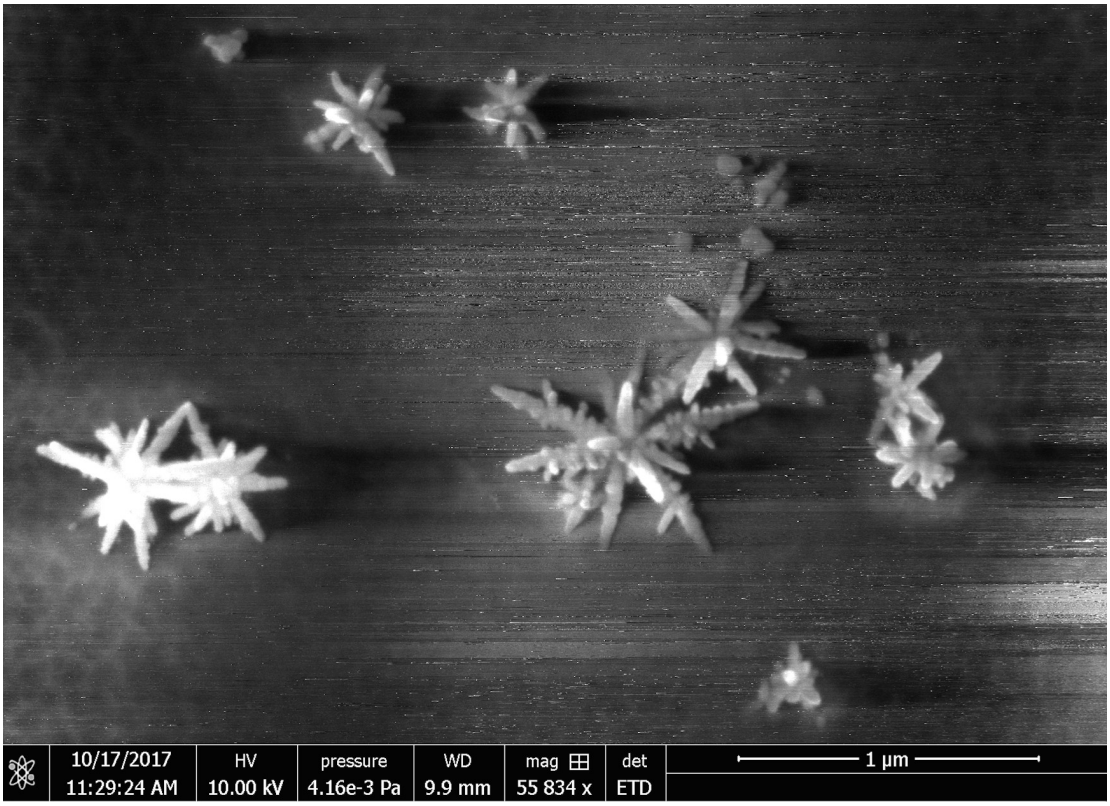

Figure 5.6. SEM of silver nanostars (AgNS) as synthesized on silica at 28528X and 55834X.

Due to prior knowledge of silver nanostars being capable of SERS detection, it was explored how effective the particles would be when performing these particular procedures.[79] There is a plethora of current research that delves into SERS effect when using silver nanoparticles, as well as gold nanoparticles, however, there is not as much investigation into the silver nanostar morphology compatibility.

Depositing the silver nanostars proved difficult. Different methods were attempted including bar coating, dip coating, spray coating as well as spin coating. Spray coating was applied in multiple layers to identify if the number of layers would affect the image or the efficiency of the inverse opal. Between one and ten layers were spray coated to see if there were any substantial differences, but it seemed as though spray coating would not necessarily coat the

substrate evenly, **Fig 5.7**. The silver particles appeared to cover the surface without infiltration of the porous template and instead create a new even layer on top of the existing film.

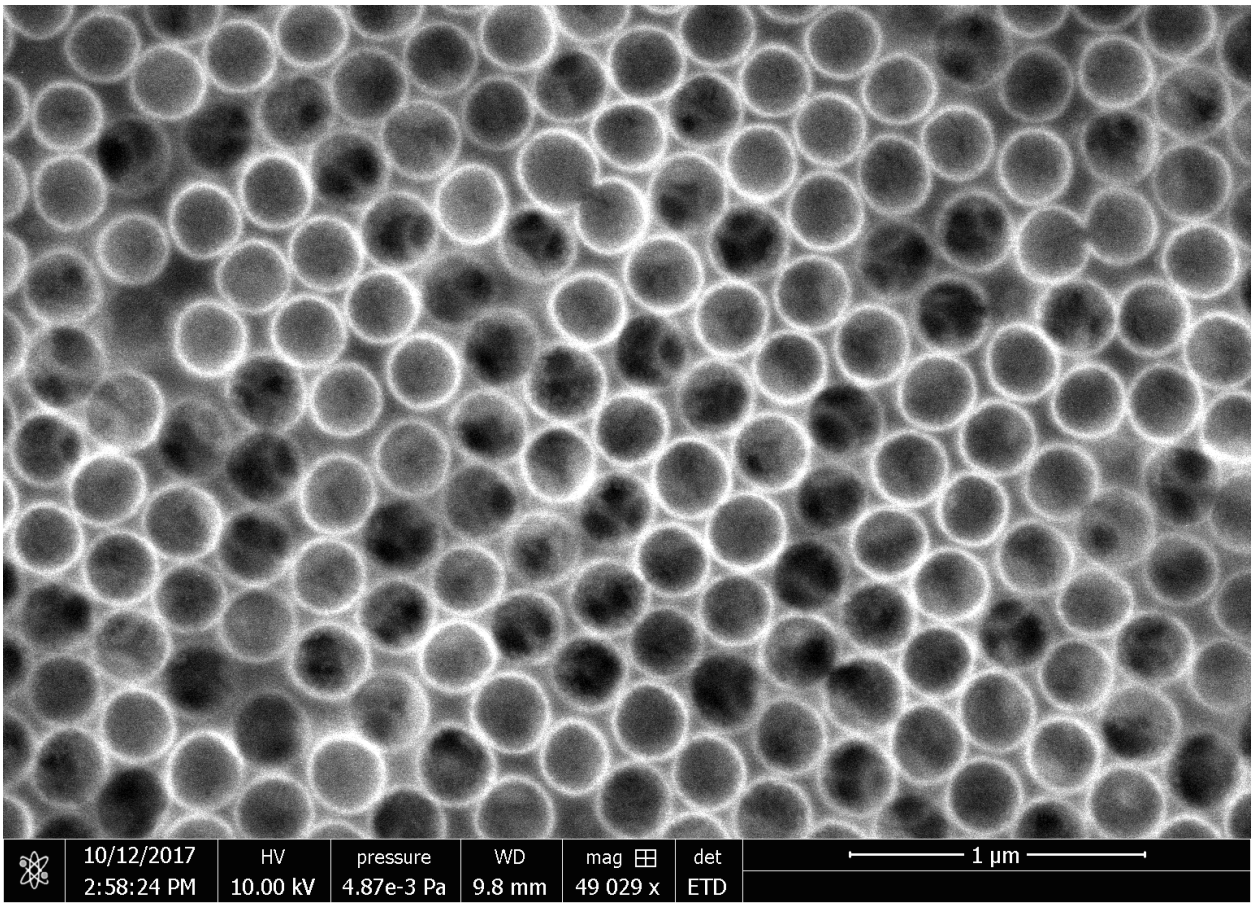

Figure 5.7. SEM image of inverse opal with two layers of AgNS spray coat deposition.

Though the SEM image looks quite different at first take, the original honeycomb pore shape can be seen if looking a bit longer at the image. It appeared as though the nanostars were coating the flat even surface rather than depositing within the pore craters. This creates for the glowing, circular result that can be seen in **Fig. 5.7** due to the conductivity of the silver present which also begins to distort the image.

A separate issue with this method resulted in the inadequate uniformity of the nanostars, **Fig 5.8**. Despite the AFM image that obtain only consisting of one spray coat layer, there are still aggregates of nanostars in a non-uniform pattern. This prohibits the nanostars from entering the pore and will prevent it in the future. As the clusters aggregate and build up on the smooth surface, entry access to the pores will continue to be blocked.

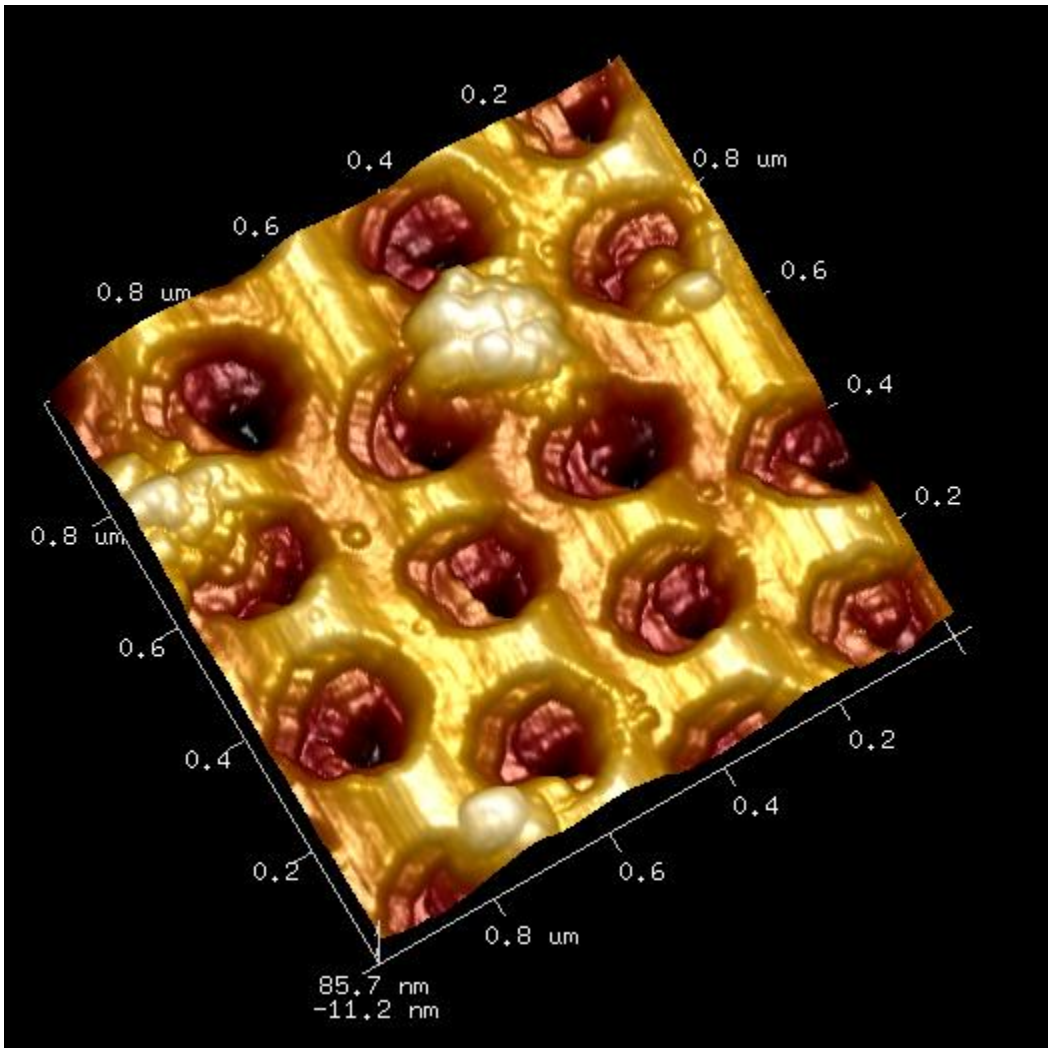

Figure 5.8. AFM image of inverse opal template with one layer of silver nanostar spray coat deposition.

Although the spray coat deposition method was not quite as refined as intended under optical imaging, the substrates were still analyzed. Upwards of five silver layers were deposited in this manner. The aim included the silver binding to the R6G when deposited which would allow for a SERS active substrate in this mechanism. However, the Raman spectrum proved that the R6G was undetectable via this substrate, **Fig 5.9**.

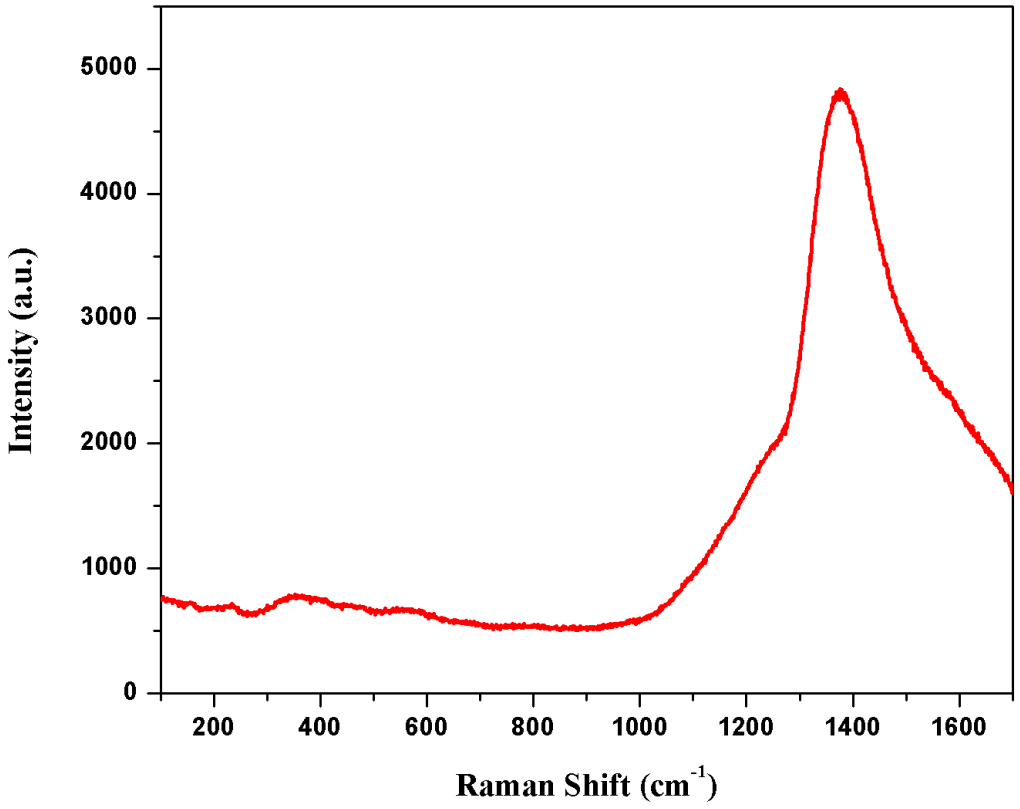

Figure 5.9. Raman spectrum of an inverse opal template with 5 layers of silver nanostars deposited via spray coating deposition with 1 μM of R6G deposited.

It seemed that the five layers of silver monopolized the Raman spectrum with a large peak observed around the 1360 cm^{-1} mark. From the SEM **Fig 5.7**, the two layers of silver nanostar deposition via spray coating appeared to be slightly saturated. Instead, the same

substrate was attempted using only one layer of spray coated silver nanostars and using a higher concentration of R6G for differentiation, **Fig 5.10**.

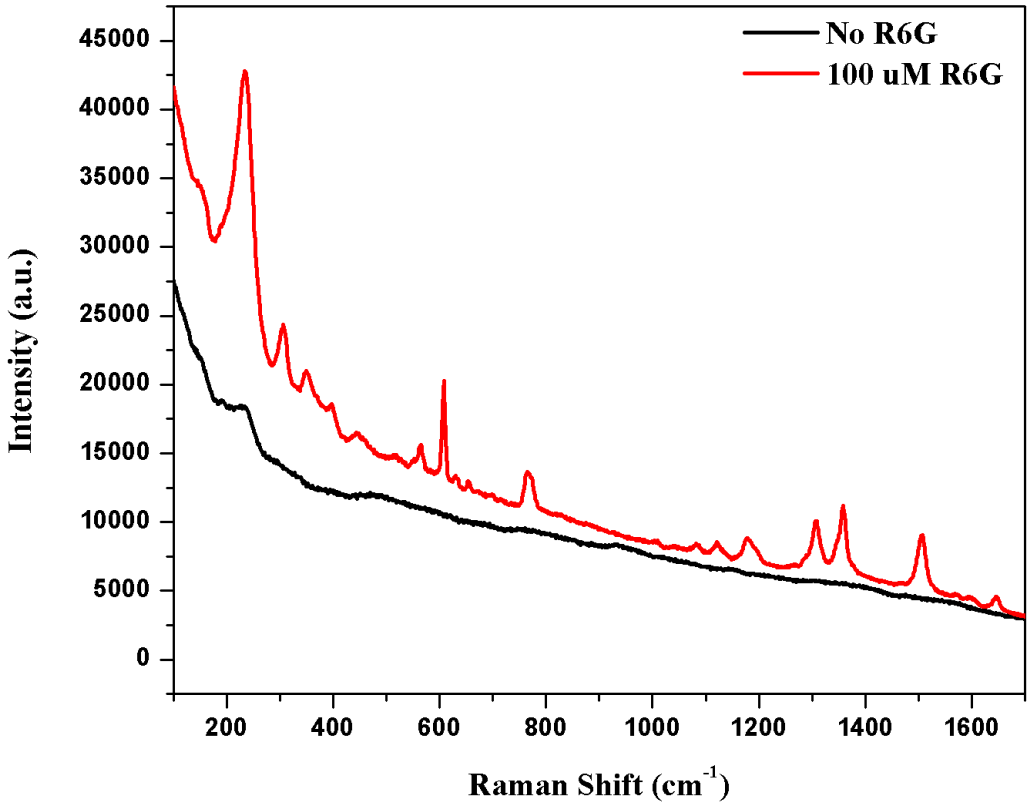

Figure 5.10. Raman spectrum of inverse opal template with one layer of silver nanostars (AgNS) using spray coat deposition versus the same substrate with 100 µM of R6G deposited.

The Raman exhibited a characteristic R6G spectrum when using the 100 µM concentration. Important to note that this is a much higher concentration than previously used. However, this was not as intense of a spectrum as some current research has shown when solely using silver at lower concentrations. This implies that there may be some sort of diminishing effect when the inverse opal template is added to the mix rather than enhancement. Although the R6G was detectable, it was not nearly as effective as other methods currently in use throughout other research and therefore not a viable method.

Since spray coating deposition was not effective in dispersing the nanostars within the pores, spin coating was attempted. Again, layering the nanostar material was observed to identify if any number of coatings was more effective and efficient than others. When observed under SEM, it appeared that five layers of spin coating was more dispersive of the nanostars and achieved more successful pore infiltration, **Fig 5.11**. It was thought that spin coating may help in the even dispersion of particles more so than the spray coating deposition method.

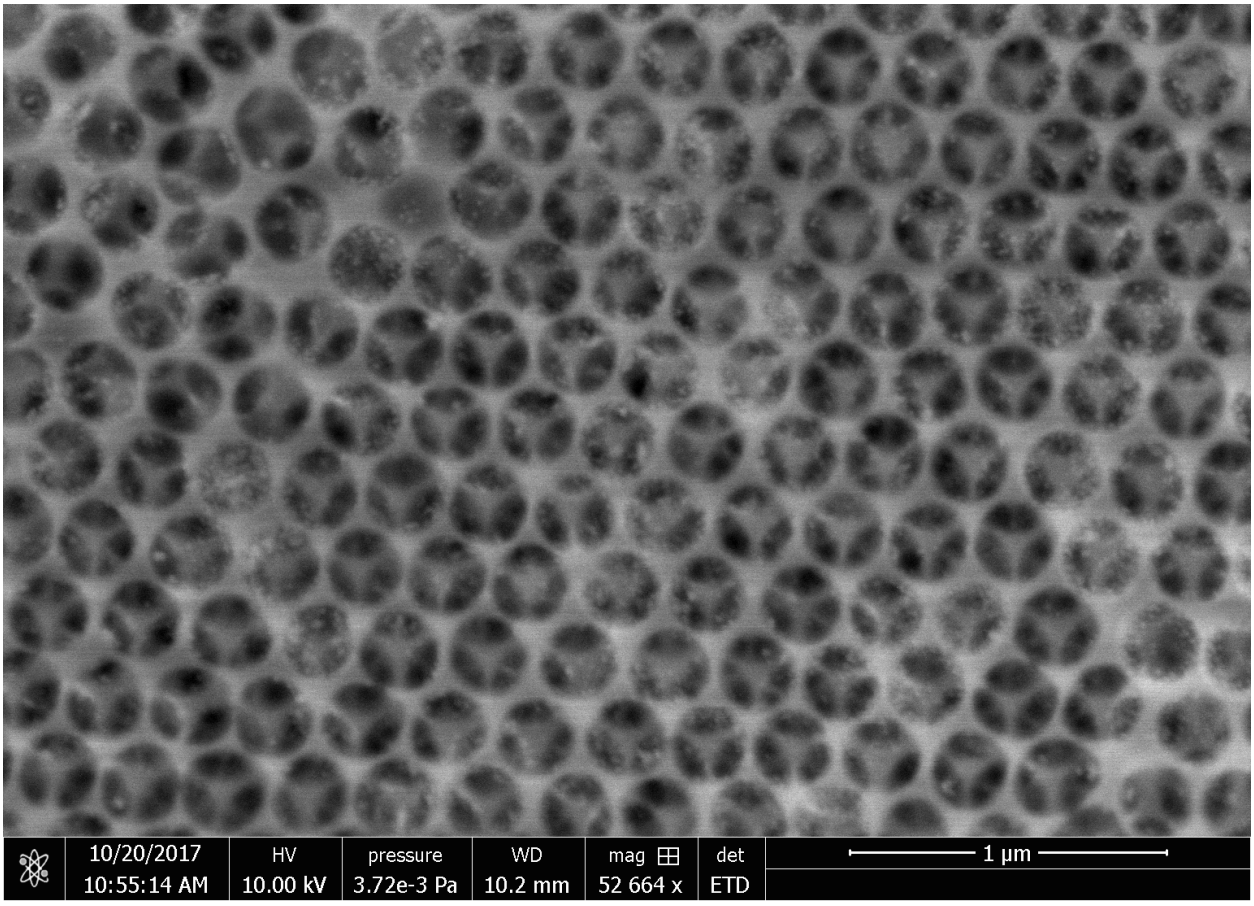

Figure 5.11. SEM image of five layers of AgNS spin coated onto inverse opal template.

Using the spin coat deposition, the nanostars were slightly more dispersed into an even format. The downside to this deposition method was that there did not seem to be large enough

deposits of the silver throughout the substrate. When the layering was increased, saturation and aggregation occurred which prevent the silver from infiltrating the pores properly, the same issue with spray coating that was seen earlier. Ultimately this method seemed more promising than spray coating but resulted in a very similar problem.

According to the Raman, the spin coat deposition did not appear to be more effective in the detection of R6G, **Fig 5.12**. In absence of R6G, the spectrum looked more detailed than when in R6G presence. In presence of 10 µM R6G, there was a shift in the spectrum. Although subtle, some peaks could be identified and appointed to R6G. Unfortunately, this was not the most effective method in terms of R6G SERS active sensors.

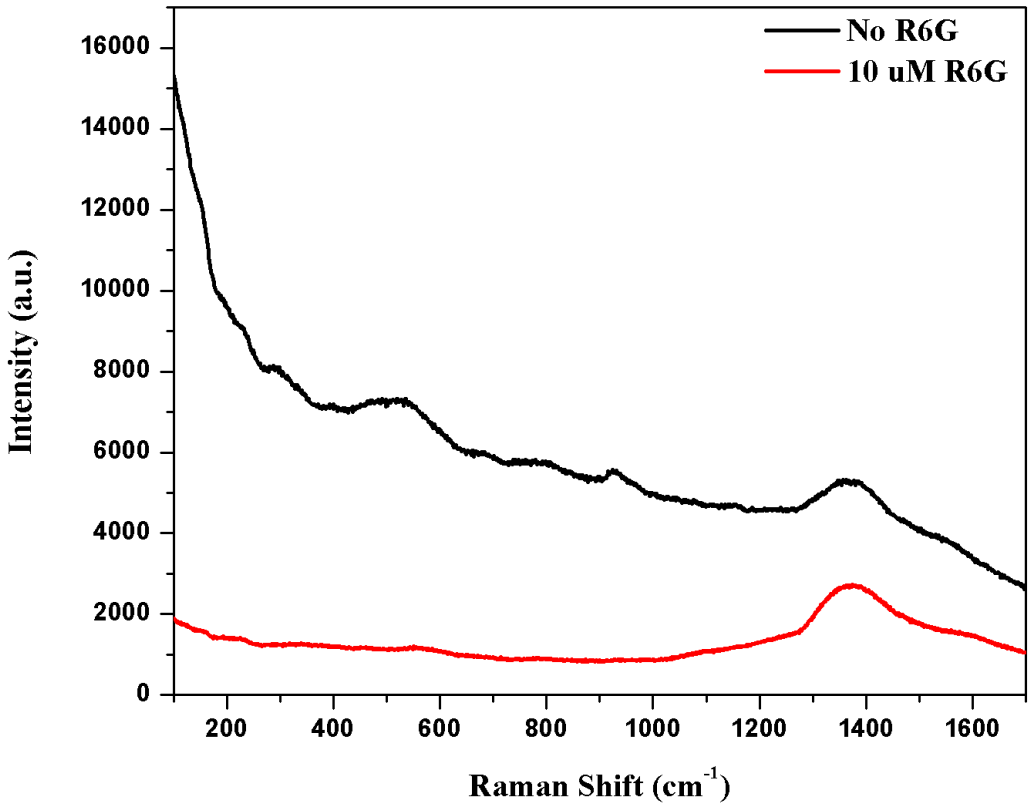

Figure 5.12. Raman spectrum of inverse opal template with five layers of silver nanostars (AgNS) deposited via spin coat versus same substrate with 10 µM R6G deposition.

From these results, it was evident that PMMA was not a fit when investigating a SERS active substrate. Although inverse opals manipulate light and refractive indexes making for a seemingly perfect Raman sensor, these studies proved that in this method it was ineffective. It was hypothesized that maybe using similar precursor material but removing the inverse opal substrate could have potential for SERS activity. The important aspect to investigate remained how to make the silver nanostars more capable than they are independently in current methods.

CHAPTER VI: MSN-AGNS SERS SUBSTRATE FOR R6G DETECTION

6.1. MSN as a SERS Enhancement Concept; AgNS SERS Substrate Methods

To take things a step further, there is no current research investigating Mesoporous silica nanoparticles (MSN) as a SERS probe. By combining these two substrates, it was questioned if a SERS active probe could be developed that provided more efficient results than current techniques on the market. Though MSN is not widely credited for Raman research, the refractive indexes and ability to manipulate light seemed suitable for research with the SERS aspect. It was a similar hypothesis as the silver/inverse opal material, however this silver particle SERS material seemed to potentially be more viable. Thus, it theoretically seemed possible to create a more efficient and enhanced silver SERS effect with MSN in addition.

Rhodamine 6G, or R6G, was selected as the target analyte for detection. R6G proves futile when acting as a target analyte. Not only does R6G display intense fluorescence independently, but also provides distinctive peaks which makes for easy recognition, proving suitable for investigation with SERS probes.[93] Since R6G is fluorescent on its own, this would also be helpful when calculating the enhancement factor since the analyte should be detected when at a higher concentration without other substituents present.

As previously described, silver nanostars (AgNS) were combined in a 1:1 ratio with 5 mM NaCl and left to stir for 10 min to incur aggregation. Post 10 minute incubation time, 0.5 mL of solution was pushed onto a pre-wet 1:1 H_2O:EtOH filter. This filter was left to dry, and then 5 mL of selectively concentrated R6G was pushed through the filter. Once the filter was dry as in no visible drops were apparent, but the filter was still damp, a Raman measurement was taken, **Fig 6.1**. Measurements must be obtained prior to complete dryness for best results.

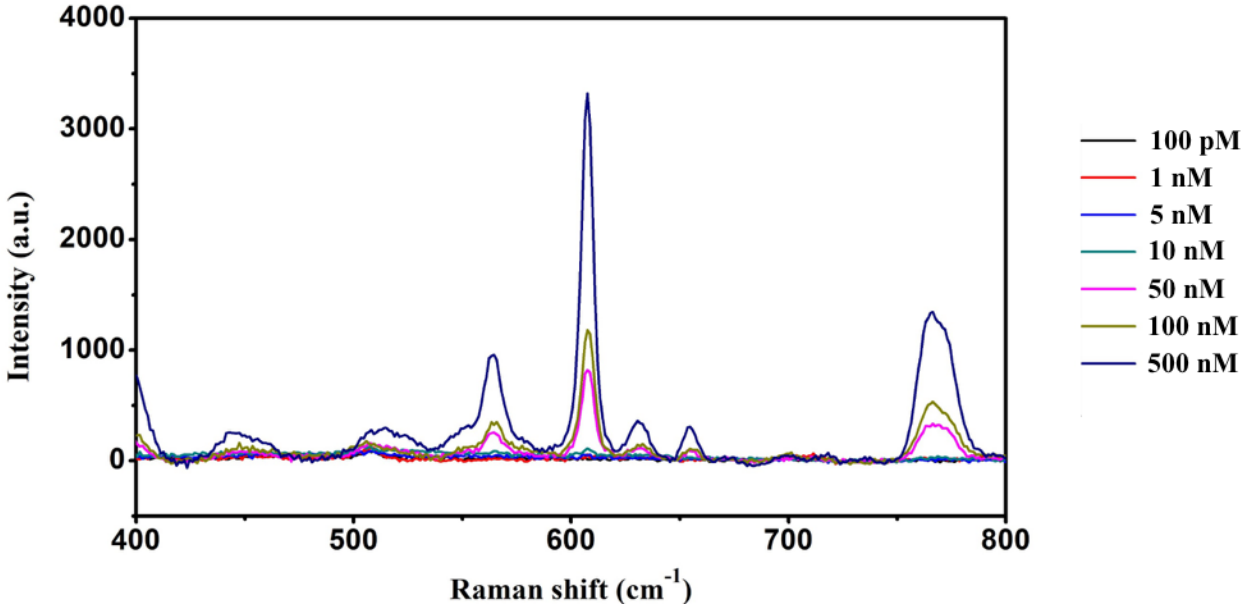

Figure 6.1. Raman spectra from AgNS substrates detecting R6G; 100 pM, 1 nM, 5 nM, 10 nM, 50 nM, 100 nM, and 500 nM.

Raman intensity at 608 cm^{-1} was used to identify a calibration curve. The Raman intensity was plotted against the concentration of R6G used, **Fig. 6.2**. It was clearly visible that there was a correlation between the concentration of R6G present and the intensity of the spectrum, particularly the 608 cm^{-1} peak.

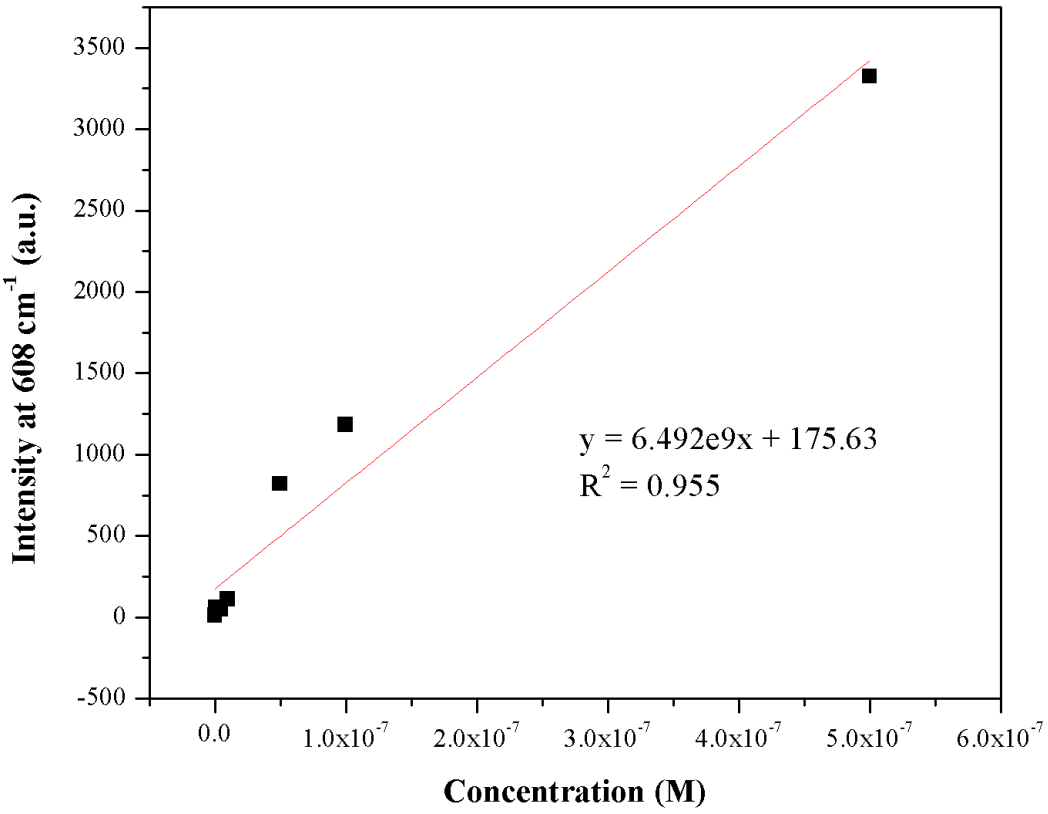

Figure 6.2. Calibration curve of Raman Intensity at 608 cm^{-1} of AgNS detecting various concentrations of R6G.

The results observed in **Fig 6.1** were taken using AgNS substrates. It is clear that there is a direct proportionality between the concentration and the intensity of spectrum, proven in **Fig 6.2**. Of course, silver nanoparticles of spherical morphology are known to be great SERS material. However, this sets the bar for new material to come in prove to be a better alternative.

6.2. R6G Raman Identification

To properly identify that this was the result of R6G being present, the peak at 608 cm^{-1} was used for confirmation. For added insurance, many peaks in the range of 100-1700 cm^{-1} could

be used, but generally 608 was the quickest and safest to identify, **Table 6.1**. Knowing which peak would be present based on the signature bending or stretching helped to pursue visualization of R6G presence when at minimal concentrations. From the tests of AgNS SERS, **Fig 6.1**, it was established that the lowest confirmed concentration of R6G was 5 nM when using these AgNS substrates.

Table 6.1. Vibrational modes of R6G SERS peaks actual versus literature.[94, 95]

Research Findings	Literature[94]	Literature[95]	Vibration Mode[95]
608	612	609	C-C-C in-plane bending
766	772	769	C-H out-of-plane bending[94]
1121	1127	1123	C-H stretching
1179	1187	1182	C-H in-plane bending
1306	1312	1310	C-O-C stretching
1358	1363	1361	Aromatic C-C stretching
1505	1509	1508	Aromatic C-C stretching, C-H stretching
1572	1575	1573	Aromatic C-C stretching
1647	1651	1647	Aromatic C-C stretching

Using current research findings in addition to literature, specific vibration modes can be assigned. The values within **Table 6.1** are critical peaks in R6G assignments. Using these measurements are incredibly useful in ensuring all R6G data presented in this paper is a result of R6G Raman characterization and not a result of a different material present or interferences.

6.3. MSN-AgNS Substrate Enhancement Versus AgNS Substrate

Further investigations were conducted to determine if MSN would cause an enhancement of R6G detection from the original AgNS substrate. As of now, there is no previous work with

MSN as a SERS substrate. A solution of 1:1:0.075 AgNS with 5 mM NaCl and MSN, respectively, was prepared and stirred for ten minutes to induce aggregation. Again, 0.5 mL was pushed through a pipette onto the pre-wet filter and left to dry. Once dry, 5 mL of concentrated R6G was pushed through and the measurement was obtained once surface had dried but the filter was still considered damp, **Fig 6.3**. The main noticeable difference in this procedure was the inclusion of MSN material into the AgNS/aggregator solution.

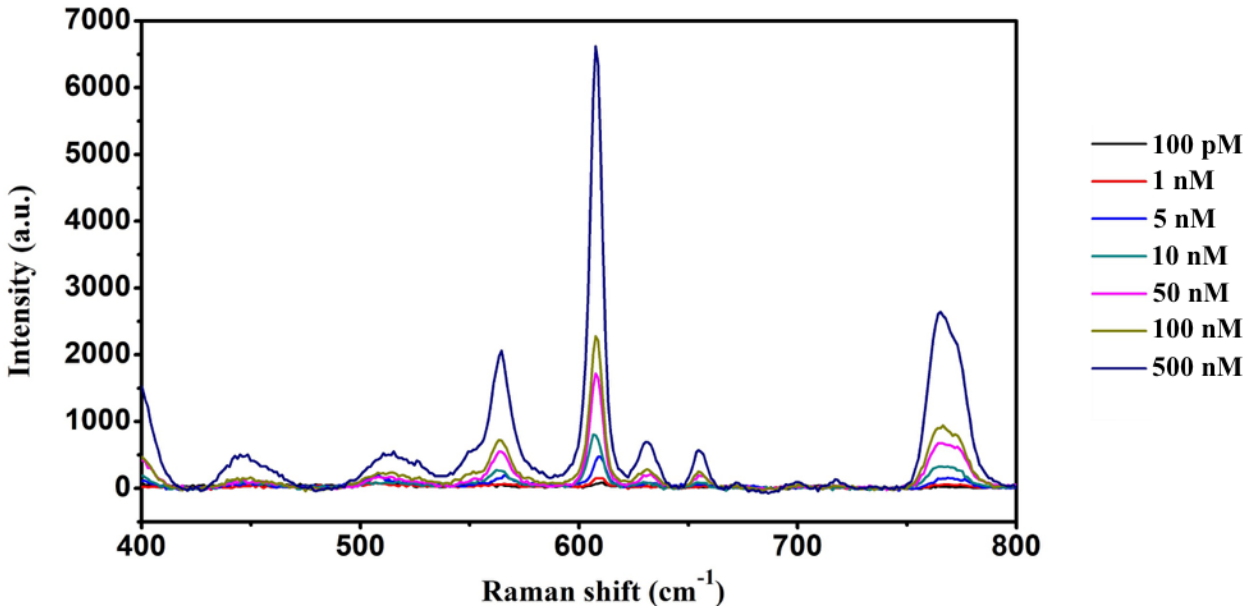

Figure 6.3. Raman spectra of MSN-AgNS SERS substrate detecting R6G; 100 pM, 1 nM, 5 nM, 10 nM, 50 nM, 100 nM, and 500 nM.

The results of MSN-AgNS SERS substrates measuring the same concentrations as the AgNS SERS substrates clearly demonstrate the significant difference in intensity values while also still demonstrating dependence between R6G concentration and 608 cm^{-1} peak intensity, **Fig. 6.4**. First and foremost, the intensity differed vastly when MSN was present versus in absence. Another noticeable difference here is that the AgNS-MSN substrates are capable of

quantifying a lower concentration of R6G than the AgNS substrates are, which will be discussed in depth.

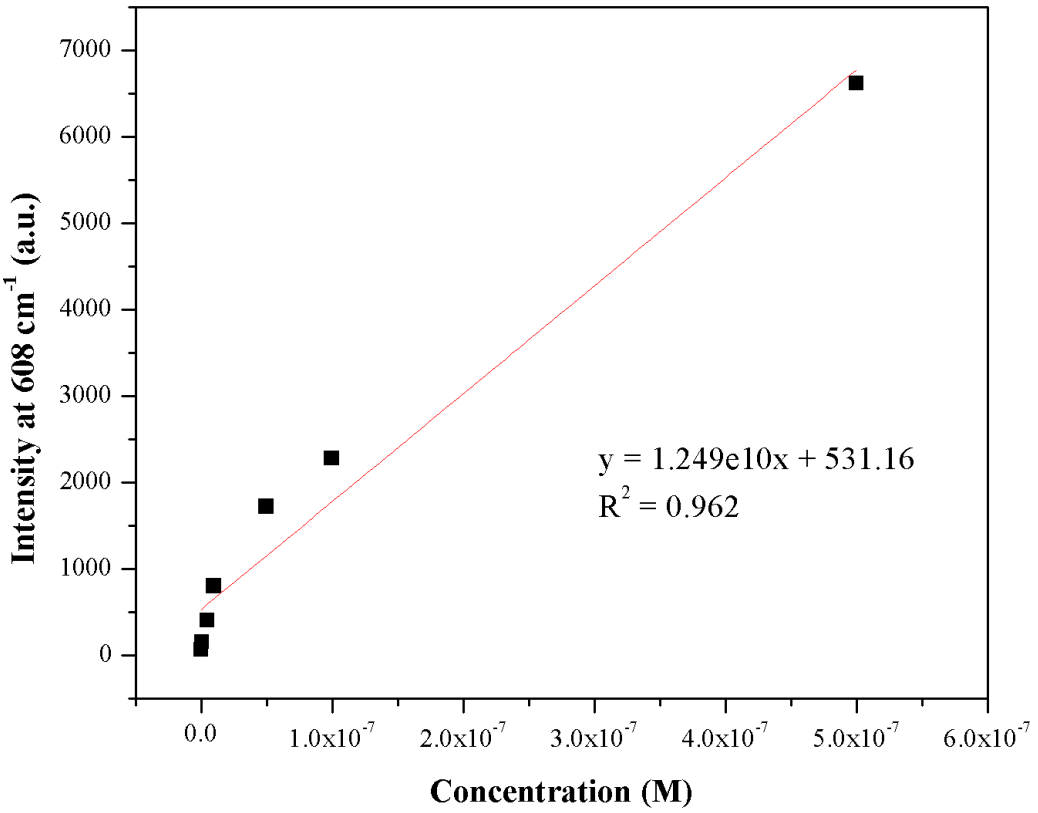

Figure 6.4. Calibration curve of Raman Intensity at 608 cm^{-1} of MSN-AgNS detecting various concentrations of R6G

To give the larger picture, **Fig 6.5 a)** demonstrates full range Raman spectra between 100 and 1700 cm^{-1} of MSN-AgNS detecting R6G. Further breakdown by examining a close up of 100 pM and 1 nM in **Fig 6.5 b)** shows the results were positive for R6G.

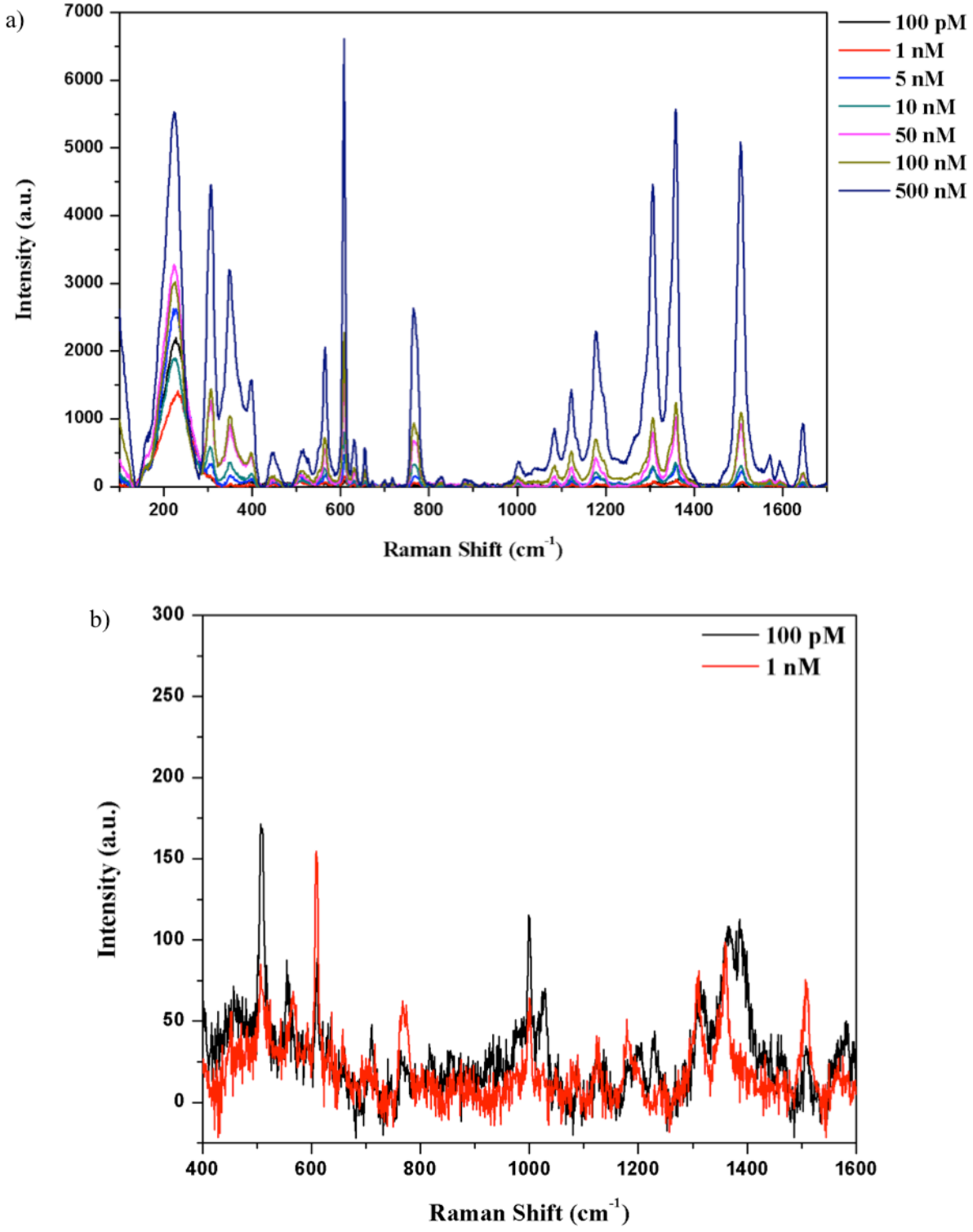

Figure 6.5. a) Raman spectra of MSN-AgNS detecting 100 pM, 1 nM, 5 nM, 10 nM, 100 nM and 500 nM R6G on full range of 100-1700 cm^{-1}. b) Raman spectra close up of 1 nM and 100 pM R6G via MSN-AgNS substrate.

Once MSN had been added into the substrate configuration, not only was the detection limit much lower than if it were absent, but the intensity values also significantly increased. When MSN was absent, 500 nM R6G was detected to have intensity of 3322 a.u. However, once MSN was combined, 500 nM R6G resulted in intensity of 6618 a.u. Detection limits alone proved the ability and effectiveness of MSN presence in solution. Without MSN, the detection limit was 5 nM R6G, yet when MSN was present fluorescence was detected as low as 100 pM of R6G. This is a 50 fold decrease in the concentration of R6G that is now distinguished from the substrates without MSN, ultimately creating a much lower detection limit and a larger detection range.

Aside from characterization, visible properties could be observed from the addition of MSN to the substrate, **Fig 6.6**. When MSN was present on the membranes, the substrate resulted in less cracking of the silver solution and tended to stay "wet" looking for a longer period of time. When MSN was not present on the substrates, there was more of the white membrane that could be visualized and did not give the same appearance of a flat, smooth, covered surface. It was also noted then when observing in close distance, the MSN-AgNS substrates displayed a pink circle of where the R6G has passed through down to ~10 nM R6G that could be seen with the naked eye the. If observing the AgNS substrates, the R6G was not quite as visible and generally reserved to the 500 nM concentration or on occasion to the 100 nM substrate. It is suggested that the MSN presence enhances SERS activity due to the porous structure which contributes to the SERS mechanism via altering the refractive indexes.

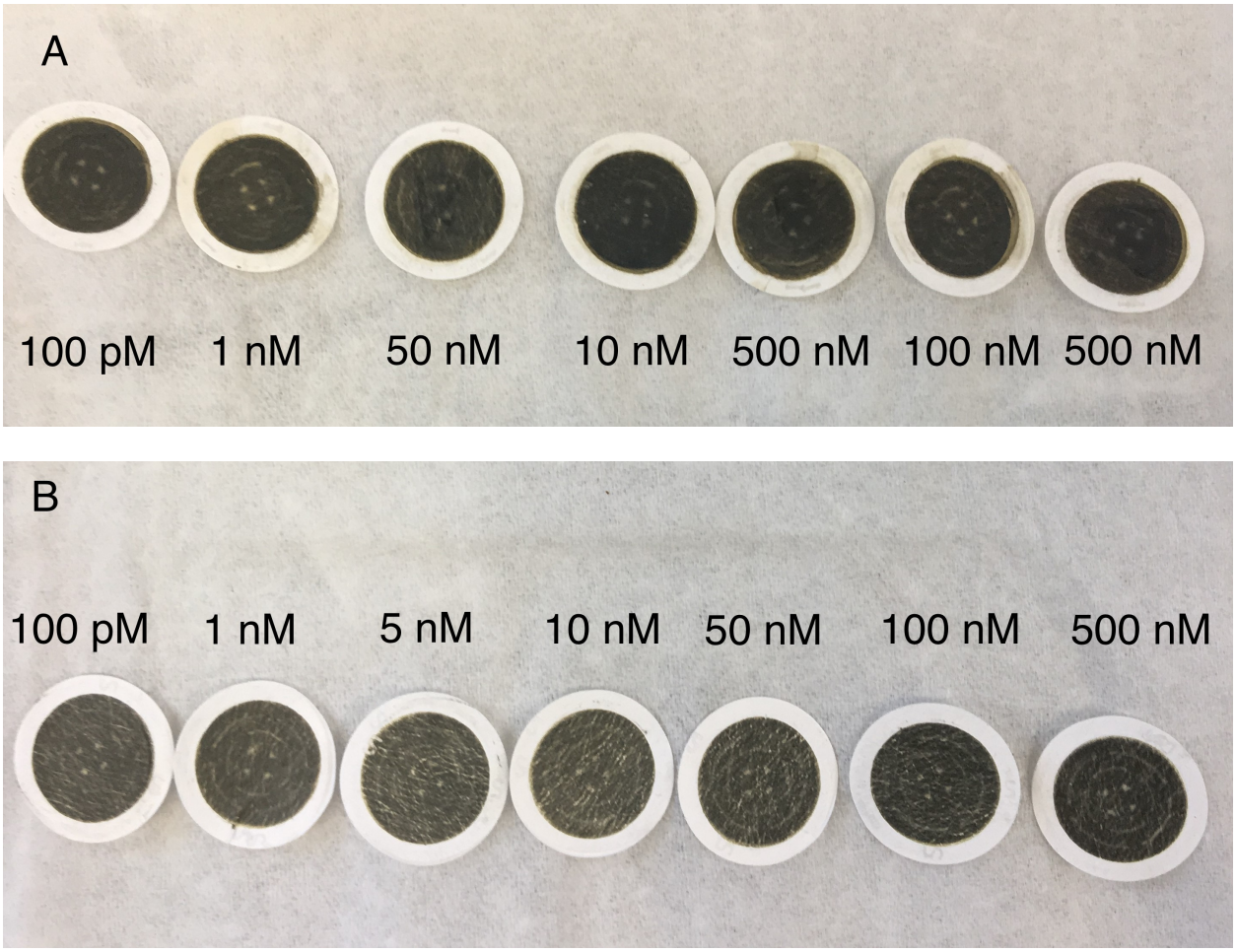

Figure 6.6. a) Substrates made with MSN-AgNS prior to R6G addition and b) substrates made with AgNS prior to R6G addition.

6.4. Enhancement Factor of Substrates with MSN Present

The differentiation between MSN presence and absence resulted in the ability to calculate the enhancement factor. This is particularly useful in determining if this method is efficient not just in presence of MSN, but as well as if it is regarded as a higher efficiency substrate comparative to other SERS methods. Enhancement factor is a calculation that allows quantification of the SERS amplification and is described as;

$$EF = (I_{SERS}/I_{Raman}) \times (N_{Raman}/N_{SERS})$$ **Equation 1**

This equation distinguishes I as intensity height and N as number of molecules of R6G. [95] To calculate for N, we can use the following equations;

$$N_{SERS} = \eta \times N_A \times V \times C_{SERS} \times (A_{laser}/A_{SERS})^{80}$$ **Equation 2**

$$N_{Raman} = N_A \times V \times C_{Raman} \times (A_{laser}/A_{Raman})^{80}$$ **Equation 3**

For better visualization, an enhancement factor was calculated for both AgNS substrates as well as MSN-AgNS substrates. For AgNS substrates that lacked MSN, an enhancement factor of 4.04×10^5 was estimated. As for substrates with MSN-AgNS, the enhancement factor was computed to be 1.12×10^6. The resulting difference between MSN-AgNS and AgNS substrates is nearly a full magnitude larger. Generally, silver SERS substrates can result in an enhancement factor ranging from 10^5 to 10^7.[96]

N_{Raman} for equation 3 is regarded as 20 mM of R6G when deposited on a blank filter membrane. Since the membrane is blank, the intensity should be small but still recognizable as the characteristic spectrum of R6G, due to R6G's innate fluorescence, **Fig 6.7**. This method would result in an intensity for the R6G which could then be utilized and ultimately converted to find the N_{Raman} and give rise to the enhancement factor.

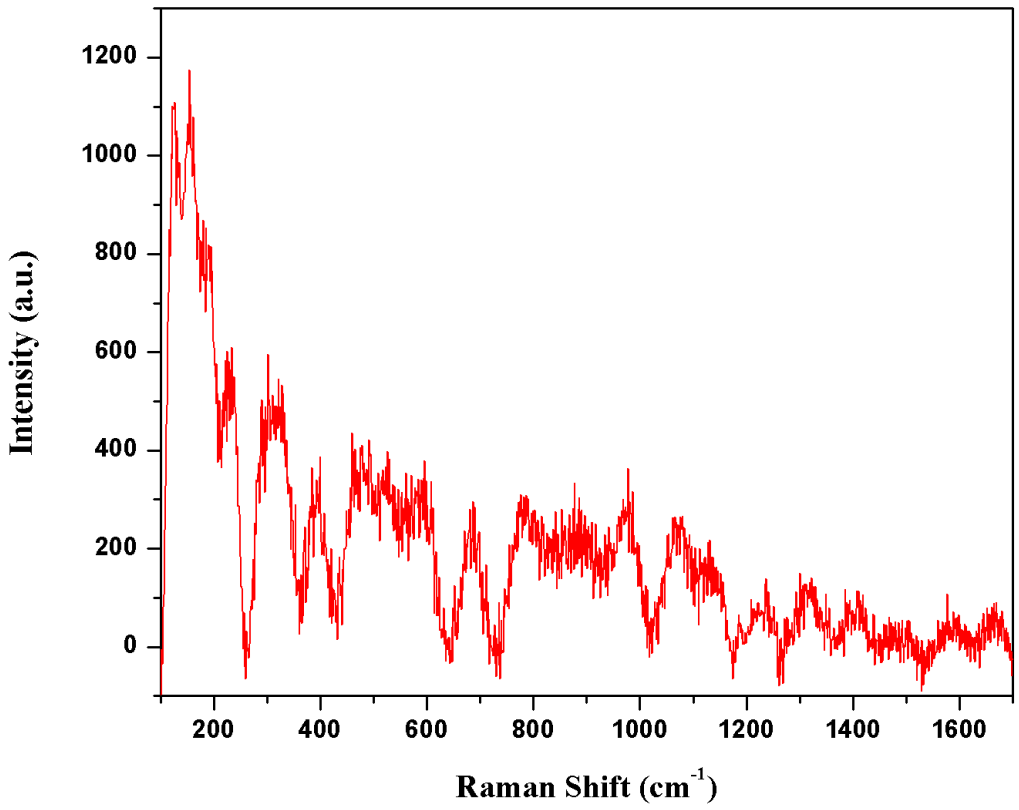

Figure 6.7. Raman spectra of 20 mM R6G on plain filter membrane.

To ensure that the measurements were that of R6G, aside from using characterization of specific bending and stretching, background measurements were observed as well, **Fig 6.8**. This would help identify what fluorescence, if any, the background solvents, materials and membrane could provide. Ultimately, this would help ensure that any fluorescence measured when using synthesized substrates was purely caused by the SERS enhancement factor relationship between materials and prove detection of the target analyte.

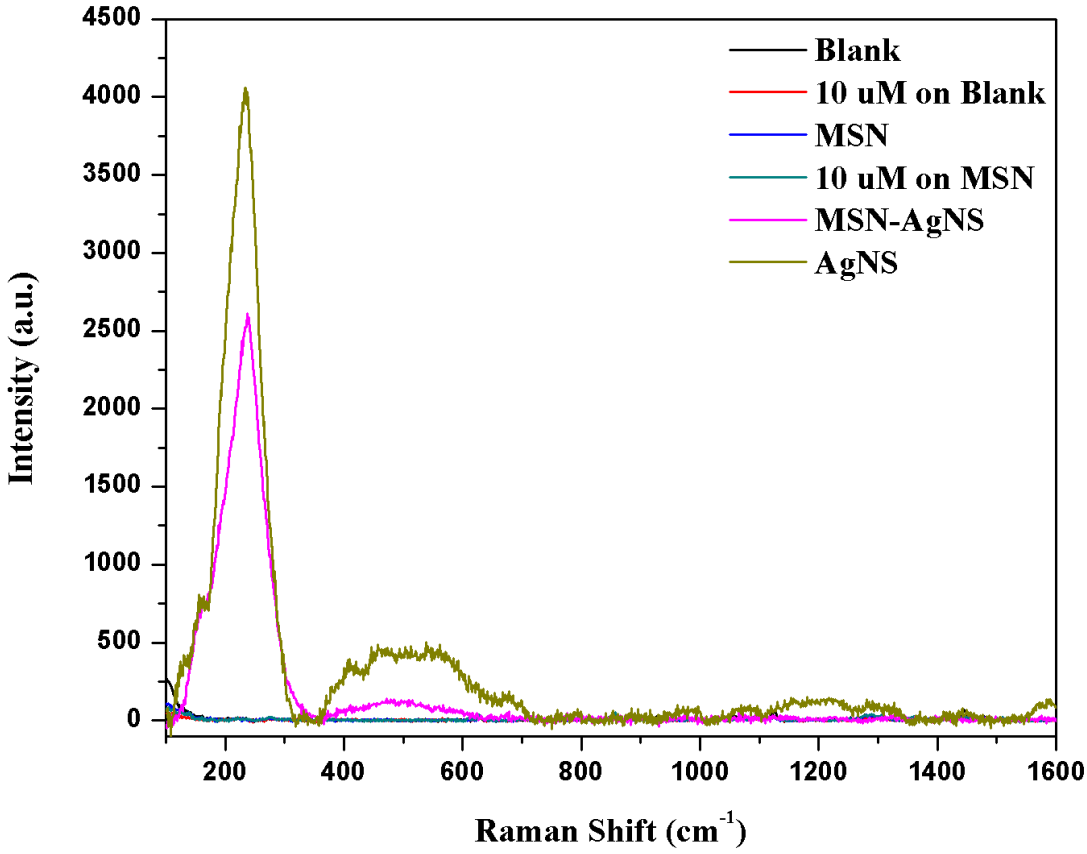

Figure 6.8. Raman spectra of blank filter membrane, 10 µM R6G on blank filter membrane, MSN on filter membrane, 10 µM R6G on MSN filter membrane, MSN-AgNS on filter membrane, and AgNs on filter membrane.

It can be seen that all 6 variations of background do not contribute any signal at the R6G characteristic peaks. The peak at 235 cm^{-1} is due to the presence of silver nanostars. Silver peak is only visibly intense when AgNS is used, either on its own or in the presence of the MSN-AgNS substrate and is not considered to interfere with R6G characterization. This ensures that all measurements incurred are solely based on the SERS mechanism involved rather than any precursor material attribution.

6.5. Current Marketed SERS Substrate R6G Detection

It has been proven that the addition of MSN to the AgNS substrates significantly increases the intensity via Raman for R6G detection. However, these results needed to be further investigated against current market materials. Ocean Optics™ makes SERS substrates which can be utilized if dealing with analytes that are active in this regard. SERS substrates can be purchased with either silver or gold nanoparticles. Using the silver nanoparticle SERS substrate, 15 µL of a 10 µM R6G was dispensed and let dry prior to Raman measurement, as stated in the procedure on the purchased material by the distributing company, **Fig 6.9**. This would give an idea if there was any increased function when incorporating MSN to silver nanoparticle SERS material.

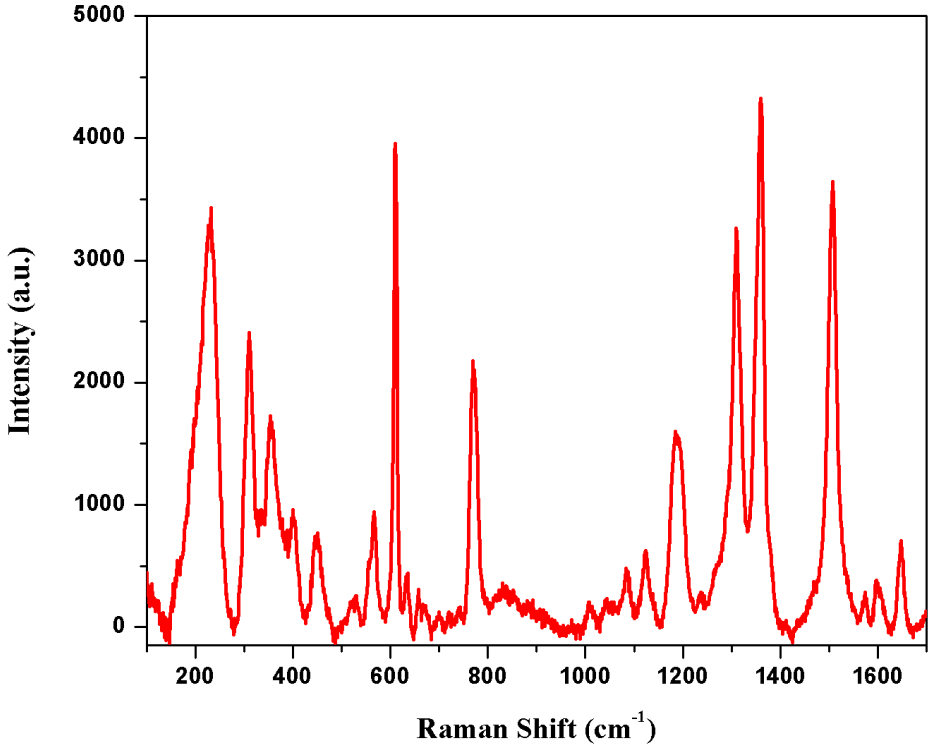

Figure 6.9. Raman spectrum of 10 µM R6G on Ocean Optics™ SERS substrate, silver nanoparticles.

From **Fig 6.9**, peak 608 cm^{-1} results in intensity of 3956 a.u. This is far less intense even when measuring a higher concentration of R6G versus the 500 nM detection of R6G via the MSN-AgNS substrate. This data ensures that the aggregation, pore size, and combination of material make a SERS active substrate while demonstrating that the detection of R6G is much more efficient under this guise.

6.6. Ratio of Precursor Materials to Form MSN-AgNS Substrates

Ultimately, before this procedure was found to enhance signal of R6G, several other variables were tested including; ratios, pre-wetting solution, pore size of membrane, solution used for aggregation, membrane holder style/make, as well as if the nanostars were significantly more efficient than the nanospheres. The ratio was the most difficult aspect of the procedure to reproduce. At first a ratio of 1:1:0.2 of AgNS:NaCl:MSN was used, which exhibited too much inconsistency, **Fig 6.10**. When multiple trials were performed, the variability of the characterization was obvious and made for varied results.

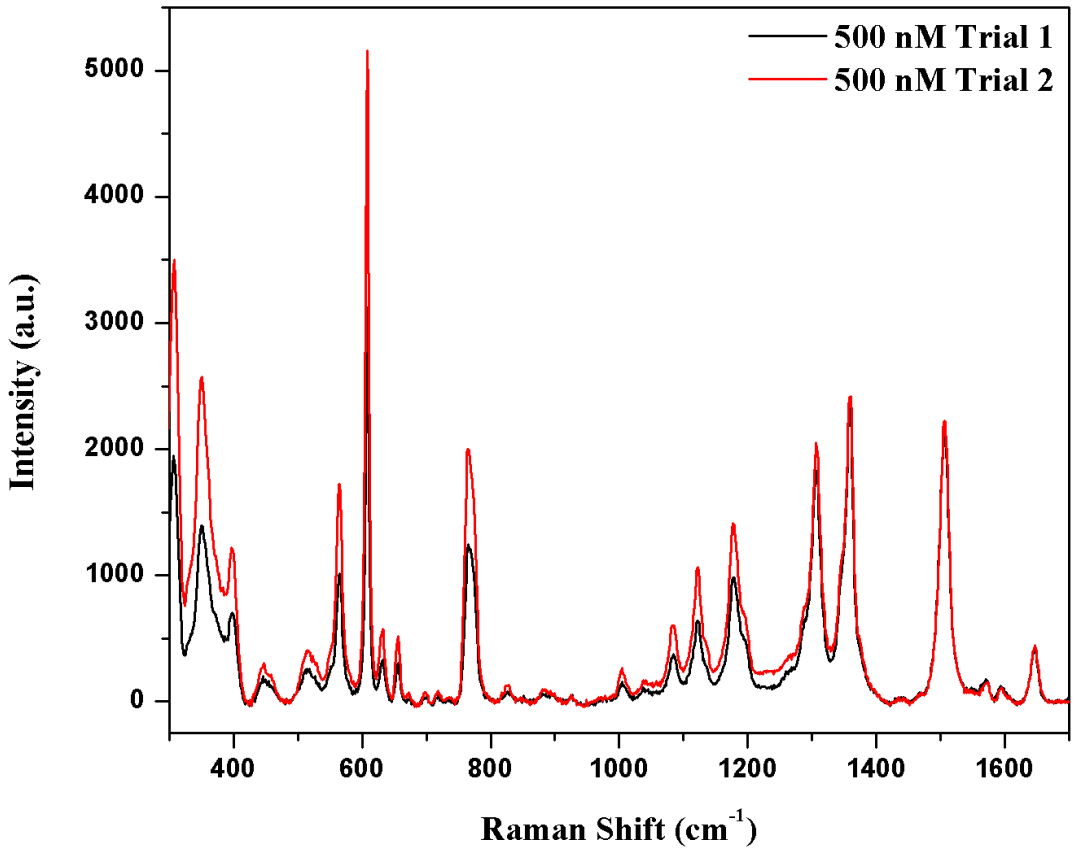

Figure 6.10. Raman spectra of 500 nM R6G on MSN-AgNS substrate using 1:1:0.2 of AgNS:NaCl:MSN.

Using **Fig 6.10**, specifically looking at the peak of 608 cm^{-1}, the differentiation can be visualized. However, these measurements were secured using the same procedure and the same R6G concentration. From this, it was decided that a 0.2 ratio of MSN in solution was too concentrated and caused discrepancies among various locations on the same filter. Though this is of course plausible regardless of ratio, it is ideal that the measurements among locations is significantly closer in value than nearly the 2000 a.u. difference seen here. It is a possibility that the MSN is contributing to an enhancement factor on its own and when present in too large of a concentration, can cause variability. A ratio of 0.1 MSN was also applied but did not yield as

significant of results as the ratio utilizing 0.075 MSN did. The 0.075 yield of MSN provided enough MSN to cause smoothing and reproducibility without causing too much cracking due to the viscosity of the material which would lead to fluorescence intensity variability.

Silver nanoparticles (of spherical morphology) were examined to identify how much of enhancement nanostars could give comparatively. The method of synthesis for the nanospheres was a procedure adapted and modified by Gao *et al*. of the original Lee-Miesel method.[83, 84, 85] Although it proved capable of detecting R6G, it was at a much lower efficiency than nanostar morphology, **Fig 6.11**. The large peak near 235 nm is due to the silver nanosphere material. Since there is such large intensity derived from this silver material, the R6G spectrum became overshadowed and difficult to correctly identify. There was also inconsistency with the correlations of concentration or intensity, as exhibited by the 500 nM not contributing to the most intense R6G spectrum. If these results worked in ideal methods, the 500 nM measurement would yield the largest response.

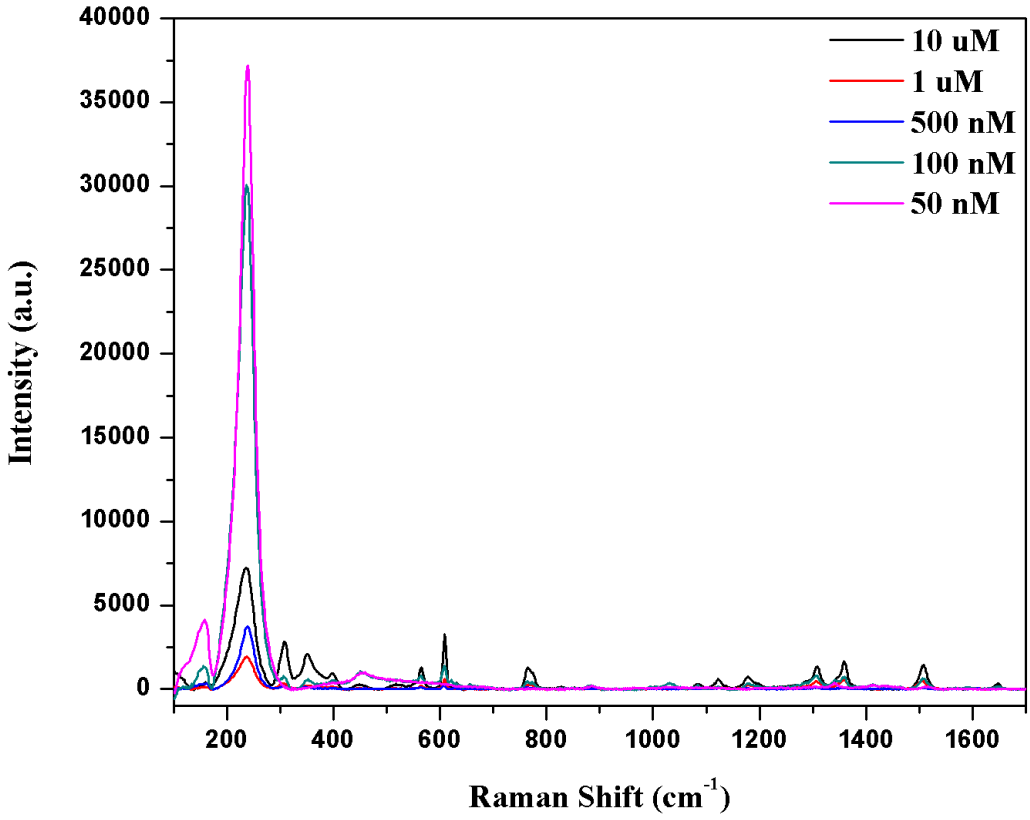

Figure 6.11. AgNP (spherical particles) detecting 50 nM, 100 nM, 1 µM and 10 µM of R6G.

Aggregation chemicals were observed to see if changing the chemical would alter any mechanism or overall effect. A chemical would be added to the silver nanoparticles (stars) to aggregate the material, the chemical either being sodium chloride or sodium citrate. When the solution was ultimately dispensed onto the membrane, this would cause large clusters of the silver to stick together. This method would form “hot spots” and aid in increasing the effectiveness of the SERS mechanism as well as uniformity.

Sodium citrate and sodium chloride were examined for aggregation effects. Both sodium aggregators were used in the same ratio to silver nanostar particles (1:1) and left to incubate for the same time (10 min at RT). This allowed for the observation if one chemical would prove to be more competent than the other. Using the nanostars, the different aggregators were added and

left to incubate before being subjected to the membrane for R6G detection, **Fig 6.12**. The membranes were then subjected to 1 µM of R6G via normal protocol and observed via Raman to identify if the aggregator had an impact on R6G detection.

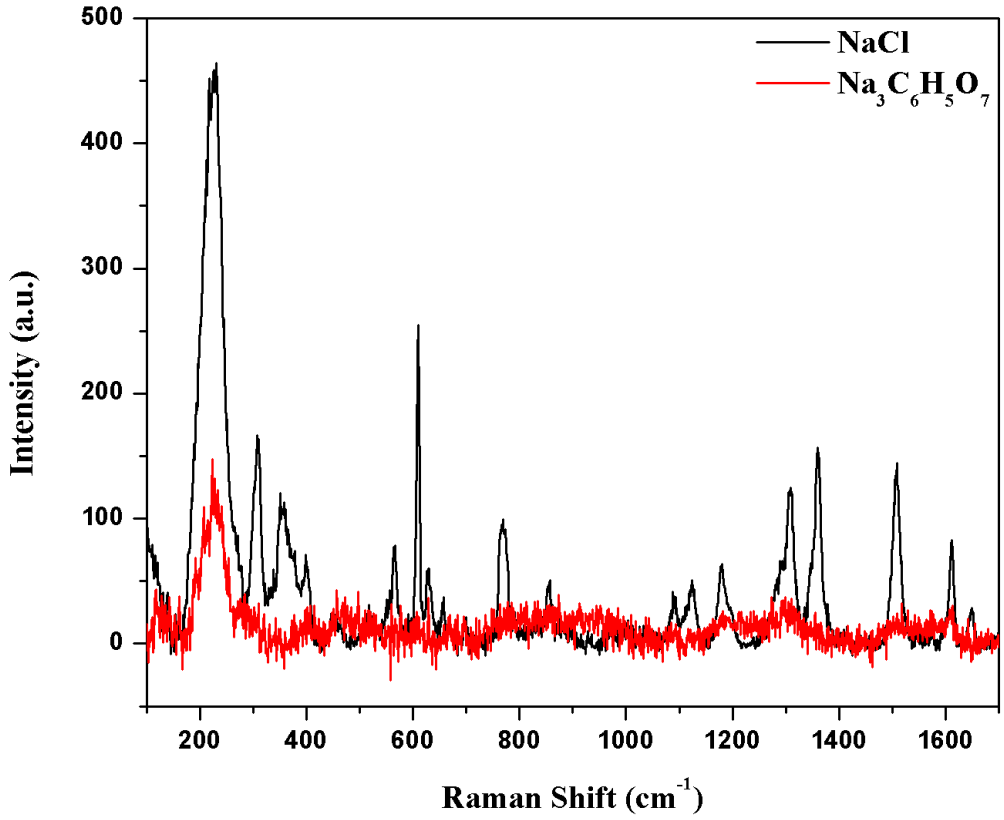

Figure 6.12. Raman spectra of 1 µM R6G detection using silver nanostars (AgNS) with aggregation chemical Sodium Citrate ($Na_3C_6H_5O_7$) versus Sodium Chloride (NaCl).

From the data in **Fig 6.12**, it was immediately confirmed that NaCl resulted in better aggregation opposed to $Na_3C_6H_5O_7$. Although the figure represents the same concentration of R6G, it is settled that when $Na_3C_6H_5O_7$ is added there is no visibility of R6G present. This allowed for the project to move forward knowing that NaCl was the best agent used. When using NaCl, the nanostars were clustering which allowed for hotspot formation and fundamentally

increased detection of R6G. Most likely this is due to the chlorine ion of sodium chloride causing agglomeration which the sodium citrate cannot cause due to the absence of a halogen ion.[97]

Aside from the chemical preparation, pore size of the membrane used could also potentially contribute to whether the substrate was more or less efficient. Two pore sizes were examined; 0.1 μm and 0.22 μm. Substrates were made using the pre-determined method designed as 1:1:0.075 of AgNS:NaCl:MSN. Again, the design was kept the same as to better determine which pore size was more advantageous under a particular set of circumstances. It was noted that on the 0.22 μm pore size, there were more visible cracks – which may not necessarily be such a negative aspect and was still characterized. Although the nanoparticles were approximately 50 nM in average diameter, the agglomeration cause by the presence of salt could potentially cause variations between the two pore sizes that otherwise could not be accounted for. The two pore sizes were enhanced under Raman, **Fig 6.13**. The membrane was subjected to 1 μM of R6G to identify if pore size had an effect on R6G detection.

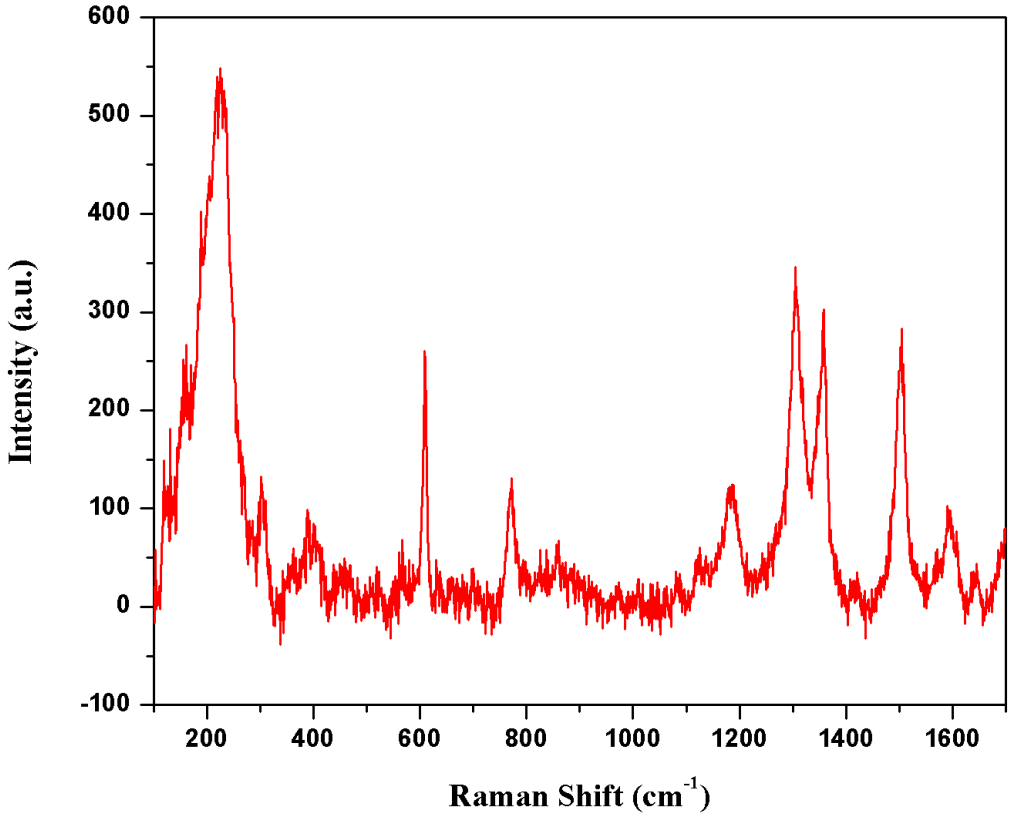

Figure 6.13. MSN-AgNS detecting 1 µM R6G on a 0.22 µm pore membrane.

The peak at 608 cm^{-1} resulted in detecting 1 µM R6G with intensity of 260 a.u. When the same substrate was deposited on 0.1 µm pore size (**Fig 6.3**) using only 500 nM R6G, there was nearly a 25 fold increase. It was immediately clear that pore size did play an impactful role on detecting R6G. In this particular case, concentrated R6G (which was not used in a full work up study due to being too concentrated) was far less detectable on 0.22 µm pore membranes than lower concentrated R6G was on 0.1 µm pore size. Most likely, these results are due to the pore size being too large for the nanostars even after aggregating and the clusters are being forced through the large pore sizes rather than being caught to form proper SERS substrates. It makes sense that these 0.22 µm substrates were visually full of more cracks than the substrates made on

0.1 μ m pore size membranes. Again, these results helped conclude that 0.1 μm pore membranes were to be used to further investigate SERS detection of R6G via MSN-AgNS substrates.

Over the course of this research, several parameters were investigated. Eventually, the primary procedure described in **Chapter 3** was developed. Upon thorough research into the properties assisting in the most ideal SERS substrate, it was identified which chemicals, ratios, membrane pore sizes, and membrane filter holders were best in developing the substrate. When MSN was introduced to the material, the detection of R6G not only enhanced, but the quantitation of R6G was not limited to 5 nM, which was the case without MSN presence.

Although there is discrepancy between the electromagnetic theory and chemical theory contributions to SERS substrates, here it is believed that the electromagnetic field of metal contributed to the SERS enhancement. If there was a chemical reaction between R6G and the MSN-AgNS causing SERS, Raman shifts would most likely be observed as the vibrations would change. Since the spectra are characteristic of R6G and there is no shifting, the electromagnetic field of the metal, in this case AgNS, is most likely the primary contribution. This research concluded that MSN is capable of SERS activity when in company with AgNS material for the detection and quantification of R6G.

CHAPTER VII: CONCLUSIONS AND FUTURE RECOMMENDATIONS

7.1. Fluorescence Chemodosimeter PSP 287 Conclusions

Regarding the detection of phosphate, there are current methods marketed that can achieve low concentration detection. Some include bulky, complex, expensive instrumentation. Aside from the cost of the instrument and training, the cost of consumable has to also be taken into account. For example, using ICP-MS, the cost of; centrifuge tubes, pipette tips, glass pipettes, chemicals to make stock solutions if not using the company's stock, or the cost of calibration verification solution, tuning solution, etc. However the reported methods of the chemodosimeter PSP 287 involve very little preparation, training, and overall a diminished cost.

In the results section of this dissertation, the chemodosimeter PSP 287 was designed in the similar method as described by Guo *et al.* method with hope of achieving similar function.[66] Though using a different molecule for sensing design than that of their work, it was hopeful that it would work in an experimentally similar way. Using this theory, the procedure was designed to use a 9:1 V/V DMSO-HEPES solution, such as the Guo method had carried out.[66] However, it was quickly realized that when using DMSO, there was no reported signal. Of course this could have been simply due to the molecule independently, but using studies of just DMSO as well as DMSO with HEPES in various ratios, it was determined that DMSO was ultimately responsible for signal quenching.

To examine the effects a little further, DMSO was subtracted from the procedure to identify if a HEPES solution would be just as effective as the reported success of Guo *et al*.[66] When using a solely HEPES buffer solution (0.02 M, pH 7.4) ion detection via fluorescence was immediate. Before moving onto the phase of ion detection, it was recognized that the stability of the material in solution should be examined. Hence, incubation studies took place between two

synthesized chemodosimeters of PSP 281 (Guo *et al.* reported chemodosimeter) and PSP 287. PSP 281 did not yield quite as fluorescent of a signal using the $2x10^{-3}$ M PO_4^{3-} ion as the PSP 287 material did. From this experiment, the molecule chosen for further work was PSP 287; 7-hydroxy-4-(hydroxymethyl)-2H-chromen-2-one.

Utilizing the incubation study, the stability of the molecule was also decided. After being subjected to 35 ^oC, the material stayed stable in solution for up to 103 hours. This acknowledged that the material could be produced and kept without repercussions from lack of stability. These results also proved that the material would last and be useful in field work detection.

Phosphate ions were the first to be worked with since there was reported literature stating success, however there was no differentiation between PO_4^{3-}, HPO_4^{2-} and $H_2PO_4^-$ phosphate ions. Considering this, it was of the utmost importance to work with all three ions to determine what, if any, distinguished results would be produced. The PO_4^{3-} ion was used in the case of the incubation study which conclusively determined PSP 287 as a more suitable chemodosimeter in these methods. The PO_4^{3-} ion yielded a much larger intensity than the HPO_4^{2-} indicating the selectivity between the two ions. In contrast, the $H_2PO_4^-$ ion did not result in any increase, but rather quenching. These two ions were selective and believed to cleave a hydroxyl group which resulted in freeing the coumarin compound to display fluorescence increase.

Before discussing the results of the deprotonated phosphate quenching, there were eight other ions sorted for detection. Based on Guo's research, these ions included; NO_3^-, NO_2^-, I^-, Br^-, Cl^-, HSO_4^-, SO_4^{2-}, and CH_3COO^-.[66] For Pi, three ions were tested; PO_4^{3-}, $H_2PO_4^-$, and HPO_4^{2-}, all sodium salts. The experiments visibly displayed the lack of fluorescence or increase at all when $2x10^{-3}$ M of NO_3^-, NO_2^-, I^-, Br^-, Cl^-, HSO_4^- and CH_3COO^- were used. This determined that the chemodosimeter PSP 287 was not selective for these ions. However both SO_4^{2-} and $H_2PO_4^-$

resulted in quenched fluorescence. It is possible that the diminished signal is due to these two ions binding to the coumarin base when in solution which decreases any fluorescence signal.

Aside from the signal being quenched, there was a linearity noticed with both SO_4^{2-} and $H_2PO_4^-$. As the concentration from the ion increased, the signal decreased. Though there is a significantly higher limit of detection with these ions comparatively to the hydrogen phosphate and phosphate ions, it could still be used for identification and larger concentrations quantification.

The two phosphate ions in contrast, PO_4^{3-} and HPO_4^{2-}, intensified as the concentration was increased. Concentrations were detectable anywhere between $2x10^{-4}$ and $2x10^{-3}$ M. These results proved not only selectivity potential, but useful in a variety of testing environments. Chemodosimeter PSP 287 and sensor material described in this project have the possibility and suitability to serve as in-field chemical sensor for ultimate quick, facile and low cost detection of phosphates at the diprotonated, protonated, and unprotonated level as well as sulfate.

It is suspected that the hydrogen phosphate and inorganic phosphate species (HPO_4^{2-} and PO_4^{3-}) were deprotonated one or both hydroxy groups of PSP 287. Once deprotonation occurred, PSP 287 was a slightly freer form of coumarin which encouraged an increase in fluorescence activity. As for the ions that exhibited diminished effects, HSO_4^- and $H_2PO_4^-$, were most likely bonding to PSP 287 at the hydroxy group(s). When the coumarin compound encountered bulkier functionalization, the innate fluorescence that free-form coumarin holds will quench, causing the on-off switch in this case.

To counter the sensor project, ICP-MS was utilized to observed sensitivity differences. Of course, the ICP-MS was significantly more sensitive, however it was much more complex in sample prep and ease of use. The system was optimized over the course of time to identify which procedure worked best. Phosphate is not necessarily an easily detected element on ICP-MS. This

is mostly due to the fact that most samples are acidified, however phosphate is not soluble in the nitric acid solution that is typically used. Aside from this, the calibration verification standard solution does not produce phosphorous, and calibration standards would have to be made from scratch.

Over the course of system optimization, it was found that the samples provided less than 10 ppb of phosphorous. The calibration curve used for this experiment was the protonated phosphate ion. To determine if the form of ion had an impact, all three ions would need to be made into calibration curves and run independently on the same set of samples. If there is no change here, then it can be concluded that there is no selectivity when using this instrument. If there is a difference in detection, though this proves that a concentration gradient exist, there is also proof in the time consumption as well as material consumption which makes this method less than ideal for detection.

Overall, the ICP-MS detection showed that phosphorous could be detected to as low as 0.1 ppb, which is significantly less concentrated than the chemodosimeter PSP 287 limit of detection. However, the main comparison between these two projects is shown for the ease of use and accessibility. In that instance, the chemodosimeter PSP 287 is much more functional and reliable for simple and slightly more concentrated samples. Other instrumentation can and will continue to be used for detection methods at the elemental level. This dissertation provided synthetic guidelines to produce a chemodosimeter PSP 287 which achieved phosphate detection down to $2x10^{-4}$ M or 200 uM. Not only did this sensor achieve sensitivity, selectivity was also performed by distinguishing between ions. These methods provide a strong sensor that is capable in ionic detection at low concentrations.

7.2. Future Directions for PSP 287 Fluorescence Detection of Phosphate Species

Future works may be done to examine further selectivity. There are countless other ionic solutions that could be potentially detectable. Although this sensor proved incredibly selective against the eleven ions tested throughout this project, there may be further research that could be performed.

7.3. MSN-AgNS SERS Substrate for R6G Detection Conclusions

Inverse opal material was also investigated in hopes of providing sensor reliable material in the quest of R6G identification. PMMA material has proven to be suitable material for optical sensors such as hydrogels. This dissertation decided to focus on subjecting inverse templated material to metal nanoparticles that would aid in R6G characterization.

The template that resulted from calcining off PMMA which left the inverse opal substrate was porous in nature and ideal for filling with silver nanoparticles. However, there was trouble in identifying a method that would allow even distribution, absence of aggregated clusters, while also filling the pores rather than blocking. To counter for this problem, spray coating, drop coating, and spin coating methods were all researched.

After many trials, it was found that the spin coating method worked the best in resolving these issues. However, the R6G deposited was still lacking the SERS enhancement. There could be several factors attributing to these disappointing results. For instance, the R6G was drop deposited on the inverse opal template with spin coat AgNS. This potentially may have been too saturating or not properly dispersed in the correct manner. It was observed via SEM imaging that five layers of AgNS spin coated onto the inverse opal substrates resulted in even layering but did not contribute to a SERS active substrate.

After several attempts of altering inverse opal template to form SERS active materials had failed, the project was deemed unsuccessful. In the future, there is hope in utilizing a PMMA or inverse opal type material to create a SERS substrate. The properties of the material are quite unique and would be suitable in forming a capable sensor.

Another project focused in this dissertation was the SERS active substrate incorporating MSN. SERS substrates have been researched since the first project was discovered in the ‘70s, however no research has been conducted that combines both current SERS methodology along with MSN. MSN material is widely used in optical projects for its ability to control refractive indexes via synthetic methods. In this project, the MSN was synthesized to add reliability and enhance a previously known SERS method.

Silver specifically is relatively popular when fabricating a SERS substrate. Primarily silver is favored because it enhances the magnetic field due it’s metallic properties while also proving that it enhances a signal comparative to gold particles. Other metals could also be applied, but are generally much less stable and reliable than gold or better yet silver. Most substrates are made using spherical silver particles, however this research focused on using a nanostar material. Nanostars are a morphology of silver nanoparticles that are not necessarily novel, but also not yet widely used in research compared to the more attainable nanospheres. The ultimate goal here was to find a fabrication method that was SERS capable utilizing both MSN and AgNS (silver nanostars).

Originally, the idea was to use an inverse opal template and project both MSN and AgNS onto it. Since this method was uneventful, the next step was to use a filter paper. Multiple variables were played with here to see what were the most effective methods and which worked better. First and foremost, the size of the filter pores. If too large, such as 0.22 μm, then the material would slip through. This resulted in the use of the perfect size; 0.1 μm pores. Next was

figuring out what was the best aggregator, sodium citrate or sodium chloride. Through many experiments, it was determined that sodium chloride aggregated the silver nanostars much more effectively than the sodium citrate was able to.

The ratio of material was the last variable to be sorted through. First, it had to be worked with on whether MSN was best added to the solution or the substrate directly. It was found that if MSN was added to the substrate first via soaking, that when the aggregated AgNS was added the MSN would become disrupted and push through the filter. This was how the AgNS/MSN/NaCl solution method was developed. Variability in the ratios between materials caused some resulting changes from SERS before the ultimate ratio was determined.

Several other factors also weighed in but were much more minor. Such as the type of substrate holder, two companies provided material. The Whatman substrates were found to be more durable and reliable in repeatability. Other substrate holders did not always provide the same surface area which increased the difficulty in proving the solution concentration was evenly distributed.

Once the method was developed and proven to work, there were several trials that had to be conducted. This would help prove that the results were reliable. As previously discussed in this dissertation, there is the nature of hot spots, which was frequently observed. For this reason, samples were taken three times from the same substrate in different spots to examine the average which would be the measurement used for presentation purposes.

The material was set against the same SERS substrate without the presence of MSN. It was a known fact that silver caused a SERS phenomenon. When the two trials were compared, it was made obvious that the absence of MSN cause a much higher detection limit and was overall lacking in terms of efficiency when compared to the trials with MSN present. With MSN added to solution, the SERS substrate was capable of detecting down to 100 pM of R6G. However

when MSN was absent, the SERS substrate was only capable of detecting down to 10, or occasionally, 5 nM of R6G. These concentrations were confirmed by identifying R6G's characteristic 608 cm^{-1} peak.

The concentration distinction of R6G was evident when MSN was present. When MSN was added to solution, the filters were visibly different. SERS substrates made with MSN and used for R6G detection would display a bright pink color on the underside whereas the substrates without MSN would not have the same visible affect. The presence of MSN was able to concentrate the R6G higher than if it were lacking.

7.3. Future Directions for MSN-AgNS SERS Substrates for R6G Detection

There may be future work to be done with these substrates examining if there are other chemicals that could be detected using this method. Of course R6G is a highly recognizable chemical via Raman, however MSN and the ability to enhance a SERS signal with silver may not be solely confined to R6G. This type of work was not performed in this dissertation but may be of future research goals.

7.4. Summary of Conclusions

This dissertation set out to develop sensors for detection that were selective and quantitative. Projects focused on selective testing of phosphate ion via a synthetic chemodosimeter and another was focused on fabricating a SERS active substrate for R6G detection. Both projects proved successful in their goals and were novel in their use and fabrication methods. Ultimately, two sensors were synthesized that could be used in current laboratories and field work facilities to perform chemical and environmental detection.

REFERENCES

1. National Research Council. (1995). Introduction to Sensors. *Expanding the Vision of Sensor Materials*. Washington, DC: The National Academies Press.

2. Billimoria, S., Mukherjee, N., Petrovskaya, A., & Khatib, O. (2008). *Tactile Sensors*. Project Report. Stanford University. Retrieved Feb, 2019 from: https://www-cs.stanford.edu/group/manips/publications/pdfs/Petrovskaya_2008_Report.pdf.

3. Philips Lifeline. (2016). *Automatic Fall Detection*. Retrieved Feb, 2019 from https://www.lifeline.philips.com/medical-alert-systems/fall-detection.html.

4. Kumar, R., & Singh, R. (2018). Prospect of Graphene for Use as Sensors in Miniaturized and Biomedical Sensing Devices. Reference Module in *Mat. Sci. Eng*.

5. Nano-Bio Spectroscopy Group. *Chemical Sensors*. Retrieved Jan, 2019 from http://nano-bio.ehu.es/files/chemical_sensors1.doc_definitivo.pdf.

6. McDonagh, C., Burke, C.S., & MacCraith, B.D. (2008). Optical Chemical Sensors. *Chem. Rev.*, 108(2), 400-422.

7. The Rayon-Matter Institue of Saclay (Iramis). *Chemical sensor of air pollutants.* Retrieved Jan, 2019 from http://iramis.cea.fr/Phocea/Vie_des_labos/Ast/ast_visu.php?id_ast=1168.

8. Lobnik, A., Turel, M., & Urek, S.K. (2012). Optical Chemical Sensors: Design and Applications *Advances in Chemical Sensors*. Prof. Wen Wang (Ed.) ISBN: 978-953-307-792-5, InTech. Retrieved from https://www.intechopen.com/books/advances-in-chemical-sensors/optical-chemical-sensors-design-and-applications.

9. Reyes, F., Grutter, M., Jazcilevich, A., & Gonzalez-Oropeza, R. (2006). Technical Note: Analysis of non-regulated vehicular emissions by extractive FTIR spectrometry: tests on a hybrid car in Mexico City. *Atmos. Chem. Phys.*, 6, 5339-5346.

10. Nanophoton. *Lesson 1. Basic of Raman scattering*. Retrieved Feb, 2019 from https://www.nanophoton.net/raman/raman-spectroscopy.html.

11. Technospex. Techincal Notes. *Introduction to Raman Spectroscopy*. Retrieved Jan, 2019 from https://www.technospex.com/resources/introduction-to-raman-spectroscopy/.

12. Stuart, D. A., Biggs, K. B., & Van Duyne, R. P. (2006). Surface-enhanced Raman spectroscopy of half-mustard agent. *Analyst*., 131(4), 568-572.

13. Sharma, B., Frontiera, R.R., Henry, A.I., Ringe, E., & Van Duyne, R.P. (2012). SERS: Materials, applications, and the future. Review. *Materials Today*, 15(1-2) 16-26.

14. Deschaines, T.O., & Wieboldt, D. (2010). Thermo Fisher Scientific Inc. *Practical Applications of Surface-Enhanced Raman Scattering (SERS)*. Retrieved Jan, 2019 from https://assets.thermofisher.com/TFS-Assets/CAD/Product-Bulletins/D19663~.pdf.

15. Faulds, K., Hernandez-Santana, A., & Smith, W. E. (2010). The inorganic chemistry of surface enhanced Raman scattering (SERS). *Spectroscopic Properties of Inorganic and Organometallic Compounds: Techniques, Materials and Applications Volume 41*, 1-21. Royal Society of Chemistry.

16. Stiles, P.L., Dieringer, J.A., Shah, N.C., & Van Duyne, R.P. (2008). Surface-Enhanced Raman Spectroscopy. *Annu. Rev. Anal. Chem*., 1, 601-626.

17. Albrecht, M.G., & Creighton, J.A. (1977). Anomalously intense Raman spectra of pyridine at a silver electrode. *J. Am. Chem. Soc.,* 99(15), 5215-5217.

18. Jeanmarie, D.L., & Van Duyne, R.P. (1977). Surface Raman spectroelectrochemistry, Part 1: Heterocyclic, aromatic, and aliphatic amines adsorbed on the anodized silver electrode. *J. Electroanal. Chem.,* 84(1), 1-20

19. Fleischmann, M., Hendra, P. J., & McQuillan, A. J. (1974). Raman spectra of pyridine adsorbed at a silver electrode. *Chem. Phy. Lett.,* 26(2), 163-166.

20. Wang, A.X., & Kong, X. (2015). Review of Recent Progress of Plasmonic Materials and Nano-Structures for Surface-Enhanced Raman Scattering. *Materials (Basel)*, 8(6), 3024-3052.

21. Radziuk, D., & Moehwald, H. (2014). Highly effective hot spots for SERS signatures of live fibroblasts. *Nanoscale*, 6(11), 6115-6126.

22. Jaworska, A., Fornasaro, S., Sergo, V., & Bonfacio, A. (2016). Potential of Surface Enhanced Raman Spectroscopy (SERS) in Therapeutic Drug Monitoring (TDM). A Critical Review. *Biosensors (Basel)*. 6(3), 47.

23. Loren, A., Eliasson, C., Josefson, M., Murty, K., Kall, M., Abrahamsson, J., & Abrahamsson, K. (2001). Feasibility of quantitative determination of doxorubicin with surface-enhanced Raman spectroscopy. *J. Raman Spectrosc.*, 32(11), 971-974.

24. Yan, T., Gu, H., Yuan, X., Wu, J., & Wei, H. (2008). Surface-enhanced Raman spectroscopy study of the interaction of antitumoral drug Paclitaxel with human serum albumin. Proc. SPIE 7280, Seventh International Conference on Photonics and Imaging in Biology and Medicine, 72800N; doi: 10.1117/12.821462.

25. McLaughlin, C., MacMillan, D., McCardle, C., & Smith, W.E. (2002). Quantitative analysis of Mitoxantrone by Surface-Enhanced Resonance Raman Scattering. *Anal. Chem.*, 74(13), 3160–3167.

26. Litti, L., Amendola, V., Toffoli, G., & Meneghetti, M. (2016). Detection of low-quantity anticancer drugs by surface-enhanced Raman scattering. *Anal. Bioanal. Chem.,* 408(8), 2123–2131.

27. Li, Y.T., Qu, L.L., Li, D.W., Song, Q.X., Fathi, F., & Long, Y.T. (2013). Rapid and sensitive in-situ detection of polar antibiotics in water using a disposable Ag-graphene sensor based on electrophoretic preconcentration and surface-enhanced Raman spectroscopy. *Biosens. Bioelectron.*, 43C(1), 94-100.

28. Yang, J., Tan, X., Shih, W.C., & Cheng, M.M. (2014). A sandwich substrate for ultrasensitive and label-free SERS spectroscopic detection of folic acid / methotrexate. *Biomed. Microdevices*, 16(5), 673-679.

29. Lu, H., Zhang, H., Yu, X., Zeng, S., Yong, K.T., & Ho, H.P. (2012). Seed-mediated Plasmon-driven Regrowth of Silver Nanodecahedrons (NDs). *Plasmonics*, 7(1), 167-173.

30. Kahraman, M., Mullen, E. R., Korkmaz, A., Wachsmann-Hogiu, S. (2017). Fundamentals and applications of SERS-based bioanalytical sensing. *Nanophotonics*, 6(5), 831-852.

31. Zhang, Q., Li, W., Wen, L.P., Chen, J., & Xia, Y. (2010). Facile Synthesis of Ag Nanocubes of 30 to 70 nm in Edge Length with CF_3COOAg as a Precursor. *Chem. Eur. J.*, 16(33), 10234-10239.

32. He, S., Chua, J., Tan, E., & Kah, J. (2017). Optimizing the SERS enhancement of a facile gold nanostar immobilized paper-based SERS substrate. *RSC Advances*, 7(27), 16264-16272.

33. National Center for Biotechnology Information. PubChem Database. *Basic Red 1*, CID=235227, Retrieved Feb, 2019 from https://pubchem.ncbi.nlm.nih.gov/compound/235227.

34. Madison, L. R., Ratner, M. A., & Schatz, G. C. (2017). SERS theory: The chemical effect of Rhodamine 6G adsorption on silver surfaces on its Raman spectrum. *Recent Developments In Plasmon-Supported Raman Spectroscopy: 45 Years of Enhanced Raman Signals* (pp. 401-414). World Scientific Publishing Co. Pte Ltd. https://doi.org/10.1142/9781786344243_0014.

35. Zhang, Y. X., Zheng, J., Gao, G., Kong, Y. F., Wang, K., Zhang, X. Q., & Cui, D. X. (2011). Biosynthesis of gold nanoparticles using chloroplasts. *Int. J. Nanomedicine*, 6, 2899-2906.

36. OMICS International. (2014). *Chemosensors*. Retrieved Feb, 2019 from https://www.omicsonline.org/chemosensors/scholarly-open-access-journals.php.

37. Wu, D., Sedgwick, A. C., Gunnlaugsson, T., Akkaya, E. U., Yoon, J., & James, T. D. (2017). Fluorescent chemosensors: the past, present and future. *Chem. Soc. Rev.*, 46(23), 7105-7123.

38. Lakowicz J. R. (2006). *Principles of Fluorescence Spectroscopy*. Massachusetts: Springer.

39. Patil, A., & Salunke-Gawali, S. (2018). Overview of the chemosensor ligands used for selective detection of anions and metal ions (Zn^{2+}, Cu^{2+}, Ni^{2+}, Co^{2+}, Fe^{2+}, Hg^{2+}). *Inorganica Chim. Acta*, 482, 99-112.

40. Lee, M. H., Kim, J. S., & Sessler, J. L. (2014). Small molecule-based ratiometric fluorescence probes for cations, anions, and biomolecules. *Chem. Soc. Rev.*, 44(13), 4185–4191.

41. Seo, J., Kim, S., & Park, S. Y. (2004). Strong Solvatochromic Fluorescence from the Intramolecular Charge-Transfer State Created by Excited-State Intramolecular Proton Transfer. *J. Am. Chem. Soc*., 126(36), 11154-11155.

42. Sheini, A., Khajehsharifi, H., Shahbazy, M., & Kompany-Zareh, M. (2017). A chemosensor array for the colorimetric identification of some carboxylic acids in human urine samples. *Sens. Actuators B Chem.,* 242, 288–298.

43. Sheet, S. K., Sen, B., Thounaojam, R., Aguan, K., & Khatua, S. (2017). Highly selective light-up Al^{3+} sensing by a coumarin based Schiff base probe: Subsequent phosphate sensing DNA binding and live cell imaging. *J. Photochem. Photobiol., A*. 332, 101-111.

44. Li, J., Zhang, C. F., Yang, S. H., Yang, W. C., & Yang, G. F. (2014). A Coumarin-Based Fluorescent Probe for Selective and Sensitive Detection of Thiophenols and Its Application. *Anal. Chem*., 86(6), 3037-3042.

45. Röttgers, R. (2007). Comparison of different variable chlorophyll *a* fluorescence techniques to determine photosynthetic parameters of natural phytoplankton. *Deep Sea Res. Part 1 Oceanoogr Res, Pap*., 54(3), 437-451.

46. Geisler, J., & Thompson, T. (2015). Biocompare. *Bench Tips - Choosing the Best Detection Method: Absorbance vs. Fluorescence*. Retrieved Sep 18, 2018 from https://www.biocompare.com/Bench-Tips/173963-Choosing-the-Best-Detection-Method-Absorbance-vs-Fluorescence/.

47. Wagner, B. D. (2009). The use of coumarins as environmentally-sensitive fluorescent probes of heterogeneous inclusion systems. *Molecules*, 14(1), 210-237.

48. Sigma-Aldrich. (2019). *Coumarin*. Retrieved Sep 12, 2018 from https://www.sigmaaldrich.com/catalog/product/sigma/c4261?lang=en&region=US.

49. Wu, P., Hou, X., Xu, J. J., & Chen, H. Y. (2016). Ratiometric fluorescence, electrochemiluminescence, and photoelectrochemical chemo/biosensing based on semiconductor quantum dots. *Nanoscale*, 8(16), 8427–8442.

50. Valeur, B. (2001). *Molecular Fluorescence: Principles and Applications*. Weinheim, Germany: Wiley-VCH Verlag GmbH.

51. European Advanced Light Microscopy Network (EAMNET). (2005). *Ratiometric Methods*. Retrieved Sep, 2018 from https://www.embl.de/eamnet/html/calcium/ratio.htm.

52. Jiang. W., Fu, Q., Fan, H., Ho, J., & Wang, W. (2007). A Highly Selective Fluorescent Probe for Thiophenols. *Angew Chem*., 46(44), 8445-8448.

53. He, L., Xu, Q., Liu, Y., Wei, H., Tang, Y., & Lin, W. (2015). Coumarin-Based Turn-On Fluorescence Probe for Specific Detection of Glutathione over Cysteine and Homocysteine. *Appl. Mater. Interfaces*, 7(23), 12809-12813.

54. Zhang, C., Wei, L., Wei, C., Zhang J., Wang, R., Xi, Z., & Yi, L. (2015). A FRET-ICT dual-quenching fluorescent probe with large off-on response for H_2S: synthesis, spectra and bioimaging. *Chem. Commun. (Camb)*, 51(35), 7505-7508.

55. Zhang, H., Zhang, C., Liu, R., Yi, L., & Sun, H. (2015). A highly selective and sensitive fluorescent thiol probe through dual-reactive and dual-quenching groups. *Chem. Commun. (Camb)*, 51(11), 2029-2032.

56. Wang, M., Wen, J., Qin, Z., & Wang, H. (2015). A new coumarin–rhodamine FRET system as an efficient ratiometric fluorescent probe for Hg^{2+} in aqueous solution and in living cells. *Dyes Pigm.*, 120, 208–212.

57. Formica, M., Fusi, V., Giorgi, L., & Micheloni, M. (2012). New fluorescent chemosensors for metal ions in solution. *Coord. Chem. Rev*., 256(1-2), 170-192.

58. Hossain, M. A., Mihara, H., & Ueno, A. (2003). Novel Peptides Bearing Pyrene and Coumarin Units with or without β-Cyclodextrin in Their Side Chains Exhibit Intramolecular Fluorescence Resonance Energy Transfer. *J. Am. Chem. Soc*., 125(37), 11178-11179.

59. Lin, W., Yuan, L., Cao, Z., Feng, Y., & Song, J. (2010). Through-Bond Energy Transfer Cassettes with Minimal Spectral Overlap between the Donor Emission and Acceptor Absorption: Coumarin-Rhodamine Dyads with Large Pseudo-Stokes Shifts and Emission Shifts. *Angew Chem. Int. Ed. Engl*., 49(2), 375-379.

60. Loudet, A., Thivierge, C., & Burgess, K. (2011). Dojindo Laboratories. *Through-bond Energy Transfer Cassettes*. Retrieved Sep 14, 108 from http://www.dojindo.co.jp/letterj/137/review/01.html).

61. Wu, Y., Peng, X., Fan, J., Gao, S., Tian, M., Zhao, J., & Sun, S. (2007). Fluorescence Sensing of Anions Based on Inhibition of Excited-State Intramolecular Proton Transfer. *J. Org. Chem*., 72(1), 62-70.

62. Shreykar, M. R., & Sekar, N. (2017). Coumarin-Pyrazole Hybrid with Red Shifted ESIPT Emission and AIE Characteristics – a Comprehensive Study. *J. Fluoresc*., 27(5), 1687-1707.

63. Wen, X., & Fan, Z. (2016). Linear Schiff-base fluorescence probe with aggregation-induced emission characteristics for Al^{3+} detection and its application in live cell imaging. *Anal. Chim. Acta*., 945, 75-84.

64. Gan, W. (2004). *Synthesis and Design of Fluorescence Ligands to Act as Sensor for Zinc* (Master's Thesis). University of North Carolina at Wilmington, Wilmington, NC.

65. Santos-Figueroa, L. E., Moragues, M. E., Climent, E., Agostini, A., Martínez-Mañez, R., & Sancenoń, F. (2013). Chromogenic and fluorogenic chemosensors and reagents for anions. A comprehensive review of the years 2010-2011. *Chem. Soc. Rev*., 42(8), 3489−3613.

66. Guo, L. E., Zhang, J. F., Liu, X. Y., Zhang, L. M., Zhang, H. L., Chen, J. H., Xie, G. X., Zhou, Y., Luo, K., & Yoon, J. (2015). Phosphate Ion Targeted Colorimetric and Fluorescent Probe and Its Use to Monitor Endogeneous Phosphate Ion in a Hemichannel-Closed Cell. *Anal. Chem.*, 87(2), 1196-1201.

67. Hussain, S. A., Dey. D., Chakraborty, S., Saha, J., Roy, A. D., Chakraborty, S., Debnath, P., & Bhattacharjee, D. (2015). Fluorescence Resonance Energy Transfer (FRET) sensor. *J. Spectrosc. Dyn*., 5(7).

68. Yuan, L., Jin, F., Zeng, Z., Liu, C., Luo, S., & Wu, J. (2015). Engineering a FRET strategy to achieve a ratiometric two-photon fluorescence response with a large emission shift and its application to fluorescence imaging. *Chem. Sci*., 6(4), 2360-2365.

69. Gardiner, D.J., Graves, P.R., Bowley, & H.J. (1989). *Practical Raman spectroscopy*. Springer-Verlag. ISBN 978-0-387-50254-0.

70. Xu, X., Li, H., Hasan, D., Ruoff, R. S., Wang, A. X. & Fan, D. L. (2013), Near-Field Enhanced Plasmonic-Magnetic Bifunctional Nanotubes for Single Cell Bioanalysis. *Adv. Funct. Mater*., 23(35), 4332-4338.

71. IDEX. Semrock. *Surface-Enhanced Raman Scattering (SERS).* Retrieved Feb, 2019 from https://www.semrock.com/surface-enhanced-raman-scattering-sers.aspx.

72. Kreibig, U., & Vollmer, M. (1995). *Optical Properties of Metal Clusters*, *Vol. 25*. Berlin, Germany: Springer-Verlag Berlin Heidelberg.

73. Haynes, C.L., Yonzon, C. R., Zhang, X., & Van Duyne, R. P. (2005). Surface-enhanced Raman sensors: early history and the development of sensors for quantitative biowarfare agent and glucose detection. *J. Raman Spectrosc.*, 36(6-7), 471-484.

74. Rycenga, M., Camargo, P.H.C., Li, W., Moran, C.H., & Xia, Y. (2010). Understanding the SERS Effects of Single Silver Nanoparticles and Their Dimers, One at a Time. *J. Phys. Chem. Lett.,* 1(4), 696-703.

75. Siemes, C., Bruckbauer, A., Goussev, A., Otto, A., Sinther, M., & Pucci, A. (2001). SERS-active sites on various copper substrates. *J. Raman Spectrosc.,* 32(4), 231-239.

76. Graff, M., Bukowska, J., & Zawada, K. (2004).Surface enhanced Raman scattering (SERS) of 1-hydroxybenzotriazole adsorbed on a copper electrode surface. *J. Electroanal. Chem.*, 567(2), 297-303.

77. White, I. M., Oveys, H., & Fan, X. D. (2006). Increasing the enhancement of SERS with dielectric microsphere resonators. *Spectroscopy*, 21(4), 36-42.

78. Morton, S.M., Ewusi-Annan, E., & Jensen, L. (2009). Controlling the non-resonant chemical mechanism of SERS using a molecular photoswitch. *Phys. Chem. Chem. Phys.,* 11(34), 7424-7429.

79. Garcia-Leis A., Garcia-Ramos, J. V., & Sanchez-Cortes, S. (2013). Silver Nanostars with High SERS Performance. *J. Phys. Chem. C*, 117(15), 7791–7795.

80. Oliveira, M. J., Quaresma, P., Peixoto de Almeida, M., Araújo, A., Pereira, E., Fortunato, E., Martins, R., Franco, R., & Águas, H. (2017). Office paper decorated with silver nanostars – an alternative cost effective platform for trace analyte detection by SERS. *Sci. Rep*., 7(1), 2480.

81. Radu, D. R., Pizzi, N. A., & Lai, C. Y. (2016). Functionalized stellate microporous silica nanospheres for Co_2 mitigation. *J. Mater. Sci*., 51(23), 10632-10640.

82. Chi, H. H., Radu, D. R., Dezayas, G., Penney, M., & Lai, C. Y. (2017). Stellate MSN-based Dual-enzyme Nano-Biocatalyst for the Cascade Conversion of Non-Food Feedstocks to Food Products. *J. Thermodyn. Catal*., 8(2), 185.

83. Gao, S., Glasser, J., & He, L. (2016). A Filter-based Surface Enhanced Raman Spectroscopic Assay for Rapid Detection of Chemical Contaminants. *J. Vis. Exp.*, (108), 53791.

84. Lee, P. C., & Meisel, D. (1982). Adsorption and surface-enhanced Raman of dyes on silver and gold sols. *J. Phys. Chem*., 86(17), 3391–3395.

85. Yu, W. W., & White I. M. (2012). A simple filter-based approach to surface enhanced Raman spectroscopy for trace chemical detection. *Analyst*., 137(5), 1168–1173.

86. Schroden, R., Balakrishnan, N., Stein, A., & Ward, M. D. (2001). University of Minnesota Materials Research Science and Engineering Center. *Inverse Opal Photonic Crystals, A Laboratory Guide*. Retrieved from http://citeseerx.ist.psu.edu/viewdoc/download?doi=10.1.1.466.4091&rep=rep1&type=pdf .

87. Lisensky, G., & Horger, J. Synthesis of Inverse Opal Photonic Crystals. Beloit College. MRSEC Education Group. Retrieved from: https://education.mrsec.wisc.edu/synthesis-of-inverse-opal-photonic-crystals/

88. Zagotto, G., Gia, O., Baccichetti, F., Uriarte, E., & Palumbo, M. (1993). Synthesis and Photobiological Properties of 4-hydroxymethyl-4'-methylpsoralen derivatives. *Photochem. Photobiol*., 58, 486-491.

89. Ritchey, J. A. (2010). *Design and Applications of 4-YL-(methyl)coumarins and Their Derivatives* (Doctoral Dissertation). University of Illinois at Urbana-Champaign, Champaign, IL.

90. University of Puget Sound. *Characteristic IR Absorption Frequencies of Organic Functional Groups.* Retrieved Jan, 2019 from http://www2.ups.edu/faculty/hanson/Spectroscopy/IR/IRfrequencies.html.

91. Fulmer, G.R., Miller, A.J.M., Sherdan, N.H., Gottlieb, H.E., Nudelman, A., Stoltz, B.M., Bercaw, J.E., & Goldberg, K.I. (2010). NMR Chemical Shifts of Trace Impurities: Common Laboratory Solvents, Organics, and Gases in Deuterated Solvents Relevant to the Organometallic Chemist. *Organometallics*, 29(9), 2176-2179.

92. Clevenson, H., Desjardins, P., Gan, X., & Englund, D. (2014). High sensitivity gas sensor based on high-Q suspended polymer photonic crystal nanocavity. *Appl. Phys. Lett.*, 104(24), 241108.

93. Jaworska, A., Wojcik, T., Malek, K., Kwolek, U., Kepczynski, M., Ansary, A.A., Chlopicki, S., & Baranska, M. (2015). Rhodamine 6G conjugated to gold nanoparticles as labels for both SERS and fluorescence studies on live endothelial cells. *Microchim. Acta*, 182(1-2), 119-127.

94. Zhong, F., Wu, Z., Guo, J., & Jia, D. (2018). Porous Silicon Photonic Crystals Coated with Ag Nanoparticles as Efficient Substrates for Detecting Trace Explosives Using SERS. *Nanomaterials*, 8(11), 872.

95. Zhai, W. L., Li, D. W., Qu, L. L., Fossey, J. S., & Long, Y. T. (2012). Multiple Depositions of Ag Nanoparticles on Chemically Modified Agarose Film for Surface-Enhanced Raman Spectroscopy. *Nanoscale*, 4(1), 137-142.

96. Hoppmann, E., Yu, W., & White, I. (2013). Highly sensitive and flexible inkjet printed SERS sensors on paper. *Methods*, 63(3), 219-224.

97. NanoComposix. *Salt Stability of Nanoparticles*. Retrieved Jan, 2019 from https://nanocomposix.com/pages/salt-stability-of-nanoparticles#target.